Mechanistic modelling of cropland and grassland ecosystems: focus on the water cycle and on cattle grazing

Auteur : Dumont, Clément
Promoteur(s) : Longdoz, Bernard
Faculté : Gembloux Agro-Bio Tech (GxABT)
Diplôme : Master en bioingénieur : sciences et technologies de l'environnement, à finalité spécialisée
Année académique : 2018-2019
URI/URL : http://hdl.handle.net/2268.2/7540

LIÈGE université
Gembloux
Agro-Bio Tech

MECHANISTIC MODELLING OF CROPLAND AND GRASSLAND ECOSYSTEMS: FOCUS ON THE WATER CYCLE AND ON CATTLE GRAZING

Clément Dumont

Thesis submitted for the degree of Master in Bioengineer
specialized in environmental sciences and technologies

Academic year 2018-2019

Supervisor: Pr. Bernard Longdoz

LIÈGE université
Gembloux
Agro-Bio Tech

MECHANISTIC MODELLING OF CROPLAND AND GRASSLAND ECOSYSTEMS: FOCUS ON THE WATER CYCLE

Clément Dumont

Thesis submitted for the degree of Master in Bioengineer
specialized in environmental sciences and technologies

Academic year 2018-2019

Supervisor: Pr. Bernard Longdoz

Acknowledgment

First of all, I would like to thank my supervisor, Pr. Bernard Longdoz, for his constant assistance and wise advice. Whenever we reached a hindrance, he helped us find a way to go on with our work and complete this thesis. I will not forget our many weekly meetings, during which he made us discover and learn step by step the world of ecosystem modelling.

Much assistance also came from the Biodyne staff. I think of Pr. Bernard Heinesch, who attended some of our meetings, Louis Gourlez de la Motte, who offered me a great support in understanding the functioning of Dorinne experimental site, and Anne De Ligne, who shared her knowledge of complex datasets with us. Besides these scientific collaborations, the staff also made us feel as part of the research unit, and I thank them for that.

However, the most important support I received during this Master thesis came from my two colleagues, Laura Delhez and Félix Vandewattyne. Through good and bad times, we always found a way to keep on pursuing our objectives in a nice atmosphere. I could not have hoped working with more farsighted and reliable people during this semester, and I thank them a lot for their presence.

Last but not least, at this end of my studies, I want to thank my family and my friends for supporting me through these years, but especially my mother who believed in me and encouraged me to start these studies, when I thought I would not be capable of it.

Abstract

Climate change stirs up more and more citizens' interest and concern, and the role of greenhouse gases (GHG) in climate change has now been widely discussed. The agricultural sector is pointed as one of the main causes of climate change, mostly for its emissions of biogenic GHG. However, the impact of ecosystems environment and management practices on these emissions is yet not fully understood, and the response of agroecosystems to a changing environment is still questioned. This context highlights the necessity of studying and understanding ecosystem dynamics in order to design climate change mitigation strategies. To do so, mechanistic models reproducing the carbon, nitrogen and water cycles of ecosystems can be developed.

This thesis aims at modifying the ASPECTS model, developed by Rasse et al. (2001) to simulate the evolution of forest stands, into a cropland and grassland model. The main dissimilarities between forests and croplands or grasslands were identified, and the required modifications were implemented in a new version of ASPECTS, called the Terrestrial Agroecosystems Dynamics Analysis (TADA) model. This new model was then calibrated against data acquired in two cropland and grassland sites, both equipped with eddy covariance (EC) systems and meteorological stations.

In this work, the attention is paid to the water cycle. Soil evaporation and canopy transpiration were calibrated against evapotranspiration fluxes (ET) measurements, and the dynamics of water infiltration and percolation within the soil profile was compared to measures of soil water content (SWC). Soil evaporation was calibrated during bare soil conditions and resulted in a calibration RMSE of 1.37 and 2.57 mm day^{-1} and a validation RMSE of 1.82 and 2.75 mm day^{-1} for, respectively, the cropland and the grassland sites. These results could not be transferred to soils covered with vegetation, making plant transpiration impossible to calibrate. Canopy aerodynamic resistance was identified as a possible cause of this problem and a new methodology is proposed to calibrate these two processes with a wide and diverse dataset in terms of environmental conditions.

In addition to this calibration, the new grazing module was tested by comparing measured and modelled grass height. The discrepancies are mainly due to the partitioning of assimilated carbon between the shoot and root compartments and to uncertainties in the estimation of cattle intake capacity. Paths of improvement are provided for a future calibration of this grazing module, considering both available data and potentially measurable variables.

Keywords: *Water cycle - Evapotranspiration - Grazing - Ecosystem model - GHG fluxes*

Résumé

Le changement climatique soulève de plus en plus l'intérêt et la préoccupation des citoyens, et le rôle des gaz à effet de serre (GES) dans ce changement climatique a été à présent largement traité. Le secteur agricole est considéré comme une des causes majeures du changement climatique, principalement pour ses émissions de GES biogéniques. Cependant, l'impact de l'environnement des écosystèmes et des pratiques agricoles sur ces émissions n'est à ce jour pas entièrement compris, et la réponse des agroécosystèmes face à un environnement modifié est toujours débattue. Ce contexte souligne la nécessité d'étudier et de comprendre la dynamique des écosystèmes, afin de développer des stratégies de mitigation du changement climatique. Pour ce faire, des modèles méchanistiques reproduisant les cycles du carbone, de l'azote et de l'eau des écosystèmes peuvent être développés.

Cette thèse a pour but de modifier le modèle ASPECTS, développé par Rasse et al. (2001) pour simuler l'évolution de peuplements forestiers, en un modèle de culture et de prairie. Les différences principales entre les forêts et les cultures ou prairies ont été identifiées, et les modifications nécessaires ont été implémentées dans une nouvelle version d'ASPECTS, appelée le modèle Terrestrial Agroecosystems Dynamics Analysis (TADA). Ce nouveau modèle a ensuite été calibré à l'aide de données acquises dans deux sites de culture et de prairie, tous deux équipés de systèmes d'eddy covariance (EC) et de stations météorologiques.

Dans ce travail, l'attention est portée sur le cycle de l'eau. L'évaporation du sol et la transpiration de la canopée ont été calibrées à partir de mesures de flux d'évapotranspiration (ET), et la dynamique de l'infiltration et de la percolation de l'eau au travers du profil de sol a été comparée à des mesures de contenu en eau du sol (SWC). L'évaporation du sol a été calibrée sur des périodes de sol nu, et a fourni une RMSE de calibration de 1.37 et 2.57 mm jour^{-1} et une RMSE de validation de 1.82 et 2.75 mm jour^{-1} pour, respectivement, les sites de culture et de prairie. Ces résultats n'ont pas pu être appliqués à des sols couverts de végétation, rendant la transpiration des plantes impossible à calibrer. La résistance aérodynamique de canopée a été identifiée comme l'une des causes potentielles de ce problème, et une nouvelle méthodologie est proposée pour calibrer ces deux processus, avec un jeu de données vaste et diversifié en termes de conditions environnementales.

En plus de cette calibration, le nouveau module de pâturage a été testé en comparant des hauteurs d'herbe mesurées et modélisées. Les divergences sont principalement dues au partitionnement du carbone assimilé entre les compartiments de pousses et de racines, et à des incertitudes dans l'estimation de la capacité d'ingestion du bétail. Des pistes d'amélioration sont proposées pour une future calibration de ce module de pâturage, reposant sur des données disponibles et sur des variables potentiellement mesurables.

Mots-clés: *Cycle de l'eau - Evapotranspiration - Pâturage - Modèle d'écosystème - Flux de GES*

Contents

Preface

This Master thesis is a part of a collaborative project. Three Master theses are dedicated to the same objective: developing and calibrating a cropland and grassland model. The three students involved in this project are Laura Delhez, Clément Dumont and Félix Vandewattyne. Some parts of this manuscript (chapter 1, chapter 2, chapter 3) are the result of a collaborative work, and are therefore common to the three manuscripts. The rest of this project was divided according to the processes studied: the above-ground carbon cycle and plant phenology by Delhez Laura, the water cycle and the implementation of a grazing module by Dumont Clément and the below-ground carbon and nitrogen cycles and the inclusion of crop and grassland management by Vandewattyne Félix. The other Master theses will be referred in this manuscript as Delhez (2019) and Vandewattyne (2019). As a part of this project, this work focuses on the calibration and validation of three main processes involved in ecosystems water cycle (soil evaporation, plant transpiration, water infiltration and percolation), as well as on the development of a grazing module taking the effect of cattle on pastures dynamics into account.

Chapter 1

Context

1.1 Current context of climate change

Climate change stirs up more and more citizens' interest and concern, as attested by recent events ("Fridays for future" initiated by Greta Thunberg, the progress of green political parties in the European elections, etc). Public awareness is improving thanks to research conducted these last 50 years as well as media coverage (MacDonald, 1988). Scientists highlighted the role of greenhouse gases (GHG) in climate change (IPCC, 2007). They identified water vapour (H_2O), carbon dioxide (CO_2), methane (CH_4), nitrous oxide (N_2O), chlorofluorocarbons (CFCs) and ozone (O_3) as being major GHG (IPCC, 1990). These gases absorb and re-emit infrared radiation coming from Earth, thus increasing the temperature of the Earth's surface (Ramanathan & Feng, 2009). This natural phenomenon is called the greenhouse effect and allows human life on Earth. If Earth was devoid of it, the mean surface temperature would be around 34°C colder than it is currently (MacDonald, 1988; Paterson, 1996; Wallington et al., 2004).

Even if these gases are essential, some of them have seen their concentration increase rapidly since the industrial revolution and have recently reached alarming atmospheric concentrations. Ice core analysis revealed that atmospheric CO_2 and CH_4 concentrations are at their highest value in 420,000 years (Petit et al., 1999). Most scientists attribute these recent peaks to human activities (IPCC, 2013). They discern natural from anthropogenic sources or sinks of greenhouse gases and endeavour to quantify each of them. In this respect, some GHG are more studied than others. Scientists consider that water vapour is not directly affected by human activities on a global scale while the stratospheric and tropospheric ozone is affected by it but has a short lifetime and its variations are minor compared to its elevated concentration (Wallington et al., 2004; Ebi & McGregor, 2008). However, these two gases are gaining growing interest as recent research proved their contribution to the significant impact of aviation on climate change (Pitari et al., 2015; Brasseur et al., 2016). On the contrary, research on CO_2, CH_4 and N_2O is more widespread because of the increase in their concentration, along with the stability and warming power of these gases (figure 1.1).

In order to quantify the individual impact of each of these gases, the Intergovernmental Panel on Climate Change (IPCC) introduced a new index: the global warming potential (GWP). It represents the warming effect caused by a release of 1kg of GHG after a certain period (IPCC, 1990). The table 1.1 shows the GWP of some GHG expressed in CO_2 equivalent and integrated over various time scales. For example, the release of 1 kg of N_2O will heat Earth surface 270 times more than 1 kg of CO_2 in the 20 years to come.

Table 1.1: Global warming potential of GHG affected by human activities (IPCC, 2014)

	Lifetime (yr)	Time horizon 20 yr	100 yr
carbon dioxide	-	1	1
methane	12.4	84	28
nitrous oxide	121	264	265
HFC-152a	1.5	506	138

The most studied greenhouse gas is the carbon dioxide which has the topmost radiative forcing according to figure 1.1. It is part of the carbon cycle which involves exchanges between oceans, terrestrial ecosystems and the atmosphere. Carbon is also stored in each of these three reservoirs. The atmospheric reservoir accumulates the CO_2 produced by human activities and the other reservoirs and also provides CO_2 to absorbing elements (oceans, terrestrial ecosystems). Oceans are considered as a net CO_2 sink due to their biological and solubility pump (Falkowski, 2000). However, accumulating CO_2 can lead to ocean acidification (IPCC, 2013). In regards to terrestrial ecosystems, two opposite processes come into play: photosynthesis and respiration. Besides these natural mechanisms, humans introduced new sources such as fossil fuel combustion, cement production and land use change (Schimel, 1995).

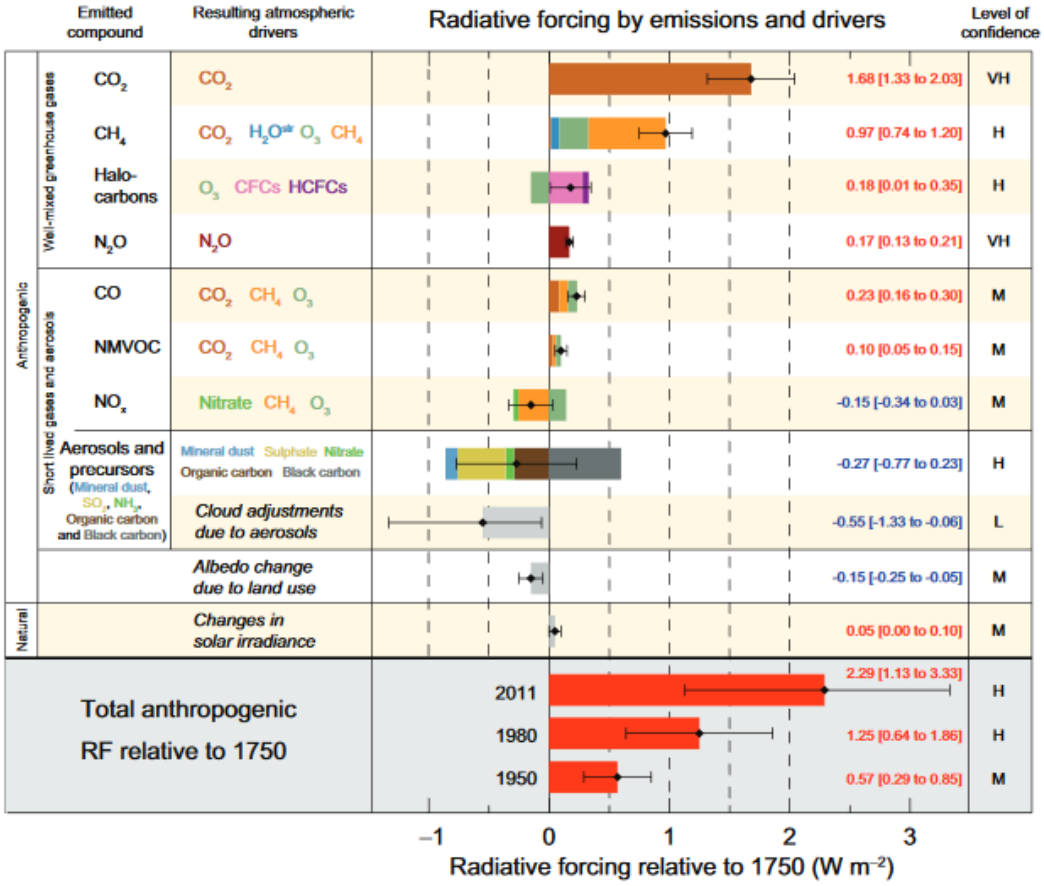

Figure 1.1: Radiative forcing components (IPCC, 2013)

Although less present in the atmosphere than CO_2, methane also plays a crucial role in climate change. Aside from contributing to the greenhouse effect, it generates tropospheric ozone which enhances the greenhouse effect

(Dentener et al., 2005). Methane has several sinks located in the air, such as oxidation by hydroxyl radicals (OH) and reaction with chlorine radicals, and in the soil like oxidation by methanotrophic bacteria (Kirschke et al., 2013). According to Nisbet et al. (2014), human activities induce about two-thirds of methane emissions. The four major sources of methane are natural wetlands, the digestive systems of ruminants, rice fields and fossil fuels exploitation (Wahlen, 1993; Khalil & Shearer, 2000).

In addition to its own radiative forcing, nitrous oxide intervenes in ozone concentration but this time, in depleting the stratospheric layer (Ravishankara et al., 2009). This ozone layer is reputed for blocking UVs that cause cancers. Nitrous oxide is emitted into the atmosphere by soil microbial processes, oceans, fertilisers use or fossil fuels combustion (IPCC, 2007). Recent studies highlighted a sink on Earth's surface besides the destruction by solar radiation in the stratosphere (Chapuis-Lardy et al., 2007; Syakila & Kroeze, 2011). This additional N_2O uptake is now widely accepted and attributed to nitrous oxide-reducing microbial communities (Thomson et al., 2012; Schlesinger, 2013).

Besides greenhouse gases, scientists associate, to a lesser extent, climate change with a modification of Earth's albedo and orbit, with an increase of atmospheric aerosols, etc. (Charlson et al., 1992; Lohmann & Feichter, 2005; Canadell & Raupach, 2008). The IPCC estimates the radiative forcing of these elements in its recurrent reports. The latest assessment can be visualized in figure 1.1. It is needless to say that all these combined elements disturb the Earth's radiative energy budget with a net accumulation of heat (Hofmann et al., 2006).

During the Paris Agreement in 2015 (COP 21), attention was drawn to the different climatic scenarios established by the IPCC (UNFCC, 2015). These scenarios are called Representative Concentration Pathways (RCPs) and correspond to the different evolutions of radiative forcing up to 2100 compared to 1750 (IPCC, 2013). For instance, the most severe RCP, named RCP8.5, forecasts a radiative forcing of $8.5 W/m^2$ in 2100. This scenario leads to an increase of average surface air temperature between 2.6 and 4.8°C by 2100 relative to the 1986-2005 average, a mean sea level rise between 0.42 and 0.85m and a reduction of 94% of the Arctic sea ice cover in September. RCP2.6, the most optimistic scenario, predicts an increase in air temperature between 0.3 and 1.7°C, an average sea level rise between 0.26 and 0.55m and 43% less of Arctic sea ice cover in September.

These changes are just a sample of all the consequences of climate change. The IPCC foretells long-term changes in ocean and atmospheric circulation, in the water cycle as well as in vegetation structure and biodiversity. The repercussions of these changes are quite laborious to determine, as it is difficult to forecast the occurrence and the impact of extreme events for which the IPCC shows less confidence than in its previous reports (IPCC, 2013). However, predicting the response of ecosystems to climate change is crucial in order to preserve them, and requires a fine understanding of their dynamics.

1.2 Roles of terrestrial ecosystems in climate change mitigation

In 2015, the contribution of agriculture to GHG emissions in the European Union was estimated by the European Environment Agency to 9.58% of total GHG emissions (Eurostat, 2017). In figure 1.2, the different sources of GHG emitted by agriculture are detailed. These gases are considered as *biogenic* GHG, as they are originating from plants, animals and microbial communities, with a variability in the emission rates driven by natural and anthropogenic perturbations (Tian et al., 2016). Note that the CO_2 emissions originating from fossil fuel combustion (material transport, greenhouse heating, grain drying, etc.) are not included in the agricultural sector, but are imputed to the energy section, as in the inventories of the IPCC. Also, the emissions represented in figure 1.2 have been converted into CO_2 equivalents (considering their global warming potential) before being expressed in percents.

The three main GHG emitted by agriculture are CH_4, N_2O and CO_2. The most important source of GHG comes from enteric fermentation, in the form of methane (figure 1.2). During the digestion of ruminant animals and some non-ruminant animals (e.g. horses and pigs), the breakdown of carbohydrates by microorganisms leads to CH_4 emissions (Jensen, 1996). The amount of methane emitted during enteric fermentation will mainly depend on the quality of the feed intake and on the type of digestive system of the animal (Hiller et al., 2014). Another source of

methane emission comes from manure decomposition under anaerobic conditions. Anaerobic conditions will tend to occur more rapidly with a larger number of animals confined in a small area (e.g. pig and poultry farms). Rice cultivation also leads to methane emissions, since this type of cultivation requires a flooding of the soil during long periods, CH_4 emissions by soil being higher in anaerobic conditions (Baldocchi et al., 2012).

The largest source of N_2O emissions from the agricultural sector results from bacteria activity in soils during the nitrogen cycle. In agricultural soils, different sources may feed the nitrogen pool: animal wastes, inorganic fertilisers, crop residues, biological N fixation, etc. Different forms of nitrogen are present in soils: organic nitrogen, ammonia, nitrites and nitrates. From the ammonia pool, a part will be converted to NO_2 and NO_3 by bacteria during the nitrification process and some of the nitrate pool will return to the atmosphere in the form of N_2 during the denitrification process. As a consequence, a fraction of the nitrogen that enters the agricultural soil returns to the atmosphere in the form of N_2O during these nitrification and denitrification reactions (Braker & Conrad, 2011), with a rate depending on soil microbial communities, on soil temperature (Rees et al., 2013), water and aeration (Robertson & Groffman, 2007) and on the type of nitrogen input (Wang & Dalal, 2015). Therefore, soil management in regards to its N inputs and to the influence of N cycle driving factors is an important aspect to consider since an adequate use of soils could reduce N_2O emissions.

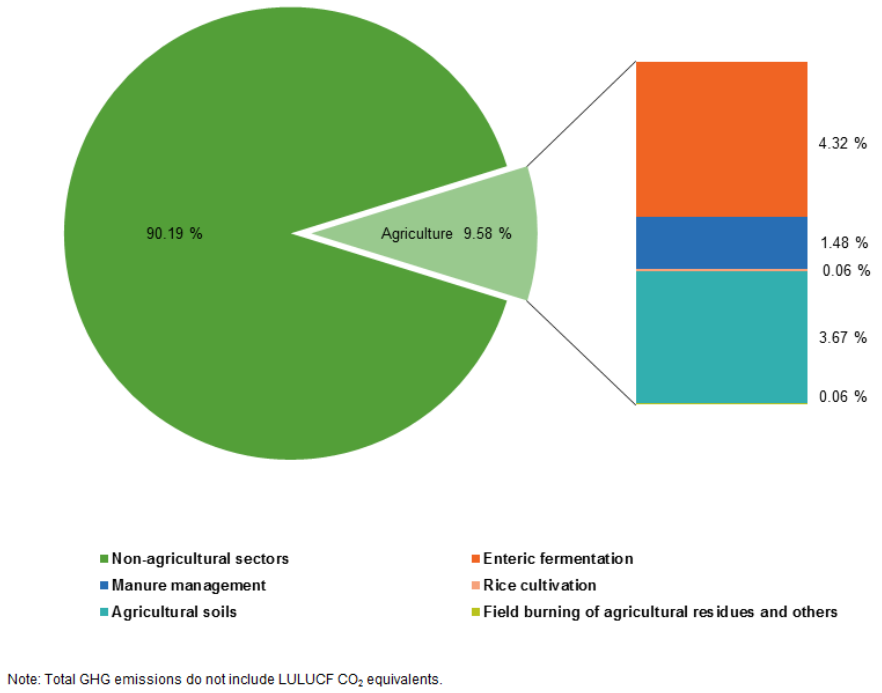

Figure 1.2: GHG emissions from the agricultural sector in 2015. Note that emissions due to land use change are not displayed in this chart (source: Eurostat, 2017).

Even though CO_2 has a lower global warming potential than other GHG, this gas remains important for the agricultural sector. Terrestrial ecosystems can both act as sinks and sources of carbon dioxide (Lal, 2004), as illustrated in figure 1.3. Through photosynthesis, plants convert atmospheric CO_2 into organic carbon at a rate called the gross primary productivity (GPP). A part of that assimilated carbon is emitted to the atmosphere as CO_2 through above- and below-ground growth and maintenance respiration, called the above- and below-ground autotrophic respiration (ARa and ARb). The balance of GPP and ARa plus ARb is called the net primary productivity (NPP) and results in an increase of plant biomass. When plant tissues return to the soil, a part of their organic carbon can be stored in the soil in the form of stabilized organic matter (Jones & Donnelly, 2004), while

some of it will be mineralized by soil microorganisms, emitting CO_2 to the atmosphere, besides microorganisms own respiration. These soil emissions are accounted as heterotrophic respiration (HR), or as soil respiration (SR) if the below-ground autotrophic respiration is also taken into account. All these CO_2 fluxes emitted by plants and soil are grouped under the term total ecosystem respiration (TER), or ecosystem respiration (R_{eco}). The balance of GPP and TER gives the net ecosystem exchange (NEE) of CO_2. For most ecosystems, this balance tends to be negative, i.e. the ecosystem acts as a sink (Smith et al., 2000). In Europe, it was estimated that CO_2 uptake by ecosystems has offset nearly 10% of Europe's fossil fuels emissions (Schulze et al., 2009). Some scientists consider soil carbon stocking as a potential climate change mitigation strategy. The «4 per 1000 » initiative, launched by France in December 2015 at the COP 21, aims at increasing soil carbon stocks with an annual growth rate of 0.4%, i.e. 4‰ per year. This increase of carbon sequestration in soils would halt the increase of CO_2 concentration in the atmosphere, thus reducing global warming (Kon Kam King et al., 2018).

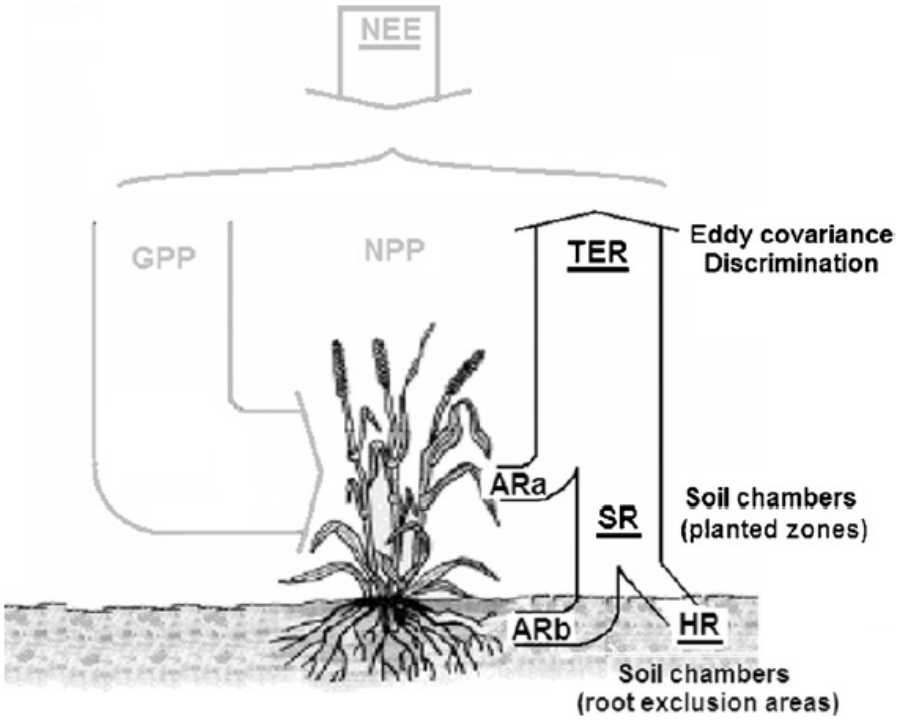

Figure 1.3: Schematic representation of carbon fluxes over an ecosystem (Suleau et al., 2011). NEE: net ecosystem exchange, NPP: net primary productivity, GPP: gross primary productivity, SR: soil respiration, HR: heterotrophic respiration, ARa: above-ground autotrophic respiration, ARb: below-ground autotrophic respiration.

However, for many croplands, most of the biomass is exported during the harvest, and the carbon temporally stored in that biomass will be emitted when the biomass is eaten, burned or transformed. These types of ecosystems tend to be lower carbon sinks (Schulze et al., 2009). Buysse et al. (2017) measured that over a period of 12 years characterized by three crops (sugar beet, winter wheat and seed potato), a Belgian intensively managed cropland behaved as a net C source when considering C exportation at harvest and C importation (manure, slimes). Terrestrial ecosystems can also emit important amounts of carbon dioxide when their land use changes from one type to another (Li et al., 2018). An example of this phenomenon unfolds during a deforestation to obtain an arable land. When human activities require the transformation of a forest soil into a cropland, in addition to the potential release of the C contained in the removed wood, an important ploughing is performed during which soil organic matter is exposed to the air, and some carbon is released, leading to a peak in CO_2 emissions. Overall, any perturbation induced to arable soils can affect stabilized organic matter, leading to carbon dioxide emissions (Houghton et al., 2012). Therefore, conservation agriculture, promoting reduced tillage can be seen as a potential

GHG reduction strategy (Rutkowska et al., 2018), although other studies highlighted the fact that CO_2 and N_2O emissions could be enhanced by reduced tillage (Conrad, 1996; Lognoul et al., 2017).

Besides the direct effects of GHG emissions by agroecosystems, terrestrial ecosystems can affect Earth's surface energy budget, by changing biophysical processes like surface roughness inducing modifications of the wind speed and the exchange of latent heat (transpiration), and soil surface reflectivity, i.e. albedo (Bonan, 2008b; Liang et al., 2010). With a higher albedo, i.e. a clearer land surface, more reflection of incoming radiation will occur, leading to a decrease of Earth temperature. Therefore, land use change can directly affect Earth temperature, as some types of vegetation have higher albedos (Mika et al., 2001; Costa et al., 2007; Loarie et al., 2011) thus reducing radiation forcing, while bare soils tend to increase radiative forcing.

As presented beforehand, the agricultural sector is highly linked to global warming and some mitigation strategies must be designed in the field of agriculture, in order to reduce GHG emissions by this sector. Tian et al. (2016) estimated that nowadays, the cumulative warming capacity of biogenic CH_4 and N_2O emissions was half offset by the cooling effect resulting from land CO_2 uptake. Some improvements must be made in order to reduce our N_2O and CH_4 emissions while increasing the potential carbon sequestration in agricultural soils. However, this reduction should not only be achieved through reducing activities (such as reducing heads of livestock) but mainly through a reduction of emission intensity, i.e. emitting less per unit of production (Eurostat, 2017). The latter requires more scientific investigation and a better understanding of ecosystem dynamics so as to provide the most suited farming practices to farmers and stakeholders. Moreover, agroecosystems do not only affect GHG concentration in the atmosphere, but their usual functioning can be jeopardized by climate change. Therefore, mitigation strategies will also have to consider the feedback of climate change on ecosystem dynamics, like the reaction of agroecosystems to more frequent drought, or to higher CO_2 concentrations in the atmosphere.

During these last decades, forest ecosystems have been mainly studied for they high carbon sequestration potential. However, other ecosystems such as croplands and grasslands can potentially store high amounts of carbon. According to Schulze et al. (2009) who estimated ecosystems GHG balances with top-down and bottom-up approaches, European croplands and grasslands have higher NPP than forests, indicating a high potential to mitigate climate change. However, when considering CH_4 and N_2O emissions mainly linked to management practices, European forests maintain on average a negative GHG balance while grasslands and croplands tend to have a neutral or positive balance, i.e. a net emission of GHG to the atmosphere (Schulze et al., 2009). This work will mainly focus on croplands and grasslands dynamics, as these ecosystems are more affected by human activities than forest ecosystems, and must be well understood in order to design management practices with lowest environmental impacts. The current knowledge of how grasslands and croplands management may affect GHG emissions will be summarized in sections 1.3 and 1.4 and some potential mitigation strategies will be detailed.

1.3 Grasslands management and GHG emissions

Grassland ecosystems cover about one-quarter of the Earth's ice free land area (Ojima et al., 1993; Steinfeld et al., 2006) and contribute to the livelihoods of more than 800 million people (Reynolds et al., 2005), providing ecological and socio-economical resources, as they contribute to livestock production and to biodiversity (Soussana et al., 2007; Peeters, 2009; Peichl et al., 2012).

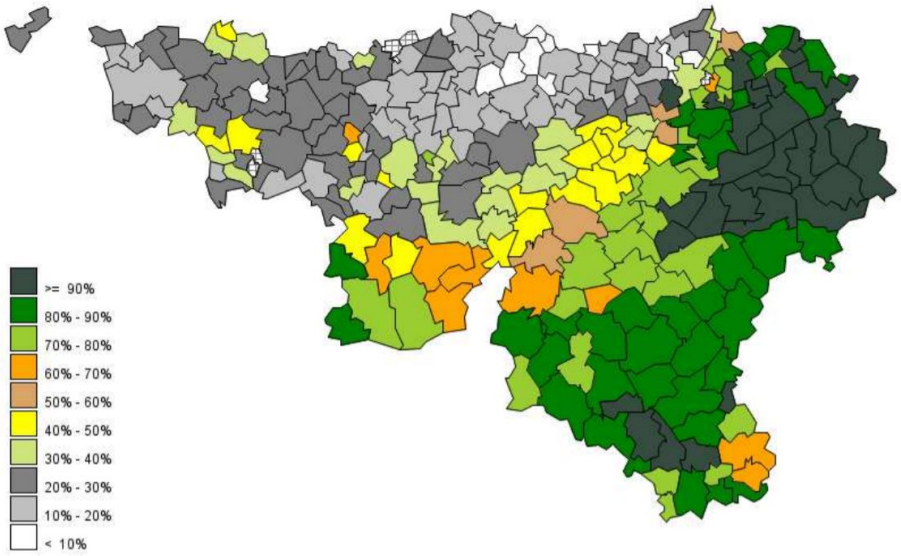

Figure 1.4: Distribution of grasslands in Wallonia in 2017. The color levels represent the percentage of grasslands in the utilized agricultural land of each commune. Source: Wallonie Agriculture (SPW), 2019a.

Like in the rest of the world, grasslands are particularly important in Wallonia, Belgium. In 2018, the number of farms with cattle reached 7,988, which corresponds to 63% of Walloon farms (StatBel, 2018). In Wallonia, the typical cattle breed is the Belgian Blue breed. The total population amounted 1,113,904 heads in 2018, with 22% of suckler cows and 18% of milk cows (StatBel, 2018). In terms of Walloon utilized agricultural land (UAL), permanent grasslands cover around 43% of UAL, while temporary grasslands cover 5% of UAL (StatBel, 2018). The distribution of grasslands in the Walloon region in terms of UAL is given in figure 1.4. In 2017, the breeding sector reached 57.9% of the Walloon agricultural production, which accounted for 1,893 million euros (Wallonie Agriculture SPW, 2019b). The production of beef meat and milk products accounts for 22% and 25% of the agricultural production respectively, in terms of euros.

Besides being a sector of great importance in Wallonia (in terms of land surface and economy), cattle breeding is more and more studied for its interactions with global warming (figure 1.5). In a breeding farming system, GHG exchanges occur at different locations: in the cowsheds for landless systems or outside stocking season, in the cropland for mixed crop-livestock farms and in the grassland for grazing systems. In each system, machines also emit CO_2 through fuel consumption. In this work, exclusively grazing systems will be studied, so the emissions from stables and fodder production will not be further detailed. A particular attention will be given to the exchanges of CO_2, CH_4 and N_2O for their radiative forcing, although other GHG may be exchanged between grasslands and the atmosphere.

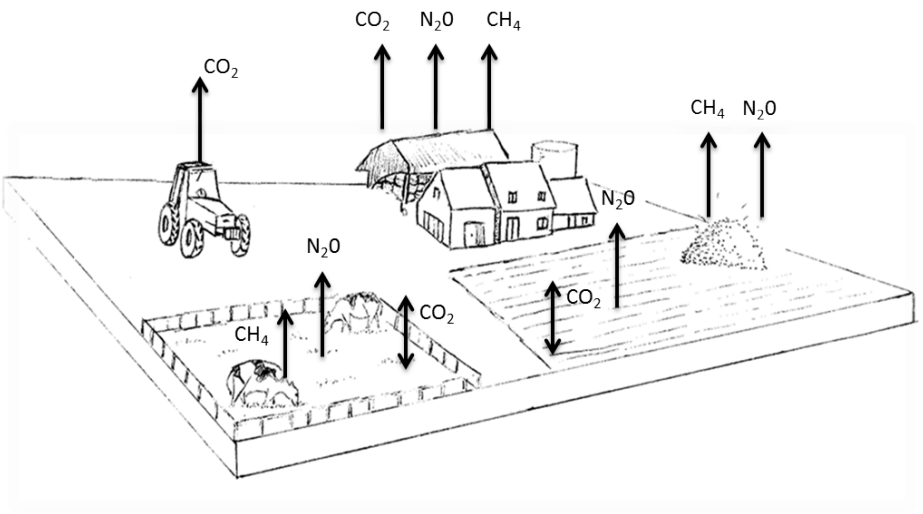

Figure 1.5: Overview of the GHG exchanged between a breeding farm and the atmosphere (Gourlez de la Motte, 2019).

Nitrous oxide exchanges occur at the soil surface, and are the result of both production and consumption processes (Butterbach-Bahl et al., 2013). N_2O can be produced via nitrification and denitrification, and consumed by microbial processes such as denitrification. N_2O fluxes vary with soil biotic (inter- and intraspecies competition, food webs, plant–microbe interaction) and abiotic (soil moisture, temperature, pH, etc.) factors, but N_2O emission peaks often occur after the application of organic (solid manures and liquid slurries) and inorganic fertilisers, increasing soil N availability (Laville et al., 2011). In grazed grasslands, a continuous input of N might originate from livestock excreta (urine and feces), fueling N_2O production (Saggar et al., 2013). N fixation may also be higher in some grasslands, due to the presence of legumes, increasing N availability (Lüscher et al., 2014). In addition to direct soil N_2O emissions, high N applications can lead to N losses from volatilization and leaching, which is also contributing to indirect N_2O emissions downstream from the grassland (Robertson & Vitousek, 2009).

Overall, very few fertilised agricultural soils act as N_2O sinks (Syakila & Kroeze, 2011), but ways of reducing these emissions are investigated. Improvements can be done in the understanding of soil N cycle through a better characterization of microbial communities, of their role in this cycle and their interaction with plants (Butterbach-Bahl et al., 2013). In their review, Saggar et al. (2013) summarize strategies to mitigate N_2O emissions: increasing C inputs, reducing N inputs from animal excreta and chemical fertilisers (to reduce NO_3^- availability), feeding animals with low protein feed, improving soil aeration and increasing pH. During late-autumn/winter and early spring, soils generally remain wet due to high precipitation, and denitrification is accelerated either by soil compaction by cattle, or by low pasture N uptake and low N immobilization due to low soil temperature (de Klein et al., 2006; Bhandral et al., 2007). Minimizing N inputs during these critical months can potentially reduce N_2O emissions. Inputs can be lessen by reducing the time animals spend grazing in the field (de Klein et al., 2006), enabling farmers to have a better control over animal excreta, that can be collected and applied to the field when the risk of N_2O emissions is minimal (van der Meer, 2008). This would however tend to change a grazed pasture into a mowed one, having a different dynamics. Animals feed can also be adapted so as to reduce the concentration of N in urine (Mulligan et al., 2004), and plant composition can be changed in order to control N inputs into soils through atmospheric N fixation (Saggar et al., 2013).

In pastures, methane can be produced at three spots: in soils, in animals manure, and directly in the rumen of ruminants (Baldocchi et al., 2012; Hiller et al., 2014). In soils, CH_4 can both be produced and consumed. Production occurs during methanogenesis, which is the final step of the anaerobic breakdown of organic matter (Whalen, 2005). Singe-celled archeas are the microorganisms responsible for methanogenesis and are found in water-saturated microsites in the soil, with high C content. CH_4 consumption is the result of biological oxidation by both

aerobic and anaerobic methanotrophic bacteria (Tate, 2015). This process is influenced by soil factors such as soil temperature and air-filled porosity, which depends on soil water content. Soil moisture is often driving most of the variability observed in CH_4 consumption (Price et al., 2004; Hörtnagl et al., 2018). Net CH_4 uptakes were reported by Smith et al. (2000) and Conrad (2009) in well-aerated soils, methanotrophy being larger than methanogenesis. Therefore, soil aeration through soil structure conservation seems to be one of the mitigation strategies towards a reduction of soil CH_4 emissions. Smith et al. (2000) also identified soil bulk density, water-filled pore space, gas diffusivity, soil temperature and water table height as the most common drivers of CH_4 fluxes variability. Note that the magnitude of these fluxes is much lower than emissions of CH_4 due to the presence of livestock, discussed below.

In grazed grasslands, methane emission is also a direct result of the presence of cattle. In the rumen of ruminants, the microbial degradation of carbohydrates present in fodder, also called *enteric fermentation*, leads to net CH_4 emissions (Jensen, 1996). Afterwards, carbohydrates that are not digested and remain in livestock excreta can be converted into methane during manure degradation. Methane emission from enteric fermentation is primarily related to feed intake quantity and composition, i.e. the substrate for methanogenic archaea (Hiller et al., 2014). Partially replacing forage with concentrate in the ruminant diet is assumed to reduce CH_4 production (Beauchemin et al., 2008), but some of this reduction may subsequently be offset by correspondingly increased manure-derived methane emissions, because of higher amounts of undigested fibre which can be a substrate for manure microbes (Hindrichsen et al., 2006), and by higher CO_2 emissions during feed production. Therefore, farmers must ensure that an adaptation of cattle feeding to reduce enteric methanogenesis will not be compensated by increased manure emissions, and simultaneous measurements of methane emissions by livestock and their manure must be conducted (Külling et al., 2002). According to Knapp et al. (2014), the most significant reductions of methane emissions by cattle can be achieved by combinations of genetics and management strategies, to increase feed efficiency and life-time productivity of individual animals and herds. Increased feed efficiency, besides leading to reduced CH_4 emissions per unit of feed intake, is also presented as an economic benefit for farmers.

Overall, some studies concerning grasslands in Europe reported that these ecosystems could behave as net CH_4 sources (Merbold et al., 2014; Dumortier et al., 2017), sinks (Kammann et al., 2001) or both (Merino et al., 2004), mainly depending on the presence of cattle and on soil management. However, most of these papers studied soil and cattle emissions separately, without taking into account the impact of cattle on soil CH_4 emission, such as soil compaction. Systems like the eddy covariance technique allow measuring these sources simultaneously, but their response to environmental and management factors may be hard to disentangle.

In grasslands, like in other ecosystems, CO_2 fluxes are the consequence of concurrent plant photosynthesis and autotrophic and heterotrophic respiration, i.e. plant and soil respiration respectively. These processes have already been presented in section 1.2. In their review of nine European grassland sites, with different management and environmental conditions, Hörtnagl et al. (2018) reported average annual CO_2 uptakes, with higher uptakes in spring, followed by summer and autumn. On average, grasslands were net CO_2 sources in winter. However, in grazed grasslands, the magnitude of the CO_2 sink can partially be offset by cattle respiration. Jérôme et al. (2014) measured on a Belgian intensively managed pasture that with an average stocking density of 2 livestock units ha^{-1}, livestock CO_2 emissions represented 8% of total ecosystem respiration. On the same pasture, Gourlez de la Motte et al. (2019) estimated that cows respiration accounted for between 37% and 52% of the NEE, thus reducing the potential CO_2 sink of pastures. Therefore, neglecting cattle respiration in the estimation of the carbon dioxide net exchange of a pasture could lead to a systematic and non-negligible bias. Besides their direct effect on CO_2 emissions, cattle also indirectly impact vegetation and soil activities (Jérôme et al., 2014). Thanks to measures of CO_2 exchanges between a Walloon pasture and the atmosphere, Jérôme et al. (2014) pointed a significant decrease of ecosystem GPP during grazing periods. This would most likely be due to defoliation by grazing animals, leading to a reduction of the leaf area index (LAI) (Rogiers et al., 2005). Plants trampling by animals, taken into account by Vuichard et al. (2007) in their grassland model, could also explain a reduction in GPP, as shoot material is partly damaged. On the contrary, during non-grazing periods, GPP tended to increase, as biomass could re-grow. The effect of cattle on plant and soil respiration is harder to evaluate. On the one hand, autotrophic respiration is supposed to decrease, due to a reduction of above-ground biomass (Cao et al., 2004; Lin et al., 2011) and soil respiration can be lowered as a consequence of a decrease in canopy residues and a reduction in living roots and

exudates to the soil (Cao et al., 2004; Bahn et al., 2006; Raiesi & Asadi, 2006; Polley et al., 2008; Lin et al., 2011). On the other hand, grazing may favour radiation penetration and temperature rise, thus enhancing both root and microbial components of the soil respiration (Bahn et al., 2006; Lin et al., 2011). Finally, soil physical properties can change as a result of soil compaction by cattle, consequently modifying soil respiration (Cao et al., 2004). The separate effect of cattle on these processes is hard to disentangle, and studies report both plant and soil respiration increases (Lin et al., 2011) and decreases (Owensby et al., 2006; Polley et al., 2008; Lin et al., 2011) under the presence of livestock. As a result, low to moderate grazing intensities can lead to positive C sequestration (Allard et al., 2007), while overgrazing may have a negative effect on soil C stocks (Dlamini et al., 2016).

In recent years, a few studies carried out full GHG budgets of grassland sites, considering CO_2, N_2O and CH_4 fluxes. Hörtnagl et al. (2018) summarized the results of nine studies, and noted that CO_2 was the predominant component of annual GHG budgets. Only 21% of the net CO_2 sequestration were offset by N_2O and CH_4 emissions. This observation is supported by Schulze et al. (2009) who evaluated this offset at 18% for European grasslands. However, carbon sequestration is fragile and reversible (Soussana & Lemaire, 2014). Sequestred carbon can be re-emitted towards the atmosphere during a soil disturbance such as a pasture renovation (Merbold et al., 2014; Drewer et al., 2017) or a land use change from pasture to crop (Guo & Gifford, 2002). What is more, considering steady management and environmental conditions, carbon stocks tend to reach an equilibrium (Smith, 2014). However, an appropriate management must be developed in order to maintain these carbon stocks.

Overall, the GHG budget of a grassland is mostly affected by management practices, such as the grazing period, the stocking density, the frequency of cutting and fertilising, etc. that impact the geochemical cycling of carbon and nitrogen (Schulze et al., 2009; Lal, 2010). Soussana & Lemaire (2014) noted that under too high stocking densities, herbivores tend to uncouple C and N cycles, leading to environmental problems due to N excesses in soils, such as nitrate leaching and N_2O and ammonia emissions. This would be due to carbon losses in the form of CO_2 and CH_4 during the digestion of ingested biomass, while only a small amount of N is used to produce meat or milk, and most of the nitrogen contained in the biomass returns to the soil at high concentration in urine patches. At low density, this higher N cycling tends to increase net primary productivity and C sequestration (Soussana & Lemaire, 2014; Gomez-Cassanovas et al., 2016), which however level off at high stocking densities, along with increased environmental problems. Farmers should therefore adapt their stocking rates and grazing schedules in order to reduce this uncoupling of C and N cycles (Soussana & Lemaire, 2014). Moreover, site-specific conditions of managed grasslands tend to change over relatively short timescales, depending on the frequency and intensity of management events, combined with environmental conditions (Hörtnagl et al., 2018). Therefore, environmental conditions boosting the emission or uptake of GHG are not persistent, and their detection requires a continuous GHG fluxes follow-up, at a fine time scale, in order to develop site-specific GHG mitigation strategies.

1.4 Croplands management and GHG emissions

Even though world land area occupied by crops only represents 12% of the total land area, it has been steadily increasing for 30 years, as depicted in figure 1.6. This evolution is directly correlated with the population growth and, therefore, with the increase of global food demand (Bajželj et al., 2014). Also, this global trend is principally due to developing countries that promote croplands in order to deliver food security and improve their economy (FAO, 2016; Burney et al., 2010).

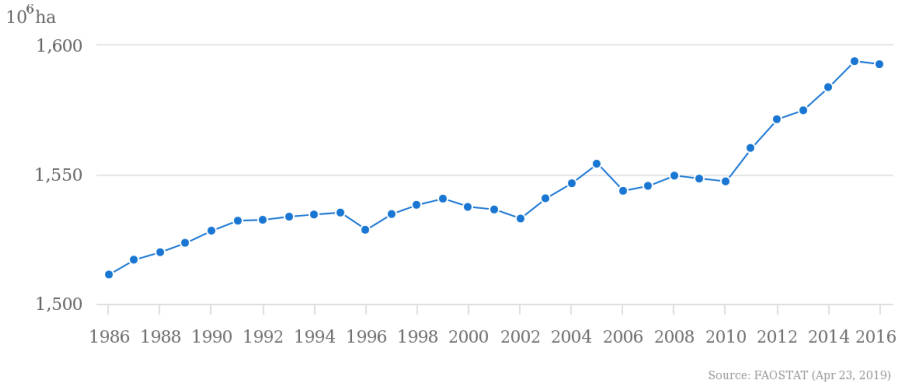

Figure 1.6: World land area used as crops (FAO, 2016)

As a developed country, Belgium is not subject to this steady growing trend. However, its territory is mainly occupied by crops. Belgian croplands represent about 28.8% of the country land area while forests and permanent pastures and meadows account for, respectively, 22.6% and 15.8% (FAO, 2016). In regards to agriculture, Belgium is reputed for its production of winter wheat, maize, potatoes and sugar beets, the first three being in the top ten of the most GHG-emitting crops (Carlson et al., 2017). This classification is based on the GHG emissions originated from the total production of each type of crops. The other seven crops identified by Carlson et al. (2017) are, in descending order, rice, barley, coconut, oil palm, soybean, rapeseed and sugarcane. It should be noted that, in this section, croplands represent all cultivated fields, including rice paddies.

As for pastures, the three major greenhouse gases associated with crops are methane, nitrous oxide and carbon dioxide (figure 1.7). Croplands can be either a source or a sink for these greenhouse gases (Falloon et al., 2009; Ciais et al., 2010). They naturally emit CO_2 by soil organic carbon (SOC) decomposition and plant respiration but absorb CO_2 by photosynthesis of autotrophs (i.e. carbon-fixing organisms). They also produce N_2O through nitrification and denitrification processes, as mentioned previously for grasslands. Aerobic soils generally act as a CH_4 sink while oxygen-deprived soils (such as rice paddies) induce methanogenesis and thus, CH_4 emissions (Ciais et al., 2010).

Considering natural and anthropogenic processes, methane emissions from rice paddies account for 48% of global cropland GHG emissions, 32% come from peatland drainage for land use change to agriculture and 20% are assigned to N_2O emissions from N fertiliser application (Carlson et al., 2017). As a matter of fact, croplands are the terrestrial ecosystems with the GHG balance the most affected by human activities. The main management operations are the tillage, the addition of N fertilisers and manure, the seeding with a selected species and the use of irrigation or flooding. Scientists highlight the importance of crop management in cropland emissions and its potential in climate change mitigation. Smith et al. (2008) outlined several mitigation possibilities when technologies and practices are adapted. These possible actions are described hereafter. Nevertheless, note that this subject is still not fully understood, especially the role of agricultural soils, and lots of research are still ongoing.

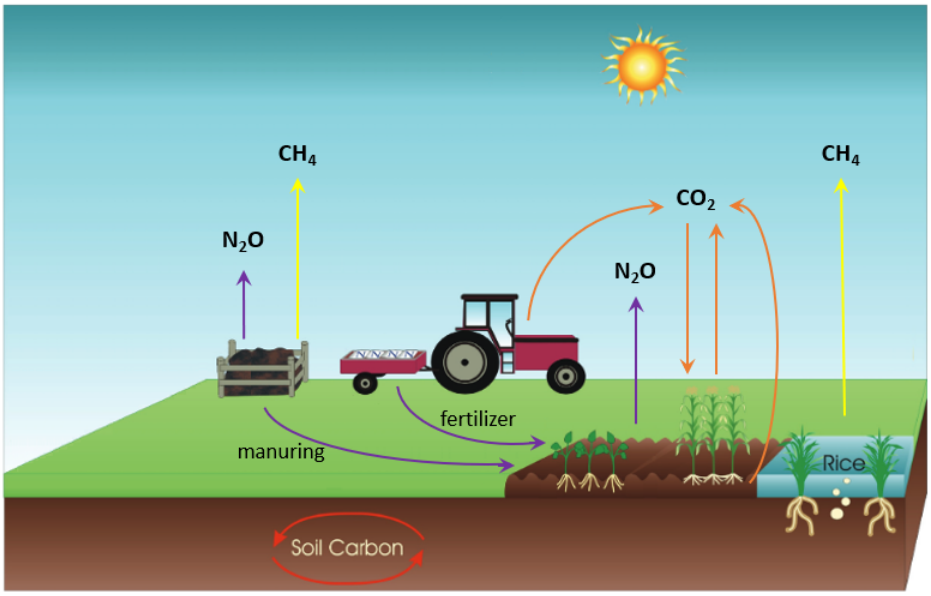

Figure 1.7: Major cropland GHG fluxes.

Tillage is an agricultural technique performed by farmers in order to facilitate seedling, to destroy unwanted weeds and to blend organic residues into the soil. In spite of these benefits, tillage breaks macro-aggregates apart, enhances soil erosion and amplifies SOC oxidation (Lal & Kimble, 1997). This latter drawback leads to a decrease of soil fertility but it can be prevented by adding organic residues (Stavi et al., 2011). A way to promote carbon storage is to adopt conservation tillage or no tillage instead of conventional tillage. With this practice, only a shallow surface layer is exposed to large temperature and water content variations and thus to favourable conditions for mineralization. Furthermore, reduced tillage would reduce the use of fossil fuel (Smith et al., 2008). According to Stavi & Lal (2013), a system without tillage requires 50% to 80% less energy. However, the burying of organic residues is limited with reduced tillage and it can lead to an increase of N_2O emissions, but this consequence is complex and not well investigated (Xiong & Khalil, 2009; Lognoul et al., 2017). Lognoul et al. (2017) assumed that a reduced tillage emits more N_2O because crop residues stay close to the surface where microbial abundance and edaphic conditions are favourable to N_2O production. On the other hand, conventional tillage buries crop residues deeper but alters microbial communities (Falloon et al., 2009).

In addition to tillage, farmers apply N fertiliser or animal manure on crops to improve their crop yields as nitrogen is a limiting element for plant growth. This application generates an increase of N_2O emissions according to Lokupitiya & Paustian (2006) but they can be reduced by improving fertiliser use efficiency thanks to wise choices in application partitioning, dates and quantities (Smith et al., 2008). N_2O emissions are enhanced when available nitrogen surpasses plant needs (Xiong & Khalil, 2009). Reducing the N fertilisers application can also be achieved by adding a legume crop to the rotation. However, note that this type of crop may also be a source of N_2O (Rochette & Janzen, 2005). As written in the previous section, there also exist indirect nitrogen emissions by leaching and volatilization. Furtermore, animal manure needs to be stored before being applied to the field. This storage releases a great amount of CH_4 outside of the cultivated ecosystem (Vergé et al., 2007).

Regarding the flooding and intense irrigation, methane is predominantly emitted by rice paddies due to anaerobic conditions. Three actions can be implemented in order to weaken this significant source. Foremost, these wetlands could be drained during the non-growing season but also one or several times during the growing season. Nevertheless, the second option is a trade-off because, even though it reduces CH_4 emissions, it might lead to an increase of N_2O emissions. Secondly, farmers could use rice cultivars with low exudation rates (Aulakh et al., 2001). Ultimately, the timing and decomposition stage of organic residues additions could be better adjusted.

Aside from crop management practices, human beings affect carbon crop cycling by developing new technologies and cultivars. Scientists design unique cultivars in order to improve crop yields or to resist some stress conditions or attacks of pathogens. Some modified genotypes possess better drought resistance or a different root/shoot ratio (Fischer & Maurer, 1978). For instance, Rezaei et al. (2018) found that modern winter wheat cultivars need 14-18% less degree-days than cultivars from 1950s and 1960s between emergence and flowering. All these modifications affect the amount and timing of photosynthesized carbon as well as its distribution among plant organs. Some of the improved varieties or cultivars also increase NPP and/or have a deeper and larger root system.

In addition to these modifications related to the operations already existing, there are also innovative practices that help to mitigate climate change. In order to improve carbon sequestration, farmers could extend their crop rotations, avoid bare fallow, irrigate drylands or bury biochar (charcoal) which consists of a long-term soil carbon pool and improves soil fertility. Those practices would increase the below-ground carbon reservoir.

All things considered, cropland is an ecosystem getting more and more space and concern over time. Even though crops are not exclusively a greenhouse sink or source, they might act as a source in the future because of the increase of N fertiliser use in order to meet the global food demand (Xiong & Khalil, 2009). All the practices previously mentioned confirm that croplands have a significant mitigation potential but which often prove to be trade-offs. CH_4 and N_2O budgets might still have unidentified or incomplete sources or sinks (Frankenberg et al., 2005; Yanai et al., 2013). According to Robertson (2004), the assessment of the GHG mitigation effects needs a holistic system approach wich will provide a global view and consider these notable compromises. In the same perspective, Lobell et al. (2006) highlighted the significance of regarding different aspects of crop management, illustrating their point by studying the effect of tillage on albedo and not the biochemical effect of tillage as most scientists. Finally, it is germane to note that the conducted experiments sometimes resulted in contradictory outcomes (Xiong & Khalil, 2009). Indeed, terrestrial agroecosystems are complex and have numerous interactions that depend on site-specific conditions.

1.5 Effects of climate change on terrestrial ecosystems

GHG emissions lead to climate change which disturbs the environment of terrestrial ecosystems. These changes impact ecosystems processes which can potentially influence society through a perturbation of ecosystem services, and which affect global warming through altered GHG emissions. This is called the feedback phenomenon. The environmental variables modified by climate change and leading to ecosystems perturbations are the air temperature, the air CO_2 concentration and water. In addition, these variables are also involved in the change of extreme events (flood, drought, etc.) frequency that also impacts agricultural lands (Tubiello & Fisher, 2007).

Temperature The average surface air temperature tends to increase due to climate change (UNFCC, 2015). This rise has several impacts on ecosystems. Plants can benefit from it as well as they can be disadvantaged depending on thermal amplitude, on species and on the localization (Bosello & Zhang, 2005). Temperate areas will tend to see their yields increase as temperature rises, while initially warmer areas will undergo reduced productivity following the positive or negative impact of temperature on photosynthesis (Parry et al., 2001). This will lead to the expansion of suitable croplands in North and to a decrease of arable lands in tropical areas (Zabel et al., 2014). Moreover, the temperature increase will impact plant and soil respiration. Soil CO_2 emission will increase due to abnormal higher temperatures (Bond-Lamberty & Thomson, 2010) but respiration will tend to stabilize as temperature levels out (Luo et al., 2001). Temperature will also have effects on pests (Chidawanyika et al., 2019), weeds and diseases (Bosello & Zhang, 2005). Finally, heat waves will decrease the ecosystem primary productivity (Reichstein et al., 2013). As an example, the European mega heat-wave of 2013 led to a 30% decrease of GPP according to Ciais et al. (2005).

CO_2 increase Atmospheric CO_2 concentration will enhance plant photosynthesis and reduce photorespiration (Bosello & Zhang 2005) as well as maintenance respiration (Ryan, 1991). These combined effects lead to an increase of biomass and yields according to Kimball et al. (2002) but only for reproductive organs as reported by Jablonski et al. (2002). The amplitude of the modification of photosynthesis and respiration will differ depending on the

species, with higher benefit for C3 metabolic plants than for C4 ones (Kimbal et al., 2002), and on the environment, with a stronger effect in the cooler and wetter zones (Bosello & Zhang, 2005).

Water Climatic models predict disturbed precipitation regimes and evaporation rates but these predictions are variable depending on the location (Bosello & Zhang, 2005). This will most likely lead to a shift in soil water content and will therefore impact several fluxes that depend on soil moisture: evapotranspiration, photosynthesis, soil respiration, CH_4 and N_2O emissions.

Other variables Other environmental variables will also probably change in the future like radiation spectrum, air humidity and atmospheric ozone concentration. The way they will be modified and their impact are less known, but these examples highlight the necessity to understand and quantify the link between environment, ecosystem functioning and GHG exchanges.

1.6 Ways to study GHG fluxes over different biosystems

In order to understand the impact of a biosphere on the atmospheric GHG concentrations and the way climate change alters the ecosystem processes involving gas fluxes exchanged with the atmosphere, these GHG fluxes have to be studied. All of them have different dynamics and responses depending on environmental conditions, phenology and management operations. To quantify them and capture their variabilities, two interconnected ways exist: measurement and modelling. Measurements provide the relation between fluxes and environmental drivers that models use to describe the processes.

1.6.1 Measurements

Several methods can be used to measure the exchanges between a biosystem and the atmosphere. They differ by their spatial and time scale, their reliability and feasibility. The methods of measurement can be divided into two categories. One of them is based on the measurement of the temporal variation of reservoirs content for one element, that can be equalized to the sum of the exchanged fluxes of molecules including this element. This method provides the total gas flux when all the quantities transferred in solid and liquid phases are known. On the other hand, chamber technique and eddy covariance (EC) technique directly measure the gas fluxes between a biosystem component and the air and allow to study their responses to environmental drivers (Randerson et al., 2002).

An ecosystem can be seen as a combination of reservoirs interconnected by fluxes of matter (carbon, nitrogen, water, etc). The considered reservoirs are often the above- and below-ground plant biomass, the soil organic matter (which can be divided into its different forms), its nitrogen pools, etc. To evaluate the variation of these reservoirs content, one or more soil or vegetation pools must be sampled. This method requires at least two sampling made at different moments to calculate a temporal variation. This kind of method is mostly used for forest aerial vegetation, for which circumference inventories coupled with allometric equations are used to calculate the differences in biomass (Brown, 2002). The follow-up of grass biomass is also realized in this way but using grass height instead of circumference. For example, the combined measurement of shoot and root biomass at the beginning and the end of a given period of time can be used to assess the NPP of the plot over that period. In addition, soil carbon storage over a period of time can be assessed by measuring the content of SOC of soil samples at the end and beginning of that period (Arrouays et al., 2017). In some cases, the quantification of content variation of a reservoir can be laborious (important number of samples and working force to cover the spatial variability). Another drawback of this method is the time scale that could be greater than a decade to accurately measure the variation of stocks when soil is included (Randerson et al., 2002; Goidts & van Wesemael, 2007). This method cannot, therefore, be used to study fluxes dynamics in response to an external factor at a fine time scale and is sometimes hardly expanded to an entire biosystem.

Presently, the two widely used methods for biosystem gas fluxes measurements are the chamber technique and the eddy covariance technique. Both methods allow measuring the net exchange of gases between a biosystem and its environment. According to the convention commonly used, gas fluxes coming from the ecosystem to the atmosphere,

i.e. emissions, are considered positive while incoming fluxes, i.e. uptakes, are considered negative. This convention will be used in the rest of this thesis. When direct gas fluxes assessment is used for CO_2 measurement, the NEE is equal to the sum of TER and GPP. On the one hand, a chamber encloses the subject of study (or its surface in the case of the soil) and the temporal evolution of the concentration of the gas of interest in the chamber is measured. The increase or decrease of this concentration is proportional to the gas emission or uptake. This method involves a perturbation of the local environment (Longdoz et al., 2000) and hardly covers all the components of the ecosystem (Baldocchi et al., 1988). On the other hand, the eddy covariance (EC) technique consists in determining the exchange between an ecosystem plot and the atmosphere by measuring, at high frequency (10Hz or more), the gases concentration and the wind vertical velocity in the boundary layer above the ecosystem and by computing the covariance of these two variables (Aubinet et al., 2000). In addition to gas exchange measurement, this technique allows to measure sensible and latent heat and momentum transfer. This method of measurement is the most used technique to measure the NEE of a whole ecosystem, due to its numerous advantages compared to the chamber technique. Therefore, its functioning and advantages will be further detailed.

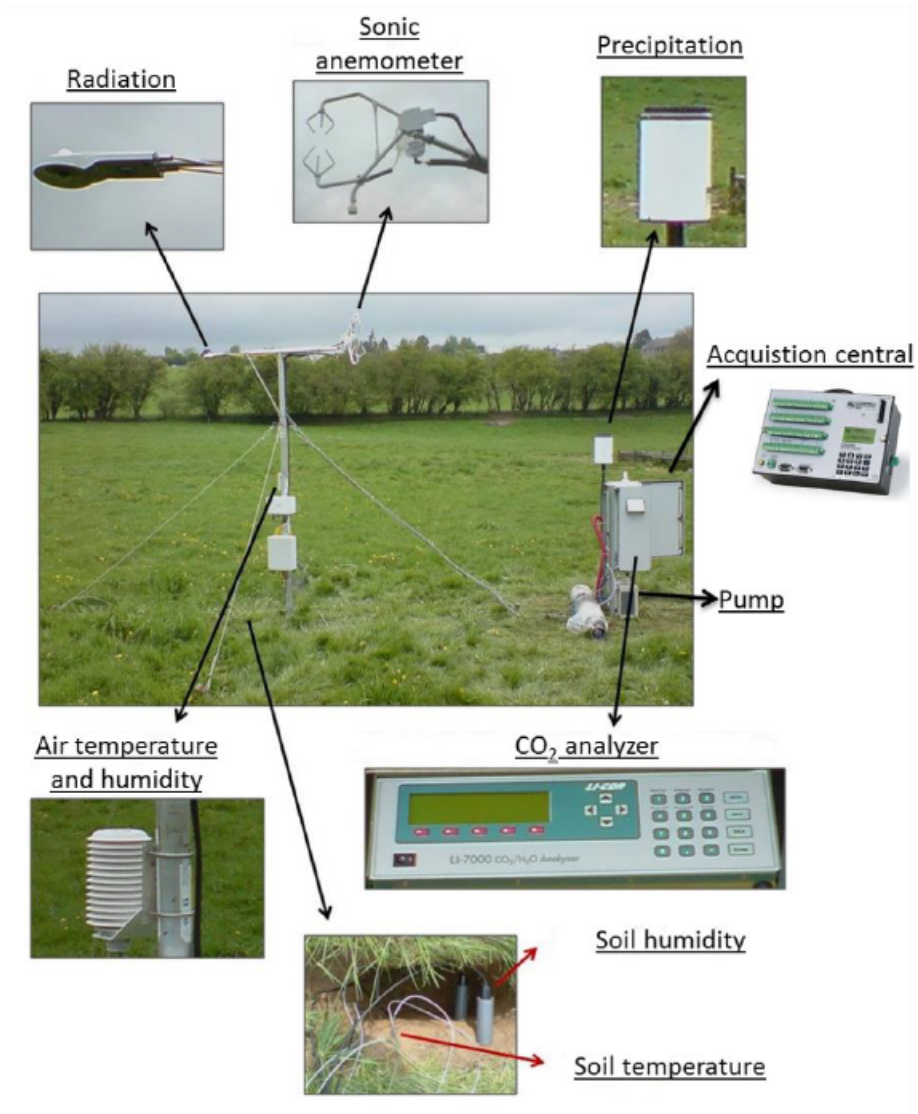

Figure 1.8: Example of typical eddy covariance and meteorological measurement devices. Terrestrial observatory of Dorinne (Gourlez de la Motte, 2019).

The instrumentation of the EC technique is composed of a gas analyser (infrared gas analyser, IRGA), a tri-dimensional sonic anemometer, a tower or a mast (named flux tower) to support them and a data logger system. A typical installation is illustrated in figure 1.8.

The purpose of the tower is to have certain sensors positioned above the canopy level. It is the case for the sonic anemometer and the sampling point where the air analysed by the IRGA is pumped. The sonic anemometer measures the three components of wind speed. The pumped air is analysed to obtain the dry mixing ratio of the gas. These data are measured at high frequency (in general at 10 or 20 Hz). The fluctuations of wind vertical velocity and gas concentration around a mean value are multiplied in order to obtain the covariance, which is proportional to the exchanged gas flux. Additionally, a micro meteorological station is installed so as to measure all meteorological drivers that have an impact on these fluxes. These drivers are typically the precipitation, the different radiations fluxes, the air and soil temperature, the air and soil humidity and the atmospheric pressure. This technique allows a time resolution lower than a minute (Randerson et al., 2002) but the spatial scale will depend on the topography and the wind characteristics (turbulence, strength and direction). The area sampled by the eddy covariance is called the footprint and its fetch can vary from one to more than 10ha. Another advantage of this method is that the measure has almost no impact on the subject.

Unfortunately, the eddy covariance method implies a lot of devices that can have failures. In addition, different corrections, filterings and quality controls have to be done on the raw data (Aubinet et al., 2000). This process removes from 20 to 60% of the collected data (Papale et al., 2006). To be complete and to be able to compute an annual, seasonal or daily sum, the dataset has to be gap filled (Falge et al., 2001; Moffat et al., 2007). The meteorological data are generally used to accomplish this task by means of functional or statistical relationships relating them to fluxes.

Another way to study the response of an ecosystem to the environmental conditions is to completely enclose it. It may be done in ecotron chambers. These devices allow to control all (or a part of) the environmental conditions and, by using a panel of sensors, to measure the response of the whole ecosystem, such as fluxes of matter or biomass growth. However, these installations remain anecdotal and as they will not be used in the present work, ecotron chambers will not be further detailed.

1.6.2 Modelling

A relatively complete and continuous assessment of an ecosystem growth can be carried out through the combination of eddy covariance and chamber measurements with soil and vegetation sampling (for an estimation of reservoirs evolution). However, continuous samplings can be very laborious and provide only an overview of the reservoirs and fluxes dynamics, at best at a daily time scale. The eddy covariance technique, on the other hand, provides half-hourly measurements, but this technique delivers only net gases exchanges, and does not give an insight of the internal ecosystem functioning, i.e. the fluxes between the main reservoirs.

Faced with that reality, ecosystems modelling can be seen as a powerful tool in order to complete the datasets collected with other methods and to help understanding some phenomena for temporal or spatial scales that could be difficult to assess. Indeed, with an accurate representation of agroecosystems into reservoirs and fluxes, the evolution of a cropland, a grassland or a forest can be simulated. Yet, this does not dispense from carrying out numerous measurements during the elaboration of the model, as ecosystem models rely on a lot of data, mainly during their calibration. According to Thornley (1998), ecosystem modelling can also present the following advantages:

- Modelling allows having an integrative but explicit approach of complex problems, such as ecosystems behaviour, in the sense that many components (plants, soil, animals, water, environment, etc.) interact with each other and some existing interactions that are impossible to quantify together experimentally could be simulated.
- Models help disentangling processes and understanding how things work. The responses of an ecosystem to the temporal and spatial variability of a driving factor can be studied through the analysis of the different

mechanisms that lead to such responses, mechanisms which are represented in the model and are not always easy to investigate in real situations. Overall, a better understanding of the system, even imperfect, can suggest ways to intervene and optimize its behaviour.

- Models are powerful tools to make predictions in experimental conditions that are impossible or impractical to create. Once a model has been calibrated and validated on existing data, simulations can be made to predict how an ecosystem will react to different environments. This approach is especially interesting to anticipate reactions to global change.

For the reasons discussed here, the fine understanding of ecosystems dynamics and gas exchanges that is required to provide climate change mitigation strategies, will require the use of a modelling tool. However, the development of a model relies on the acquisition of various data that will be used in order to set up, calibrate and validate the model.

1.6.2.1 Basic principles

A model is an abstraction of a reality that might be hard to study, to diagnose or to measure. It constitutes an appropriate level of reduction and idealization where only the processes important for the goal targeted are emphasized. The study of ecosystem dynamics may require modelling for the various reasons that have already been presented. To do so, the processes involving different ecosystem components can be expressed by means of mathematical expressions. Models are designed to study specific situations, and their construction depends on the aim that is pursued. No model represents reality as it is, and they are only valid in their limitations (Yilmaz, 2015). According to Box & Drapper (1987), "*all models are wrong but some are useful*".

Models can be classified according to different criteria, depending on whether they associate probabilities to some simulated events (stochastic or deterministic), whether they study changing behaviours (dynamic or static), and whether they are based on equations having non predefined form or coming from scientific laws (empirical or mechanistic).

Stochastic models involve that some random elements are included in the predictions, so that an output corresponds to a distribution of probability over a range of values. Consequently, given the same inputs, each simulation gives distinct results (Obropta & Kardos, 2007). A *deterministic* model provides definite and specific predictions, based on causal relationships between inputs and outputs. Results only depend on parameters values and initial conditions. This approach is acceptable for most of the problems, but for uncertain processes such as rainfall, migration of diseases or pests and death, stochastic models could be preferred (Thornley, 1998). In the context of ecosystem modelling, used to simulate the regular functioning of a forest, a crop or a pasture, a deterministic model seems more adapted, as the laws simulated correspond to biochemical or physical processes and the environmental inputs are specific values that have been recorded. Using defined numeric inputs allows unambiguous relationships between outputs (predictions) and inputs. Overall, the best approach is to first build a deterministic model to test its accuracy, and if the complexity of the mathematical description used to reach the predefined objectives is too high in regard to the means available, then randomness can be introduced to characterize a more complex stochastic problem (Thornley, 1998).

A *dynamic* model simulates the evolution of quantities with time, by means of a set of ordinary differential equations, with time being the independent variable, such as:

$$\mathrm{d}C_{roots}/\mathrm{d}t = \ldots \tag{1.1}$$

to express the evolution of carbon stock in plant roots with time. For dynamic models, the choice of a modelling time step is of great importance, as it will affect the interpretation of the model results. Time steps can go from sub-hourly to multiyear, depending on the type of problem that is studied. On the other hand, *static* models do not make time-dependent predictions. For example, a static model could be a set of equations predicting directly the grain dry mass at the end of the growing season without simulating its development. Most of the time, static models are also empirical.

Empirical models are not based on scientific principles, but use mathematical or statistical equations with no predefined form, that are fitted to experimental data in order to provide predictions from observations. An empirical model can be seen as a black box, as few information is provided by the model about the relationship between the inputs and outputs of the model. On the contrary, a *mechanistic* model provides and requires an understanding of the processes being modelled and the form of the equations used are determined by the knowledge about these processes. Mechanistic models are also called *process-based* models. A mechanistic model is constructed on two or more levels of organization, with a partitioning of the phenomena that are to be predicted on the upper level into processes represented on the lower level, which can themselves be split into other mechanisms and so on (Thornley, 1998). For example, crop growth rates (upper level phenomenon) can be modelled as a sequence of processes as photosynthesis, respiration, carbon allocation, transpiration and nutrients uptake (lower level mechanisms). These processes can also be subdivided into a number of mechanisms and so on. At the end, the lowest level of a mechanistic model is always empirical. For example, photosynthesis can be expressed by means of an empirical relationship between incident light and produced sugar (less mechanistic), or through a sequence of biochemical reactions that happen during the photosynthesis, each described by an empirical formula (more mechanistic). In the latter example, photosynthesis will be seen as a process-based model itself, based on assumptions about within-leaf processes. However, any model has to stop at a given level of description, and therefore, a mechanistic model is always incomplete. The best method is to first build a two-levels model, and then to split the lower level processes that give the most inaccurate results and that could be improved. The development of a process-based model requires a good knowledge and understanding of the modelled problem, and a good prior identification of what the important elements are, and how they relate to each other.

In this work, the model developed to study the dynamics of terrestrial ecosystems is a deterministic, dynamic and mechanistic model. Deterministic because no distribution of probability is associated to the processes that are simulated in the model, the values of the inputs being known (measured), dynamic because the aim is to study the temporal evolution of ecosystem response to a changing environment, and mechanistic because the system modelled is rather complex, some phenomena being described at an important level of precision, in order to gain a better understanding of the interactions between its components.

1.6.2.2 Cropland and grassland models

Describing and comparing all the existing models is impossible in view of their number. For example, in the review of van Wijk et al. (2014), when only searching for models which simulate crop management at the scale of a farm or of a farm-household, 126 models described in 480 papers were found. It is relevant to believe that by changing the type of model, much more could be found. In this chapter, a brief history of the models designed to describe agroecosystems from plot to exploitation scale will be provided followed by an overview of the main characteristics of the most used models. The signification of the different model acronyms and the sources used for each one are given in the Appendix A.

This chronicle of models development is based on the work of Jones et al. (2016). It targets not only models that deal with the impact of croplands and grasslands on climate change but all the models relative to agricultural systems.

The first model for agricultural systems was developed by Heady (1957) and his team in the 1950s. The purpose was to create a tool to optimize decisions at farm scale with the aim to improve the yield. The use of models in order to understand complex natural systems started to be more and more popular in 1964 with the work of the International Biological Program. They created several ecological models including grassland models. Despite that, several scientists stayed highly skeptical about this method. In 1972, two programs promoted the use of models in this field of study. The first one from the USA which was intended to build models to predict crop production all around the world in order to tackle the shortage and the price increase of agricultural commodities. This program led to the creation of the first versions of a model called CERES-Wheat and CERES-Maize (Ritchie & Otter, 1985). The second program was the Integrated Pest Management project created in the USA and supported by the FAO and was designed to regulate the increase of pesticide use. The project led to the creation of several submodels simulating the apparition and scattering of insects and diseases. They are still currently included in modern models

like DSSAT (Jones et al., 2003). The Agricultural System journal was launched in 1976 and allowed to publish scientific research in this domain, leading to the legitimization of model use. Two of the most widely used models were created afterwards: EPIC (Williams et al., 1989) thanks to the US Soil and Water Conservation Act and APSIM (McCown et al., 1996) in Australia.

In the 1980s, the development of personal computers and World Wide Web induced large progress in this field of study. It led to the creation of networks such as the International Consortium for Agricultural System Application, to the establishment of global datasets and to the release of open source models like APSIM and DSSAT. It gave access to use the models but also gave the opportunity to modify these codes, and led to a community-based development of these models.

Models studying the relations between agroecosystems and climate change were adopted in 1986 by the International Geosphere Biosphere Program and in 1990 by the IPCC. The goals of these programs were to assess the impact of climate change on agriculture and to search adaptations and mitigation of agricultural practices. It was followed by the Agricultural Model Intercomparison and Improvement Project (AgMIP) in 2010 in which various models were compared and improved, before using them to assess the impact of agriculture on climate and vice-versa (Rosenzweig et al., 2013).

In the current context of food system improvement (quality and quantity) under climate change, institutes and universities endeavour to develop their own model to fit to their local specificities. As a result, numerous models are studied, compared and improved nowadays. The following paragraphs summarize how these various models may differ from each other.

Time scale The level of complexity and the accuracy of the results provided by ecosystem models are tightly linked to the time step of the processes and climate variables that are used as inputs (Hoogenboom, 2000). While yearly time scales are often adequate to estimate the evolution of soil reservoirs over hundreds of years, the choice of monthly climate data as input often leads to under- or overestimates of crop yields because the temporal variability of the plant growth rate has a finer resolution (Nonhebel, 1994). Therefore, many crop growth models are run with daily time steps and daily input data, also because weather data are often acquired at this temporal scale: DNDC (Li et al., 1992), STICS (Brisson et al., 2003), CERES-EGC (Gabrielle et al., 2006), ANTHRO-BGC (Ma et al., 2011), CQESTR (Gollany et al., 2012), DayCent (Necpálová et al., 2015), etc. However, many physiological and physical processes involved in carbon, water and energy agrosystem cycles proceed at shorter time-scales, and their response to the environment is non-linear in the course of the day (Puech-Suanzes et al., 1989; Hirasawa & Hsiao, 1999). Faced with that reality, and taking advantage of the new technologies increasing the frequency of fluxes and environmental measurements, models developed to reproduce these cycles have time steps shorter than a day (often one hour or one half-hour and sometimes less) such as in SPA (Williams et al., 1996), PaSim (Riedo et al., 1998), ASPECTS (Rasse et al., 2001), ORCHIDEE-STICS (de Noblet-Ducoudré et al., 2004), ChinaAgrosys (Wang et al., 2007), etc. These kinds of models allow to analyse the intra-day variability of most phenomena, they often provide a better accuracy (Wattenbach et al., 2010) and reduced instabilities, but they can lead to longer computational time, which is nowadays a minor problem, considering the improvement of computer processors.

Spatial description Ecosystem models can be classified according to the number of dimensions they represent. Most of the ecosystem models are developed considering only the vertical dimension (horizontal homogeneity), where materials or energy can be exchanged between (from top to bottom) the atmosphere, the canopy layers, the plant stem, and the soil layers. In such models, reservoirs content and fluxes are expressed by unit of area, and the results are extrapolated to the whole plot using a simple multiplication by the studied area. This method implies some homogeneity in the non considered dimensions of the modelled field (Faivre et al., 2004). For non-homogeneous but patchy distributed zones, a same agroecosystem model can be applied to sub-zones, where distinct initial values and parameters will be set with, for the most sophisticated models, lateral flows between the sub-zones. This approach, named model spatialization, is used to evaluate the evolution of biosystems on regional, continental or worldwide scales (de Noblet-Ducoudré et al., 2004), with climatic data inputs provided by atmospheric general circulation models (GCM). A well-known example of this kind of model is ORCHIDEE described by Krinner et al. (2005). For such models, remote sensing is often used to assign land cover types to the studied sub-areas, and to extract

some information like the dominant vegetation, the soil moisture, etc. (Tsvetsinskaya et al., 2001). However, some scientists claim that the hypotheses and validity domains of one-dimensional crop models at plot scale are not adapted (too restrictive) to larger surfaces even when they try to estimate and integrate lateral flows (Faivre et al., 2004). In some situations, the need of simulating horizontal fluxes between grid cells leads to bi- or three-dimensional models (Faivre et al., 2004). This is particularly justified by a focus on the hydrology of the simulated site, as phenomena like runoff or lateral drainage can greatly affect soil water content and pollutant concentration at the watershed outlet (Beaujouan et al., 2001).

Modelling focus Every model does not have the same purpose. Some of them focus on a certain agroecosystem such as PaSim for grassland (Vuichard et al., 2007; Ma et al., 2015) or CERES-EGC (Gabrielle et al., 1995), DSSAT (Jones et al., 2003) and EPIC (Williams et al., 1989) for cropland while others show more multidisciplinarity like Daycent which is able to simulate croplands, grasslands, savannas and forests (Parton et al., 1998). Agroecosystems are composed of the atmosphere, soil, fauna and flora. A model can either focus on some of these components or keep a global view. For example, RothC (Coleman & Jenkinson, 2014) and CQESTR (Gollany et al., 2012) focus on the soil components and mostly on the soil organic carbon turnover while the model of Hutchings & Gordon (2001) focuses on the herbivores on grassland and the model of Jouven et al. (2006) mainly concerns herbage growth. The attention might also be aimed at a particular process like in EPIC, a model that focuses on soil erosion (Williams et al., 1989). Due to these various points of interest, every model does not simulate the same cycles and fluxes. Generally, carbon and water cycles are the most represented ones but, for example, ChinaAgrosys (Wang et al., 2007), JULES (Best et al., 2011) and ANTHRO-BGC (Ma et al., 2011) simulate the energy balance. The nitrogen cycle is also sometimes neglected like in RothC and CQESTR (Gollany et al., 2012; Coleman & Jenkinson, 2014).

Levels of complexity All the cycles or processes can be described with more or less precision (Wang et al., 2007). The level of complexity adopted in a model mainly depends on the accessible computational power and the accuracy of the available data used for parameterization and validation. For instance, three major levels of complexity exist in canopy models: the big-leaf, two-leaf and multi-layers models. The big-leaf model considers the canopy as a single representative leaf, assuming that the response of this leaf to the environment is similar to the whole canopy response. Two-leaf models, on the other hand, simplify the canopy as being two leaves, a sunlit one and a shaded one, and show significant improvements compared to big-leaf models. The results of two-leaf models are nearly as good as multi-layers models which divide the canopy in several horizontal layers and, therefore, are time consuming (de Pury & Farquhar, 1997). These latter models allow a better characterization of the system, as they estimate the vertical evolution of sunfleck penetration and leaf photosynthesis within the canopy (Wang & Leuning, 1998; Clark et al., 2011). However, a complex description of the system can provide some difficulties (Hogue et al., 2006). Calculations certainly require a greater amount of time, especially during the parameter tuning (Xiao et al., 2014). It might also lead to an overparametrization, when the parameters are too numerous or their spatial and temporal variability are too complex compared to the values coming from data or literature (Bastidas et al., 2006), or to difficulties in the initialisation, calibration and validation procedures, especially when measured data used to compare the simulation are lacking. Besides the intrinsic complexity of a model, the difficulties coming from its coupling with other models must also be taken into account. The combination of models is required according to the desired results and available data. For example, a soil-vegetation-atmosphere (SVAT) model has to be combined to a general circulation model when large spatial scale weather forecasting is necessary (Sellers et al., 1997). As a consequence, this kind of coupling increases the complexity of the whole system. In addition to this level of complexity, which is related to the definition of the simulated object, another level concerns the type of approach describing the processes. Still in the perspective of photosynthesis, an example of two notable approaches exists. In order to estimate the assimilated CO_2, Farquhar et al. (1980) developed a biochemical approach including a chain of complex reactions whereas Monteith (1972) and Monteith & Moss (1977) introduced the radiation use efficiency, computing directly the plant biomass growth (including photosynthesis, plant respiration and allocation to plant growth) as the product of this efficiency and the intercepted radiation.

Land management representation Different types of management can be done in croplands and grasslands. The various operations are the sowing/planting, fertilisation, irrigation, fertigation, soil tillage, mulching, harvesting, etc. Some models take all of these practices into account like STICS (Brisson et al., 2003) and DNDC (Li et al., 2012) but some operations are neglected in other models, as tillage in the DSSAT model (Jones et al., 2003).

Moreover, each practice can be implemented differently based on the selected approach or level of complexity, as explained above. For instance, tillage simulation can be translated into several impacts on the system. In the EPIC model, tillage leads to the mixing of the topsoil nutrients and residues, to the variation of bulk density, to the leaching of organic carbon, to a variation of surface roughness and to soil erosion (Izaurralde et al., 2006). In comparison, RothC model does not take the leaching of organic carbon into account and, according to Nieto et al. (2010), it can lead to a certain discrepancy in the modelled SOC value. In general, tillage simulation is a source of issues in models but all the other practices also have to be well represented to ensure the suitability of the results (Brilli et al., 2017). Besides soil and plant management, grassland models can also include cattle management, such as livestock composition and diet, feeding frequency, stocking periods and intensity, like in PaSim model (Graux et al., 2012).

Modelling context Considering the differences between agroecosystem models presented beforehand, one can understand that the choice of a model will mainly depend on the objectives pursued. Primarily, cropland modelling was used as a decision-making tool for crop management (Asseng et al., 2009; Li et al., 2012), in order to maximize yields, for economical purposes. Afterwards, eco-physiological sub-models, simulating plant growth and fluxes of matter in the atomsphere-plant-soil continuum, were added into crop models, providing more complete tools such as STICS (Brisson et al., 2003), and allowing the study of the influence of environmental conditions on ecosystem behaviour. Other crop models have also included crop physiology and molecular biology processes for plant breeding programs (Slafer, 2003). In the same way, the first grassland models provided useful information about production such as optimized cutting events and cattle stocking rates (Graux et al., 2012).

1.7 Objectives

In view of the questions that remain regarding the response of ecosystems to their environment and to management practices, this thesis aims at reproducing and understanding the dynamics of grasslands and croplands by means of an ecosystem model. To achieve this, a model designed and validated for forest stands is used. The main steps of this work are:

- The implementation of the required processes into the forest model to transform it into a cropland and grassland model. This first objective implies a fine understanding of the forest model, and an identification of the dissimilarities between forest ecosystems on the one hand and cropland and grassland ecosystems on the other hand. The scientific literature and various models are then reviewed in order to implement the appropriate equations in a new model, which is the result of a collaborative work, also described in Delhez (2019) and Vandewattyne (2019).
- The sensitivity analysis, calibration and validation of the water cycle. This task relies on dataset acquired at one cropland and one grassland experimental sites, both equipped with flux towers and meteorological stations. The processes calibrated are the soil evaporation, the canopy transpiration and the infiltration and percolation of water within the soil profile. Along with this calibration and validation, paths of improvement are provided.
- The pooling of results of calibration carried out in Delhez (2019) and Vandewattyne (2019) and the test of the grazing module. No calibration of this module is carried out so far, but both measured and modelled grass heights are compared and the discrepancies between observations and predictions are analysed. This leads to recommendations for a future calibration of this grazing module.

Chapter 2

TADA model

As presented in the previous chapter, a fine understanding of ecosystem functioning may require the use of ecosystem modelling. We propose to develop a new model based on an existing one. The original model chosen for this work is the ASPECTS model, developed in 2001 by Rasse et al. ASPECTS was first built in order to study the evolution of carbon reservoirs in temperate forest ecosystems (Rasse et al., 2001). Afterwards, this model was used to predict evaporation from forest stands under changing climate (Misson et al., 2002) and a nitrogen cycle was added in 2002 by Rasse. Although ASPECTS solely studies forests, this model was chosen as a basis for various reasons:

- ASPECTS is a process-based model, which includes mechanistic descriptions of the main ecosystem processes. This helps determining the links between driving variables and important processes as well as quantifying the feedback effects controlling the system. In addition, this mechanistic model gives an insight into the fluxes between the ecosystem components.

- With a time step of 30 minutes, ASPECTS allows studying the intra-day fluxes dynamics, as well as simulating the evolution of the ecosystem reservoirs in the long run. This may be interesting in order to study a same phenomenon on different time scales, as some short-time trends might not be visible at a monthly or yearly scales.

- ASPECTS focuses, among others, on CO_2 exchanges between the ecosystem and the atmosphere for which large datasets are available. A part of this model was calibrated against NEE data acquired with the EC technique and provided accurate estimations of NEE fluxes for several years of data (Rasse et al., 2001).

- As ASPECTS was partly developed by scientists from the University of Liège, the source codes were available for this work, and some assistance was provided by Pr. François in the understanding of ASPECTS.

One of the goals of this thesis was to modify ASPECTS, a forest model, into a cropland and grassland model. This work required a complete comprehension of ASPECTS model before identifying the processes that differ from an ecosystem to another. For these processes, existing parametrizations, routines and equations were compared in the literature, and the most suited ones were added to ASPECTS. This led to a new model called TADA (Terrestrial Agroecosystem Dynamics Analysis) which allows simulating carbon, nitrogen and water cycles in forests, croplands and grasslands.

In this chapter, an overview of the TADA model will first be given and the representation of an ecosystem into reservoirs and fluxes will be presented. Then, the main modules of TADA will be described, with a focus on the innovations compared to ASPECTS. For more information about ASPECTS, the reader will find a complete description in Bureau (n.d.). Finally, some computational considerations will be discussed.

2.1 General description

2.1.1 Model overview

As for many ecosystem models, TADA describes ecosystems as a set of reservoirs, connected by fluxes of matter or physical quantities such as heat. In figure 2.1, the ecosystem reservoirs whose content is subject to simulation are represented by solid line boxes. These reservoirs express the amount of carbon, nitrogen or water per m^2 stored in different parts of the ecosystem. Therefore, ecosystem reservoirs are expressed in gC m^{-2}, gN m^{-2} or mm H_2O (i.e. L H_2O m^{-2}) and flux densities (abbreviated into the term "flux" in this work to facilitate the reading) in gC, gN or mm H_2O m^{-2} day^{-1}. In addition, the model also simulates the soil temperature dynamics (temperature expressed in K). The dashed boxes correspond to reservoirs with a content considered as constant for the simulations. This is the case for CO_2, N_2O, N_2 and H_2O whose temporal evolution is not simulated. The main modelled reservoirs are the carbon and nitrogen stored in plant organs, soil residues and soil organic matter (SOM), the soil NH_4 and NO_3, and the water contained in various reservoirs: the canopy interception, snow, the soil surface layer and soil horizons. The soil is divided into horizontal layers having their own reservoirs. Finally, soil temperature is considered as a reservoir in each soil layer in order to simulate the evolution of temperature in time, as temperature drives a lot of soil reactions. Note that TADA is a uni-dimensional model, as no horizontal heterogeneity is taken into account in the ecosystem.

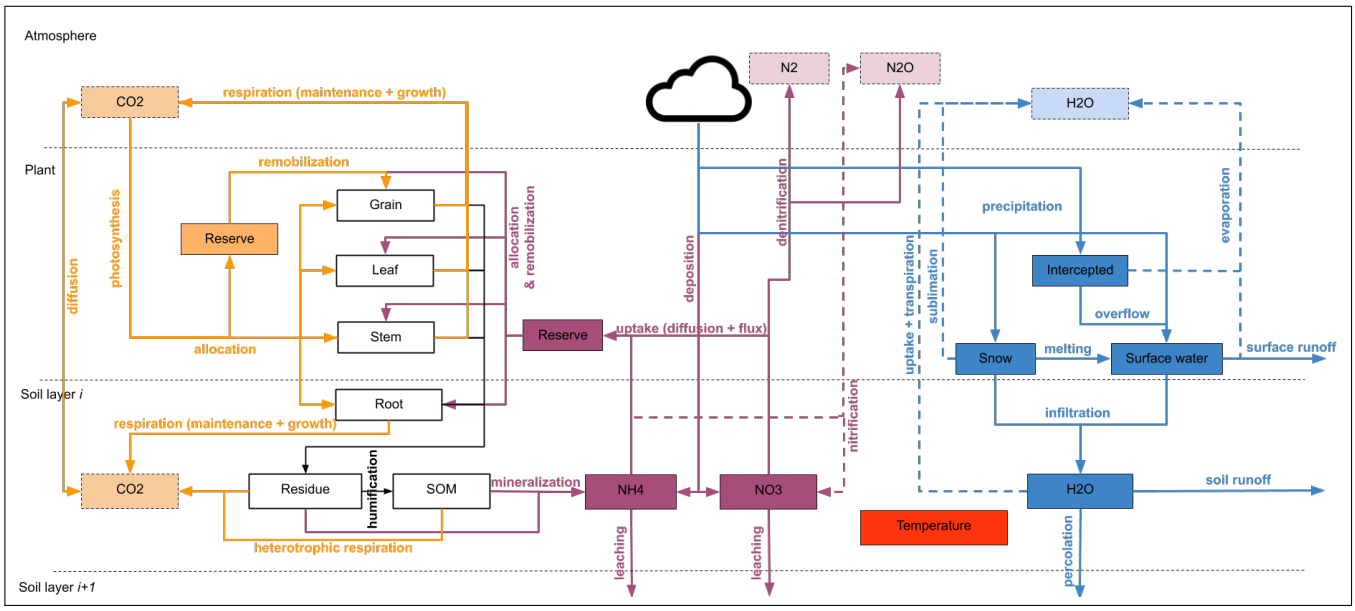

Figure 2.1: Diagram of ecosystem divison into reservoirs and fluxes in the TADA model (orange stands for carbon, purple stands for nitrogen, blue stands for water and black stands for both carbon and nitrogen).

TADA distinguishes three main cycles (carbon cycle in orange, nitrogen cycle in purple, water cycle in blue and coupled carbon and nitrogen cycles in black), interacting through various processes. For the sake of clarity, fluxes of matter due to management practices (including grazing) are not represented in figure 2.1, but will be detailed below, and in sections 2.2.4 and 2.2.5, as parts of the C and N cycles. The main input of the carbon cycle corresponds to plant photosynthesis. A part of this assimilated carbon goes back to the atmosphere through maintenance and growth respiration, and the remaining part is allocated to plant organs or stored in reserve, according to the plant species and its phenological stage. Through senescence, some of the carbon and nitrogen present in plants feeds the soil residue pools, which in turn provide carbon and nitrogen to the SOM pools. According to the management practices, some carbon contained in the plant organs can be exported at harvest or by cattle during grazing periods. Some carbon can also be applied to the field with manure or directly from animals excreta, thus feeding the litter pool.

Two main inputs of the nitrogen cycle are the NO_3 and NH_4 included in the atmospheric depositions, as well as fertilisation and animal droppings. A part of the NH_4 pool turns into NO_3 and N_2O during nitrification, and some NO_3 returns to the atmosphere in the form of N_2 and N_2O through denitrification. Besides that output from the nitrogen cycle, some nitrogen is transported by plant uptake to an intermediate reserve pool, which feeds plants organs according to their demand of nitrogen. Some nitrogen is also lost through vertical and horizontal NH_4 and NO_3 leaching, leaving the soil profile with respectively vertical percolation and horizontal runoff. Finally, the nitrogen leaving the deepest modelled horizon is lost by the system. For croplands and grasslands, N fertilisation can fuel the NH_4 and NO_3 pools. The presence of livestock induces an export of N from the above-ground organs, as well as after a harvest. Finally, the NH_4 and litter pools are fed by, respectively, animals urine and faeces.

Water enters the system through precipitation in the form of rain or snow. A part of this water is intercepted by the vegetation, and the rest fills a soil surface reservoir. Then, water percolates into deeper soil layers or leaves the soil surface through horizontal runoff or evaporation. The soil water can move from layer to layer and goes out of the ecosystem though vertical percolation or canopy transpiration. Some ecosystem models simulate reservoirs of water in the roots, stem and leaf tissues with a transfer of water following hydric potential differences, but TADA does not.

2.1.2 Numerical resolution

The aim of a dynamic model is to calculate the temporal evolution of state variables, i.e. the variation of the content of each reservoir symbolized by dx/dt [gC, gN m^{-2} day^{-1} or mm day^{-1}) with t representing the time. This evolution is expressed by a differential equation, which can be written as:

$$\mathrm{d}x/\mathrm{d}t = F_{in} - F_{out} \tag{2.1}$$

where F_{in} represents the incoming fluxes of a given reservoir, while F_{out} represents the outgoing ones. In figure 2.1, all the inputs of a reservoir are represented by an incoming arrow and the outputs by an outgoing one. This scheme shows well that the input of a reservoir x_1 can be the output of another reservoir x_2. The different inputs and outputs are fluxes due to physical transport processes or (bio)chemical reactions, which depend on environmental conditions (e.g. meteorological conditions, soil characteristics, management, etc.), on the initial values of x and on parameters values.

In mathematical terms, the reservoirs contents (x_i) are considered as unknowns and the time t as the independent variable. Therefore, the equation 2.1 can be seen as:

$$\mathrm{d}x_i/\mathrm{d}t = f(x_{i=1,nres}, t) \tag{2.2}$$

where the variation of the reservoir content x_i depends on its value, on the value of the other reservoirs contents and on time. The numerical integration consists in computing the evolution of variables during a finite time step. Different methods exist to reach this goal, each one different by its stability, its convergence and its order. The stability reflects the risk that the model propagates and amplifies a numerical error in a large proportion. The convergence shows if the numerical solution approaches the real solution when the used time step decreases. The order of a method designates the time step needed to have an answer in the error tolerance. In other words, a method with a smaller order needs a smaller time step to have the same quality of result. The numerical integration method has to be chosen to improve these three characteristics while keeping an eye on the calculation time (i.e. the time that takes the computer to find the numerical solution).

The numerical methods can be split into three different families: single-step, iterative, and multistep methods. The single step ones calculate the value of the x variables at the end of a timestep only by using their starting value, the time step and their derivative. A common example is the Euler method. The iterative method, such as Runge-Kutta's, divides the time step to resolve the differential equation. Finally, the multistep will use a specific combination of several previous points and derivative values to calculate a new one. The increasing complexity of these methods aims to reach higher stability, convergence and order.

The TADA model uses the numerical method already implemented in ASPECTS. A 4^{th} order Runge-Kutta scheme is used to initialise the multistep Bashfor-Moulton method. The need of an initialisation is due to the fact that the method needs four previous values to calculate a new one. A routine is dedicated to the resolution of differential equations in TADA, for each time step, with a default value of 1 minute.

2.1.3 Model inputs

As explained beforehand, the TADA model can be represented as a system composed of reservoirs whose contents vary over time according to the fluxes which are simulated using a given numerical resolution. For its proper functioning, TADA requires the value of the parameters as well as additional data. These latter are named model inputs hereafter and can be divided into four general categories.

Initial reservoirs content Initial conditions are compulsory for every model, that is to say the initial value of the reservoirs content in this case. As a reminder, all the reservoirs are specified in figure 2.1. If these initial conditions are not well estimated, an unstable or transient behaviour might appear in the model outputs (Hashimoto et al., 2011). On the one hand, the content of some reservoirs is easily measurable, such as the leaf carbon content, the soil water content and soil temperature. On the other hand, the carbon and nitrogen content of roots, litter and soil organic matter in each soil layer are rarely measured because of the complexity of the needed method. However, these last reservoirs can be estimated either by relationships with other measured variables (as the root/shoot ratio) or by a steady state simulation for soil carbon reservoirs. In a nutshell, a steady state simulation is a long-term simulation with cyclic inputs after which the soil reservoirs are expected to reach an equilibrium. The values of the reservoirs at this equilibrium state can be defined as the initial values for the research applications.

Meteorological data Contrary to models coupled to an atmospheric general circulation model (GCM), TADA requires meteorological variables as inputs: global radiation, precipitation, wind velocity, atmospheric pressure, air temperature and relative humidity. Generally, these variables are measured in every standard meteorological station. The time scale of these inputs will define the minimal time scale of the outputs. For example, with one year of 30-minute meteorological data, TADA will generate results reproducing seasonal, daily and half-hourly variability. These meteorological variables are essential because they intervene in various processes implemented in TADA (photosynthesis, water interception, nitrogen atmospheric deposition, plant transpiration, etc.).

Soil data Soil characteristics, such as soil texture, horizon depth, pH and bulk density for each soil layer as well as the average slope of the studied area, etc., are regarded as parameters and thus, are inputted only once. However, some of the soil inputs can change during the simulation due to soil operations like ploughing. In that case, these inputs are subject to temporal variability. The number of homogeneous soil layers depends on the soil data. The more layers considered, the more gradual the evolution of variables over the soil profile will be. These inputs are indispensable for water movements in soil and the determination of any stress related to soil characteristics (water stress, pH stress). As for the previous categories, soil data can be measured or at least assessed with field observations.

Management This last category was very simplified in ASPECTS (limited to wood harvesting) but is essential for cropland and grassland ecosystems. This input is a chronological list specifying every operation the farmer makes on the crop or grassland (including those relative to livestock). Depending on the type of management, supplementary information might be required besides the nature of the operation. For instance, three additional inputs must be encoded for mineral fertilisation: the applied quantity, the fraction of ammonia and the fraction of urea. Note that this category, as well as the previous ones, is further detailed in the user guide in section 2.3.

2.2 Modules description

As presented beforehand, evaluating the evolution of ecosystem reservoirs with time requires the computation of fluxes between these reservoirs. These fluxes are calculated in different modules which can be merged into a carbon, a nitrogen and a water cycle (figure 2.2). The soil temperature module also computes the vertical gradient of temperature and the heat fluxes between soil layers. Aside from the main cycles, the phenological module evaluates the transition from one phenological stage to another, which will mainly affect carbon and nitrogen allocation pattern. Finally, a management module allows taking different crop management techniques into account such as soil tillage or nitrogen fertilisation and a grazing module considers the effect of animals on plant growth.

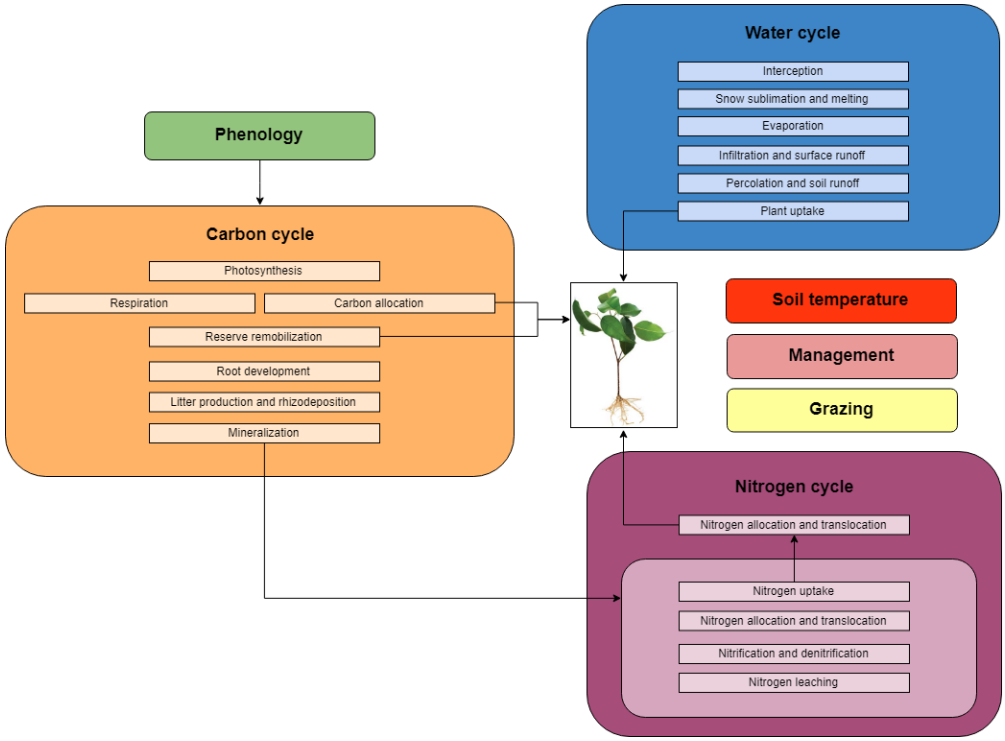

Figure 2.2: Main modules of TADA model.

In this section, the different modules will be presented, with a particular attention paid to the modules which were modified or improved in the TADA model compared to ASPECTS, and those for which some calibration procedures were performed during this project. In the interests of clarity and concision, only the water and carbon cycles, and the management and grazing modules will be detailed in this section (those on which this thesis focused). The reader will find a complete description of the other modules (soil temperature, root development and nitrogen cycle) of the TADA model in Appendix B or in Delhez (2019) and Vandewattyne (2019).

2.2.1 Water cycle

The development of a water submodel is of great importance for ecosystem models, as various plant or soil processes are controlled by the available soil water. TADA simulates the transfer of water from precipitation to soil porosity and the loss through evapotranspiration but does not compute the amount of water contained in plant organs. Therefore, the physiological processes affected by water availability (the most important one being photosynthesis) will be regulated in TADA by water stress factors depending on soil water content (SWC). Other processes such as organic matter turnover, nitrogen leaching and soil heat transfer are affected by corresponding factors.

Interception

The only climatic input of the water cycle is the measured precipitation. This precipitation falls as rain if the air temperature is above 0°C or as snow in the other case. If a precipitation is in the form of rain, a part of it is intercepted by the vegetation canopy. The fraction of the intercepted rain f_{green} is proportional to the leaf area index (LAI), as leaves will cover more space. However, as leaves are not evenly distributed and as some of them may cover others, f_{green} is computed considering the probability that a droplet reaches the foliage decomposed in many elementary layers. This leads to:

$$f_{green} = 1 - e^{5000 \log(1-LAI)} \tag{2.3}$$

The intercepted rain feeds an interception reservoir, some water evaporates from this reservoir and the difference between both fluxes gives the evolution of the interception reservoir. A maximum value of interception is computed as a function of the LAI, and once this value is overshoot, the surplus of water returns the soil as throughfall:

$$Thf = Pr_{int} - E_{int} - (wl_{\max} - wl(t)) \tag{2.4}$$

where *Thf* is the throughfall [mm day^{-1}], Pr_{int} is the intercepted rain [mm day^{-1}], E_{int} is the intercepted water re-evaporated [mm day^{-1}], wl_{max} is the maximum volume of the interception reservoir [mm], and *wl(t)* is the volume of the interception reservoir [mm].

Snow reservoir

As snow mainly falls during winter when the vegetation foliage is less developed, no interception of snow is considered. Snow directly reaches the ground and enters the snow reservoir, which is subjected to snow melting (according to the air temperature) and to snow sublimation (proportional to the gradient of vapour pressure between the snow and the air). The melted snow reaches the surface water reservoir, together with precipitations in the form of rain.

Evaporation

In TADA, a surface water reservoir is fed by three components: the melted snow, the rain falling from the interception reservoir, and the droplets directly hitting the ground. The surface reservoir is considered as a very thin soil layer (default value of 1cm, same texture as the upper soil layer) where all the soil evaporation takes place, which means that no water is evaporated from deeper horizons. Soil evaporation is calculated with Mahfouf & Noilhan's (1991) equation:

$$E_{soil} = (1 - f_{snow}) \frac{\frac{\alpha\, e_{soil}}{T_{soil}} - \frac{e_{air}}{T_{air}}}{R_g\, r_{tot}} \tag{2.5}$$

where f_{snow} is the portion of ground covered by snow, e_{soil} is the saturation vapour pressure of soil water [Pa] at T_{soil} temperature [K], R_g is the gas constant [461.89 Jkg^{-1}K^{-1})] and α is the relative humidity of air in the fictive soil layer.

In soil, water is retained in the smaller pores of the soil matrix, and above the free water, water vapour is in equilibrium with the liquid phase (Mahfouf & Noilhan, 1991). Therefore, vapour pressure in soil is not at saturation and must be corrected by the relative humidity (Philip, 1957):

$$\alpha = e^{[\psi_0/(R_g T_{soil})]} \tag{2.6}$$

where ψ_0 is the hydric potential of the fictive soil layer [Pa], computed according to Saxton & Rawls (2006) as a function of soil water content and soil texture.

The total resistance to soil evaporation is the combination of three series resistances, from the soil pores to the atmosphere:

$$r_{tot} = r_{\text{soil}} + \lambda_{bl} r_{bl} + \lambda_{ae} r_{ae} \tag{2.7}$$

where r_{bl} is the boundary layer resistance [s m^{-1}] and r_{ae} the aerodynamic resistance [s m^{-1}], both weighted by two parameters λ_{bl} and λ_{ae} which are calibrated against experimental data. The last term r_{soil} is a soil resistance to water vapour exchange [s m^{-1}] (Passerat, 1986, cited in Mahfouf & Noilhan, 1991):

$$r_{\text{ soil}} = \varepsilon_{cst} * 10^4 e^{-\varepsilon_{water} \frac{\theta_0}{\theta_{\text{sat},0}}} \tag{2.8}$$

where θ_0 is the soil water content (V_{water}/V_{total}) in the fictive soil layer [-] and $\theta_{sat,0}$ is the soil water content at saturation, computed according to Saxton & Rawls (2006) and depending on soil texture. Two parameters, ε_{cst} and ε_{water} give more or less weight to the variation of soil water content in the value of soil resistance. This resistance is supposed to increase as SWC falls, in order to prevent loosing too much water from soil evaporation.

The aerodynamic resistance was originally introduced to express momentum fluxes following a gradient of horizontal momentum with an analogy of Ohm's Law (Monteith & Unsworth, 1990):

$$r_{ae} = \frac{u}{u^{*2}} \tag{2.9}$$

where u is the horizontal wind speed at the reference level [m s^{-1}], u^* is the friction velocity [m s^{-1}] and r_{ae} is expressed in s m^{-1}. Note that this equation is only valid for neutral stability conditions.

For heat and water vapour exchanges, an additional boundary layer resistance must be added, as the apparent sources of heat and water vapour will often be found at lower levels in the canopy than the apparent sink of momentum (Monteith & Unsworth, 1990). Thom (1972) provided an empirical equation for boundary layer resistance:

$$r_{bl} = \frac{6.2}{u^{*0.67}} \tag{2.10}$$

with r_{bl} expressed in s m^{-1}.

To calculate the resistances presented above, the friction velocity is computed based on the assumption of a logarithmic wind-profile (Monteith & Unsworth, 1990):

$$u^* = \frac{0.4\, u}{\ln\left(\frac{z-d}{z_0}\right)} \tag{2.11}$$

where z is the reference level where the wind speed in measured [m], z_0 is the roughness length [m], proportional to the roughness of the elements, and d is the displacement height [m] which takes the height of the surface elements into account. Jones (1992) provided formulas expressing the roughness length and the displacement height as a function of canopy height (h [m]): $z_0 = 0.13\ h$ and $d = 0.64\ h$ for crops and pastures and $z_0 = 0.075\ h$ and $d = 0.78\ h$ for forest stands. Note that for bare soil, the displacement height is null, and the roughness length is about 0.0015 m (Jones, 1992). In TADA, canopy height is obtained from plant shoot dry mass through allometric relationships fitted to field data for winter wheat and grass respectively.

Infiltration and surface runoff

The surface reservoir, which is subject to soil evaporation, is fueled by water from precipitation. Depending on the intensity of the precipitation, all the water reaching the ground will infiltrate into the fictive soil layer or runoff will occur. This is the case if the incoming water, expressed in mm day^{-1} overshoots the maximum water flow at the saturated conductivity K_s which depends on soil texture, according to Saxton & Rawls (2006).

The infiltrated water has two fates, depending on the remaining non water-filled porosity in the fictive soil layer:

$$por = \theta_{sat,0} - \theta_0 \tag{2.12}$$

If the remaining porosity is lower than 1%, no water remains in the fictive soil layer, and all the infiltrated water percolates into the first *real* soil layer. If not, a temporal aspect is considered: if the infiltrated water replenishes less than 50% of the remaining non water-filled porosity in one time step, all the infiltrated water remains in the fictive soil layer, and otherwise, the surplus percolates into the first soil layer:

$$perco = \begin{cases} 0 & \text{if} \quad infi < \frac{0.5\,por}{\Delta t} \\ infi - \frac{0.5\,por}{\Delta t} & \text{if} \quad infi \geq \frac{0.5\,por}{\Delta t} \end{cases} \tag{2.13}$$

where *perco* is the percolating water [mm day^{-1}], *infi* is the infiltrated precipitation [mm day^{-1}] and Δt is the time step used in the simulation.

Percolation and soil runoff

The soil profile is represented as a series of homogeneous soil layers where soil parameters are equal to the values calculated in the middle of the layers. The number of layers, their depth and their texture must be specified by the user as input parameters. In each layer, the soil water content is computed according to the difference between incoming and outgoing fluxes:

$$V_i \frac{d\theta_i}{dt} = F_{i-1} - F_i - F_{lat,i} - U_i \tag{2.14}$$

where i is the considered soil layer, V_i is the volume of layer i [m^3], F_{i-1} is the flux coming from the above *i-1*th soil layer [mm day^{-1}], F_i is the water flux leaving the ith soil layer to the *i+1*th one [mm day^{-1}], $F_{lat,i}$ is the lateral soil water runoff [mm day^{-1}] and U_i is the water uptake by vegetation in soil layer i [mm day^{-1}].

Vertical fluxes are computed with an adaptation of Fokker-Planck's equation:

$$\frac{d\theta}{dt} = \frac{d}{dz}\left(D(\theta)\frac{d\theta}{dz} - K(\theta)\right) \tag{2.15}$$

where z is the depth [m], *D(θ)* is the water diffusivity [m^2 day^{-1}] and *K(θ)* is the hydraulic conductivity [m day^{-1}]. The hydraulic conductivity is calculated from the saturated conductivity with Saxton & Rawls' equation (2006):

$$K(\theta)_i = K_{sat,i}\left(\theta_i/\theta_{sat,i}\right)^{[3+(2/\lambda_i)]} \tag{2.16}$$

where $K_{sat,i}$ is the saturated conductivity [m day^{-1}] and λ_i is a texture-dependent parameter. Saturated conductivity is computed according to Rawls et al. (1998):

$$K_{sat,i} = \frac{24}{1000}\mathbf{C}_i\left(\theta_{sat,i} - \theta_{fc,i}\right)^{m_i} \tag{2.17}$$

where C_i and m_i are empirical parameters and $\theta_{fc,i}$ is the water content at field capacity, computed from soil texture according to Saxton & Rawls (2006). In their study, Saxton & Rawls (2006) compute the parameter m_i as follows: m_i=*3*-λ_i where λ_i is a texture-dependent parameter.

Water diffusivity is obtained from the hydraulic conductivity by taking the slope of the water potential formula ($d\psi_i/d\theta_i$), provided by Saxton & Rawls (2006):

$$D(\theta)_i = K(\theta)_i \frac{d\psi_i}{d\theta_i} \tag{2.18}$$

The discretization of Fokker-Planck's equation allows computing the water fluxes between soil layers:

$$F_i = K(\theta)_{moy,i,i+1}\cos(\alpha) - D(\theta)_{moy,i,i+1}\frac{\theta_{i+1} - \theta_i}{\left(\Delta z_i + \Delta z_{i+1}\right)/2} \tag{2.19}$$

where Δz_i is the thickness of soil layer i and α is the mean field slope [degree]. The first term of equation 2.19 represents the transfer of water through the soil profile by gravity, regulated by the hydraulic conductivity, while the second one stands for water transfer by diffusion following a gradient of soil water content. In equation 2.19, water diffusivity and hydraulic conductivity are taken as the mean of these values in layers i and *i+1*, weighted by the thickness of these layers:

$$D(\theta)_{moy,i,i+1} = \frac{\Delta z_i D(\theta)_i + \Delta z_{i+1} D(\theta)_{i+1}}{(\Delta z_i + \Delta z_{i+1})} \quad \text{and} \quad K(\theta)_{moy,i,i+1} = \frac{\Delta z_i K(\theta)_i + \Delta z_{i+1} K(\theta)_{i+1}}{(\Delta z_i + \Delta z_{i+1})} \tag{2.20}$$

The vertical water flux is calculated with equation 2.19 only if the soil water content in the considered layer outreaches its field capacity. Below the field capacity, the vertical flux F_i is set equal to zero. This assumption is rather correct for water fluxes due to gravity, but neglects the diffusion of water that still occurs under the field capacity. Note that for the first soil layer, the incoming vertical flux is equal to *perco* computed in equation 2.13. The bottom limit condition is a free drainage, so that no diffusivity is considered:

$$F_i = min(K(\theta)_i, K_{sub}) \cos(\alpha) \tag{2.21}$$

where K_{sub} is the substratum conductivity [m day^{-1}]. If the modelled site is based on a thicker, and low-permeable substratum, few drainage will occur, and a water table may be encountered in the soil profile. Soil water runoff may also be produced when the soil water content in layer i exceeds its saturation soil water content, or when no water can be transferred from layer i to layer *i+1* as layer *i+1* is already as its saturation value.

Plant uptake

In TADA, the total plant uptake is assumed to be equal to plant transpiration, so that the water removed from soil layers by vegetation will directly be emitted to the atmosphere. Plant transpiration, such as soil evaporation, is proportional to a gradient of vapour pressure and to a conductance for water vapour exchanges:

$$TR_x = \left(\frac{e_{leaf,x}}{T_{leaf,x}} - \frac{e_{air}}{T_{air}} \right) \frac{g_{H20tot,x}}{Rg} \tag{2.22}$$

where TR_x is the transpiration flux [mm s^{-1}], $T_{leaf,x}$ and T_{air} are the leaf and air temperatures [K], $e_{leaf,x}$ is the leaf saturated vapour pressure [Pa] at $T_{leaf,x}$ temperature, e_{air} is the partial vapour pressure of the air [Pa] and $g_{H2Otot,x}$ is the conductance to transpiration [s m^{-1}]. The subscript x denotes different types of leaves: the sunlit ones that receive direct radiation, the shaded ones that receive diffuse radiation and the clouded ones for overcast periods. The division of vegetation canopy into these different classes will be presented in the description of the photosynthetic module. The total canopy transpiration is equal to the sum of the contributions of each kind of leaves. Note that, as no leaf energy balance is implemented in TADA, leaf temperature is assumed to be equal to the air temperature.

The conductance to transpiration depends on the stomatal conductance and is inversely proportional to the boundary layer and aerodynamical resistances (Leuning, 1995):

$$g_{H2Otot,x} = \left(\frac{\frac{P_{atm}}{R_g T_{leaf,x}}}{1,6 g_{C,x}} + \frac{r_{bl}}{GAI} + r_{ae} \right)^{-1} \tag{2.23}$$

where P_{atm} is the canopy air pressure [Pa], $g_{st,x}$ is the stomatal conductance [mol m^{-2} s^{-1}] and GAI is the green area index [-]. The stomatal conductance is expressed as follows, according to Leuning (1995):

$$g_{C,x} = g_{0,x} + g_1 * An_x \tag{2.24}$$

where $g_{0,x}$ is the stomatal conductance during periods without carbon assimilation [mol m^{-2} s^{-1}], g_1 is the stomatal regulation factor [-] and An_x is the net assimilation rate of carbon [mol m^{-2} s^{-1}], computed according to Leuning (1995) in the photosynthetic module. The term g_1 is expressed by Leuning's equation (1995):

$$g_1 = strs_\theta \frac{a_1 \, f_{VPD}}{10^6 (P_{CO2} - \gamma)/P_{atm}} \tag{2.25}$$

where $strs_\theta$ is a stress factor depending on the soil water potential, ranging from 0 to 1, and taking into account stomata closure under drought conditions, a_1 is the stomatal resistance factor [-], f_{VPD} is a function depending on the vapour pressure deficit (VPD), P_{CO2} is the canopy air CO_2 partial pressure [Pa] and γ is the compensation point of photosynthesis [Pa]. In this equation, a_1 and γ are two species-specific parameters.

Once total canopy transpiration has been computed, water uptake is computed in each soil layer:

$$U_i = TR \frac{f_{up,i}}{\sum_{i=1}^{n} f_{up,i}} \tag{2.26}$$

where U_i is the water uptake in soil layer i [mm day^{-1}], TR is the total transpiration [mm day^{-1}] and $f_{up,i}$ is a factor depending on root distribution, water availability and soil aeration in layer i, which denotes the ability of roots to extract water from a given soil layer.

2.2.2 Phenology

The phenology module determines the phenological stages of plant species, i.e. plant development stages. Dynamics and processes within the plant appear to vary depending on the growth stage (Wardlaw, 1990). The number and the characteristics of these stages are specific to the modelled plant species. For instance, deciduous species go through periods with or without leaves while the main difference for perennial species that do not shed their leaves occurs between the vegetative and reproductive phase. During this latter phase, a significant part of their resources is allocated to the reproductive organs. In order to take these dynamics into account, a subroutine estimating the beginning and the end of the phenological stages has been implemented for each ecosystem in the TADA model.

2.2.1.1. Cropland ecosystems

A great amount of crop phenology models exists, with the temperature as a main driving variable (Salazar-Gutierrez et al., 2013). However, more complex models (like STICS) include the influence of soil humidity during germination and emergence, and the influence of vernalization and photoperiod. As vernalization might be important for some plant species, as winter wheat (Palosuo et al., 2011), the phenology module of STICS was adopted. All the equations of the STICS model are described in Brisson et al. (2008). However, some modifications have been made in order to adapt these equations to TADA. The crop phenology module adapted to winter wheat is composed of nine phenological stages as defined in table 2.1. Development units (UPVT) are accumulated during a phenological stage and the transition to the next stage occurs when this accumulation reaches a given threshold. This variable is used from the first to the seventh stage, as the two last stages are controlled by the harvest and sowing dates.

Table 2.1: Modelled phenological stages with an estimated correspondence to the BBCH scale

stages	**winter wheat phases**	**BBCH-scale**
1	sowing - germination	00-05
2	germination - emergence	05-10
3	emergence - terminal spikelet initiation	10-30
4	terminal spikelet initiation - flag leaf ligule visible	30-39
5	flag leaf ligule visible - end of leaf growth	39-55
6	end of leaf growth - beginning of grain filling	55-71
7	beginning of grain filling - physiological maturity	71-90
8	physiological maturity - harvest	90-99
9	bare soil	-

The grain germinates, meaning that the second phenological stage is reached, when the development units accumulated from sowing exceed a given threshold called $UPVT_{germ}$. These development units, taking the growing

degree-days and the soil humidity into account, are computed as follows:

$$UPVT(n) = \sum_{n=\text{sow}}^{germ} [(T_{\text{soil}}(n) - T_{\text{base}}) * f_{\text{hum}}(n)] \tag{2.27}$$

where $T_{soil}(n)$ is the daily average soil temperature at the sowing depth [°C] and T_{base} is the base temperature for germination [°C]. The coefficient $f_{hum}(n)$, defined in equation 2.28, introduces the influence of soil humidity on the seed development.

$$f_{\text{hum}}(n) = \begin{cases} \frac{S_p * \theta_{\text{soil}}(n)}{\theta_{wp}} & \theta_{\text{soil}}(n) \leq \theta_{wp} \\ S_p + (1 - S_p) * \frac{\theta_{\text{soil}}(n) - \theta_{wp}}{\theta_{fc} - \theta_{wp}} & \theta_{soil}(n) > \theta_{wp} \end{cases} \tag{2.28}$$

where S_p is a parameter related to root sensitivity to drought and θ_{soil} is daily mean of soil water content at the sowing depth, θ_{wp} is the wilting point and θ_{fc} is the field capacity.

Once the grain has germinated, the emergence is achieved when the elongation of the coleoptile, computed as in equation 2.29, is greater than the sowing depth. As for the first stage, the development units for this second stage depend on temperature as well as on soil humidity. E_{max} is the maximum elongation of the coleoptile in darkness conditions [cm], C_p [-] and B_p [°C] are parameters of the subsoil plantlet elongation curve.

$$Elong(n) = E_{\max} * \left[1 - \exp\left(-\left(B_p * \sum_{n=germ}^{\text{emerg}} UPVT(n)\right)^{c_p}\right)\right] \tag{2.29}$$

From the emergence to the beginning of the grain filling, the development units take the growing degree-days, the vernalization and the photoperiod into consideration. Therefore, the following equations are applied from stage 3 to stage 6.

$$UPVT(n) = \sum_{n=\text{emerg}}^{\text{grain fill}} (GDD(n) * RFPI(n) * RFVI(n)) \tag{2.30}$$

where $GDD(n)$ is the growing degree-days [°Cd], $RFPI(n)$ is the photoperiod coefficient and $RFVI(n)$ is the vernalization coefficient. The $GDD(n)$ term is completely described in Brisson et al. (2008) but the two last terms might need some details.

The effect of photoperiod ($RFPI$) differs following the plant species. Long-day species, such as winter wheat, have an optimal development with a maximal photoperiod whereas short-day species, such as soybean, prefer a minimal photoperiod (figure 2.3).

This photoperiod coefficient, defined in equation 2.31, is estimated from several parameters (S_v, P_{sat}, P_{base}) and from the daily effective photoperiod $Pho(n)$. This new variable is computed according to the work of Weir et al. (1984) which is based on the site latitude and the Julian day number. Note that the photoperiod is considered effective from and until the sun is at 6° below the horizon.

$$RFPI(n) = (1 - S_v) * \frac{Pho(n) - P_{sat}}{P_{sat} - P_{base}} + 1 \tag{2.31}$$

S_v is related to photoperiod sensitivity, P_{sat} is the saturating photoperiod [hr] which corresponds to the photoperiod at which the coefficient $RFPI$ reaches 1 in figure 2.3 and P_{base} is the base photoperiod for development [hr] which is the photoperiod at which the $RFPI$ reaches 0 in figure 2.3.

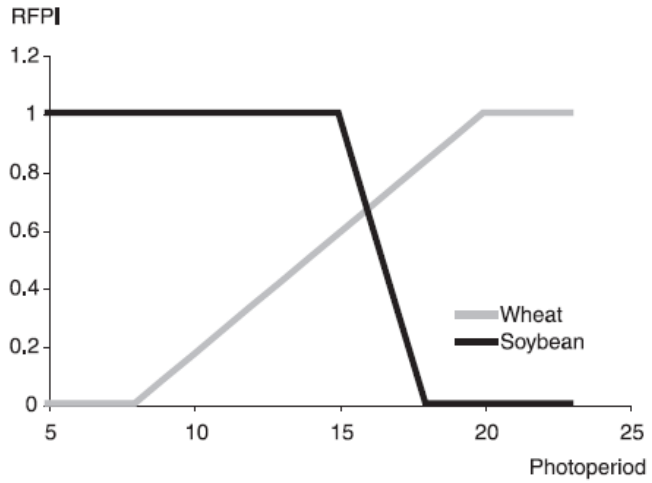

Figure 2.3: Photoperiod coefficient of winter wheat and soybean as a function of photoperiod [hr] if S_v=0 (Brisson et al., 2008)

The vernalization coefficient, whose equation is written below, must range from 0 to 1. If the cold requirement is not reached, this coefficient is lower than 1 and slows down the plant development.

$$RFVI(n) = \frac{\sum_{i=germ}^{grainfill}(VNI(n)) - VN_{\min}}{VN - VN_{\min}} \tag{2.32}$$

where $VNI(n)$ is the vernalizing value at a given day computed as in equation 2.33, VN_{min} is the minimum number of required vernalizing days and VN is the number of required vernalizing days.

$$VNI(n) = MAX\left(0; 1 - \left[\frac{T_{cold} - T_{air}}{A_{cold}}\right]^2\right) \tag{2.33}$$

with T_{cold} the optimal temperature for vernalization [°C] and A_{cold} the thermal amplitude around the optimal temperature [°C].

2.2.1.2. Grassland ecosystems

The phenology model adopted for grassland ecosystems is fully described in Lazzarotto et al. (2009). Compared to cropland ecosystems, this model is simpler as it consists of two different phases: the reproductive and vegetative phase. Lazzarotto et al. (2009) only consider the effect of temperature in the computation of the development units:

$$DU(n) = \frac{\sum_{n=1}^{N} MAX\left(0; \overline{T}_{7d}(n) - T_{base}(n)\right)}{T_{rep}(n)} \tag{2.34}$$

where $\overline{T}_{7\mathrm{d}}$ is the running mean for the daily average air temperature for a period of seven days [°C], T_{base} is the base temperature [°C], T_{rep} is normalization factor for grass development [°Cd] and N is number of simulated days. The reproductive phase starts when $\overline{T}_{7\mathrm{d}}$ exceeds the base temperature and ends when the accumulated development units reach a given threshold DU_{veg}.

2.2.3 Carbon cycle

Photosynthesis

The photosynthesis module estimates the gross assimilation rate of CO_2 by plants from the meteorological data, the green area index and the nitrogen content of the photosynthetic plant organs. The adopted model follows a biochemical approach, limiting the gross assimilation rate according to the regeneration of RuBP (Ribulose 1,5-bisphosphate) or the availability of Rubisco (RuBP carboxylase/oxygenase). Indeed, in high irradiance and below the ambient CO_2 concentration, the photosynthetic organs are Rubisco limited whereas they are limited because of the RuBP regeneration in low irradiance and above the ambient CO_2 concentration. There is a co-limitation of these two factors at intermediate irradiance (de Pury, 1995). This phenomenon, depicted in figure 2.4, is modelled with a non-rectangular hyperbola detailed in equation 2.35. The net assimilation rate A_n is estimated from the gross assimilation rate A_c from which the dark respiration is removed. It is germane to note that in this model, the whole canopy is considered as composed of two big leaves: a sunlit and a shaded leaf, justifying its name of sun/shade model.

$$\theta_{\mathrm{a}} A_{\mathrm{c}}^2 - (A_{\mathrm{j}} + A_{\mathrm{v}})\, A_{\mathrm{c}} + A_{\mathrm{j}} A_{\mathrm{v}} = 0 \tag{2.35}$$

where θ_a is a curvature factor, A_c is the gross canopy assimilation rate per unit ground area [μmol m^{-2} s^{-1}], A_v is the assimilation rate limited by Rubisco [μmol m^{-2} s^{-1}] and A_j is the assimilation rate limited by RuBP regeneration [μmol m^{-2} s^{-1}].

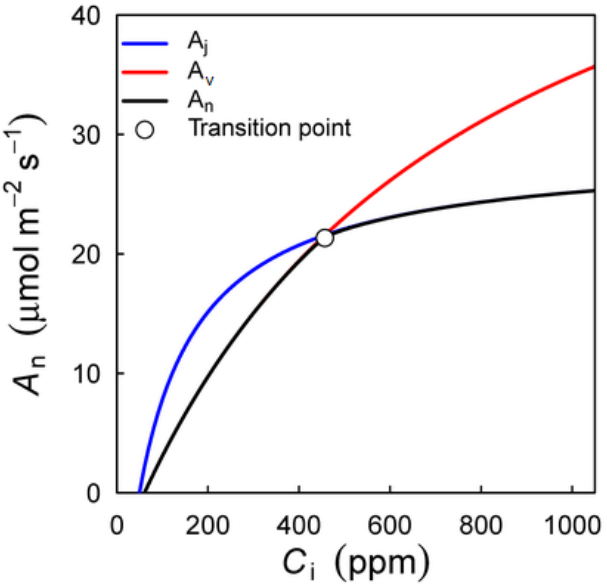

Figure 2.4: Assimilation-CO_2 concentration curve according to the Farquhar model (Duursma, 2015)

The equations of these two limited assimilation rates (A_v and A_j), as well as other elements that are not developed in this thesis, are amply described in de Pury & Farquhar (1997). A_v and A_j mainly depend on the intercellular CO_2 partial pressure C_i and, respectively, the photosynthetic Rubisco capacity (V) and the electron transport rate (J).

The **photosynthetic Rubisco capacity** V at a given temperature is derived, with a normalized Arrhenius equation, from the photosynthetic Rubisco capacity at a reference temperature V_0 which is computed from the nitrogen content of photosynthetic organs according to equation 2.36:

$$V_0 = \chi_n * (N_c - GAI * N_b) \tag{2.36}$$

where χ_n is the ratio of photosynthetic capacity to leaf nitrogen at the reference temperature, N_c is the nitrogen content of photosynthetic organs [mmol(N) m^{-2}], GAI is the green area index and N_b is the nitrogen content of photosynthetic organs not associated with photosynthesis [mmol(N) m^{-2}].

The **electron transport rate** J is related to the PPFD absorbed by the Photosystem II. This dependence can also be modelled with a second non-rectangular hyperbola. In order to obtain the PPFD absorbed by each type of leaves (sunlit and shaded), the global radiation must be divided into a direct or diffuse fraction according to the BRL model (Ridley et al., 2010):

$$f_d = \frac{r_d}{r_g} = \frac{1}{1 + e^{\beta_0 + \beta_1 k_t + \beta_2 AST + \beta_3 \alpha + \beta_4 K_t + \beta_5 \psi}} \tag{2.37}$$

where f_d is the diffuse fraction of global radiation [-], r_d and r_g are the diffuse and global solar radiation [W m^{-2}], k_t is the clearness index at a 30-minute time step, which corresponds to the ratio of r_g to the extraterrestrial radiation r_et [-], AST is the apparent solar time [hr], α is the solar angle [degree], K_t is the daily clearness index [-] which is computed as TADA reads the meteorological data, ψ is the persistence which corresponds to k_t averaged on two successive time steps [-] and β_i are fitting parameters [-]. The determination of AST, α and r_et is initially present in the ASPECTS model and is mainly based on the work of de Pury & Farquhar (1997). Once the distinction between diffuse and direct is made, the PPFD (photosynthetic photon flux density) of these two fractions are obtained as follows:

$$PPFD_b = 4.6 * 0.45 * r_b = 4.6 * 0.45 * (1 - f_d) * r_g \tag{2.38}$$

$$PPFD_d = 4.6 * 0.65 * r_d = 4.6 * 0.65 * f_d * r_g \tag{2.39}$$

where $PPFD_b$ and $PPFD_d$ are respectively the direct and diffuse PPFD [μmol m^{-2} s^{-1}], 4.6 is a conversion factor (from W m^{-2} to μmol m^{-2} s^{-1}), 0.45 and 0.65 are the fractions of PPFD in beam and diffuse solar radiation and r_b is the direct solar radiation [W m^{-2}].

The equations computing the PPFD absorbed by the sunlit and shaded leaves from the diffuse and direct fraction are all listed in de Pury & Farquhar (1997). In addition to the sun/shade distinction, the absorbed PPFD is initially computed for overcast periods in ASPECTS, allowing the computation of carbon assimilation rate under cloudy conditions.

Besides V and J, the **intercellular CO_2 partial pressure** C_i is a significant driver of the gross assimilation rate A_c. However, this variable is unknown before entering the photosynthesis module. In order to overcome this problem, a second equation is associate to equation 2.35, forming a system of two equations and two unknowns: A_c and C_i. This second equation is describing the diffusion of CO_2 though the stomata:

$$A_n = \frac{C_{atm} - C_i}{r_s} \tag{2.40}$$

where C_{atm} is the atmospheric CO_2 concentration and r_s the stomatal resistance [s m^{-1}]. The computation of the stomatal resistance requires the value of the net assimilation rate A_n (Leuning, 1995) which is equal to the gross assimilation rate A_c decreased by the dark respiration. De Pury & Farquhar (1997) assumed that the dark respiration at 25°C is equal to $0.0089V_0$. With the normalized Arrhenius function, the dark respiration can be estimated for any temperature. Finally, this system of two equations and two unknowns can be solved with the Newton-Raphson method.

Respiration

Plant growth models distinguish two functional components of dark respiration: a maintenance and a growth component. The maintenance respiration is "associated with the maintenance of existing biomass" whereas the growth respiration is "associated with the synthesis of new biomass" (Amthor, 1984). Based on the work of McCree (1970) and Thornley (1970), Amthor (1984) describes plant growth with the following equation:

$$\frac{dW}{dt} = Y_{\mathrm{G}}(P - mW) \tag{2.41}$$

where W is the dry mass of the living tissue, Y_G is the growth conversion efficiency, P is the gross photosynthesis and m is the maintenance coefficient. According to this equation, mW represents the maintenance respiration component and $(1 - Y_G)(P - mW)$ is the growth respiration component. These two elements, computed for croplands and grasslands in the TADA model, follows the same approach as in equation 2.41, considering the maintenance respiration as a function of the living biomass, with a coefficient m depending on the ecosystem, and the growth respiration as the carbon loss during the conversion of available sugar into new biomass.

The computation of cropland maintenance respiration is based on the work of Spitters et al. (1989) for the SUCROS model, as defined in the following equation:

$$RM_x = mW_x = f_x * Q10^{\frac{T_{air}-25}{10}} * W_x \tag{2.42}$$

where RM_x is the maintenance respiration of the organ x [gC m^{-2} day^{-1}], f_x is a maintenance coefficient depending on the organ (0.015 for the stem and roots, 0.03 for the leaves and 0.01 for the storage organs), W_x is the dry matter of the organ x [gDM m^{-2}], $Q10$ is the temperature coefficient with T_{air} the air temperature [K]. The total maintenance respiration is the sum of the stem, roots, leaves and storage organs maintenance respiration.

The maintenance respiration for grassland ecosystems is established from the equations proposed by Lazzarotto et al. (2009):

$$RM = mW = RM_0 * rm * [f(T_{air}) * W_{sh} + f(T_{soil}) * W_{rt}] * \frac{C_s}{C_s + \kappa_r} \tag{2.43}$$

where RM is the total maintenance respiration [gC m^{-2} day^{-1}], RM_0 is the reference maintenance respiration rate at 20 °C [gC gDM^{-1} day^{-1}], rm is the maintenance respiration weighting coefficient, W_{sh} and W_{rt} are respectively the shoot and root dry matter [gDM m^{-2}], C_s is the carbon substrate concentration [gC gDM^{-1}] and κ_r is a maintenance respiration constant. As TADA does not differentiate substrate from structural carbon, C_s is considered as a constant percentage of dry matter. $f(T)$ is a temperature response function defined as:

$$f(T) = \mathrm{MAX}\left(0; \frac{(T - T_{low})^{Q10} * (T - T_{up})}{(T_{ref} - T_{low})^{Q10} * (T_{ref} - T_{up})}\right) \tag{2.44}$$

where T_{low} ans T_{up} are the boundaries of the accepted temperature range [K], T_{ref} is the reference temperature [K] and $Q10$ is the temperature coefficient. This function can be computed for soil and air temperature.

The computation of the total growth respiration is similar for cropland and grassland ecosystems. Both of them follows the equation 2.41 but grasslands have a constant growth efficiency Y_G (equal to 0.74 according to Choudhury (2000)) while, according to Van Keulen et al. (1982), the growth efficiency of croplands is based on the carbon partitioning coefficients as follows:

$$Y_G = (alloc_{lf} * 0.72 + alloc_{st} * 0.69 + alloc_{so} * 0.73) * alloc_{sh} + alloc_{rt} * 0.72 \tag{2.45}$$

where $alloc_{lf}$, $alloc_{st}$, $alloc_{so}$, $alloc_{sh}$ and $alloc_{rt}$ are the fraction of carbon allocated to, respectively, the leaf, the stem, the storage organ, the shoot and the root compartment. They are presented in the following section.

Allocation

The allocation of net assimilates, i.e. carbon partitioning, is generally associated with the phenological stages in plant growth models (Wardlaw, 1990; Marcelis & Heuveling, 2007). In the TADA model, the partitioning between plant organs is considered constant during a phenological stage for croplands while it changes with development units and shoot/root ratio for grasslands.

The constant allocation coefficients for winter wheat crops, taken from Arora & Gajri (1998), are included in table 2.2. As a reminder, phenological stages are listed in table 2.1. Firstly, the assimilates are divided into the shoot or root compartment, with an increasing priority for the above-ground compartment as the plant develops. Then, the shoot assimilates are partitioned between the leaves, the stem and the storage organs. This latter compartment starts to grow at the beginning of grain filling. Finally, within the stem, there is a reserve compartment which increases until the grain filling period. The carbon remobilization from the reserve compartment toward the storage organs (the grain) is detailed in the following section. The 3.5 phenological stage corresponds the middle of stage 3 and the 7.5 phenological stage begins ten days after anthesis (i.e. flowering).

Table 2.2: Allocation coefficients for shoot, leaf, stem, reserve, storage organ and root compartments from emergence to physiological maturity of winter wheat

stages	$\mathbf{alloc}_{sh}$	$\mathbf{alloc}_{lf}$	$\mathbf{alloc}_{st}$	$\mathbf{alloc}_{res}$	$\mathbf{alloc}_{so}$	$\mathbf{alloc}_{rt}$
3	0.5	0.325	0.17	0.005	0	0.5
3.5	0.7	0.49	0.204	0.006	0	0.3
4	0.9	0.45	0.44	0.01	0	0.1
5	0.95	0.143	0.727	0.08	0	0.05
6	0.97	0	0.485	0.485	0	0.03
7	0.98	0	0.49	0.49	0	0.02
7.5	1	0	0	0	1	0
8	1	0	0	0	1	0

The carbon allocation adopted for grasslands is based on a teleonomic or goal-seeking partitioning (Thornley, 1995; Lazzarotto et al., 2009). The shoot/root partitioning coefficients are defined as follows:

$$\begin{cases} alloc_{\mathrm{sh}} = \frac{\varphi}{1+\varphi} \\ alloc_{\mathrm{rt}} = \frac{1}{1+\varphi} = 1 - alloc_{\mathrm{sh}} \end{cases} \tag{2.46}$$

where φ is a partitioning function computed with the following equation:

$$\varphi = \frac{W_{\mathrm{rt}}}{W_{\mathrm{sh}}} \frac{(\kappa_C + C_s)}{C_s} \frac{N_s}{(\kappa_N + N_s)} \tag{2.47}$$

where W_{sh} and W_{rt} are the shoot and root dry matter [gDM m^{-2}], C_s is the estimated constant percentage of non-structural carbohydrates in dry matter [gC gDM^{-1}] and N_s is the nitrogen substrate concentration which is estimated by the ratio of the plant nitrogen reserve on the total dry matter [gN gDM^{-1}]. κ_C and κ_N are teleonomic partitioning constants. This teleonomic partitioning aims to maintain a particular root/shoot ratio. Therefore, if the plant experiences a decrease in above-ground biomass, for instance because of grazing, the plant will respond with an amplified allocation to the shoot compartment.

In addition, the allocation pattern during the reproductive phase differ from the vegetative phase. Indeed, the plant needs resources for flowering and seed production during the reproductive phase. The allocation of new assimilates to the shoot compartment is hence prioritized during this phase. In order to take this varying allocation pattern into account, Lazzarotto et al. (2009) modified the shoot/root partitioning coefficients during the reproductive phase according to Riedo et al. (1998):

$$\begin{cases} alloc'_{\mathrm{sh}} = alloc_{\mathrm{sh}} + (1 - \lambda_{\mathrm{rep}})\, alloc_{\mathrm{rt}} \\ alloc'_{\mathrm{rt}} = \lambda_{\mathrm{rep}} alloc_{\mathrm{rt}} = 1 - alloc'_{\mathrm{sh}} \end{cases} \tag{2.48}$$

where the factor λ_{rep} is equal to 1 during the vegetative phase and lower than 1 during the reproductive phase. This factor is computed according to the grass phenology:

$$\lambda_{\mathrm{rep}} = \lambda_{\mathrm{rep,ear}} + (1 - \lambda_{\mathrm{rep,ear}})\, \mathrm{MAX}\left[0, \left(1 - \frac{\mathrm{DU}}{\mathrm{DU}_{\mathrm{ear}}}\right)\right] \tag{2.49}$$

$\lambda_{rep,ear}$ is the coefficient of preferential shoot allocation after ear emergence, DU are the development units [°Cd] computed according to the equation 2.34 and DU_{ear} is the development units at ear emergence.

Reserve remobilization

This module of the TADA model only concerns cropland ecosystems and is specific to winter wheat. During the grain filling period, winter wheat plants remobilize their accumulated reserve toward the grain. This reserve is constituted of non-structural carbohydrates (NSC) which can either be starch or water-soluble carbohydrates (fructose, fructan, sucrose, glucose).

According to Ehdaie et al. (2008), the stem water-soluble carbohydrate (WSC) content starts to decrease following a sigmoid curve several days after the anthesis. In winter wheat plants, the NSC content is mainly composed of WSC (Kiniry, 1993; Wardlaw & Willenbrink, 2000). Therefore, in the TADA model, the entire reserve compartment is assumed to follow the sigmoid function defined in equation 2.50 during the reserve remobilization.

$$y_{\text{sigm}}(t) = \frac{1}{1 + \exp(-a * (t - c))} \tag{2.50}$$

where a and c are sigmoid parameters fitting the observations of Ehdaie et al. (2008). According to their work, the stem WSC content levels out fifty days after the anthesis, thus defining the end of the sigmod curve. At that moment, it is assumed that approximately 80% of the stem WSC content has been remobilized to the grain since the beginning of the reserve remobilization. The reserve content at a given time t is hence computed as follows:

$$Res(t) = Res\,(t_f) + \frac{y_{\text{sigm}}(t)}{y_{\text{sigm}}\,(t_i)} * [Res\,(t_i) - Res\,(t_f)] \tag{2.51}$$

where $Res(t)$, $Res(t_i)$ and $Res(t_f)$ are the reserve content [gC m^{-2}] at, respectively, time t, the initial remobilization time (ten days after anthesis) and the final remobilization time (fifty days after anthesis).

According to Ehdaie et al. (2006), the efficiency of WSC mobilization and transport to the grain depends on the internode. The TADA model uses the mean value of the efficiency of the different internodes, which is equal to 75%. Therefore, at the end of the remobilization period, the amount of carbon reaching the grain corresponds to:

$$Remob_{\text{grain}} = 0.75 * (Res\,(t_i) - Res\,(t_f)) \tag{2.52}$$

Consequently, the remaining 25% are lost by plant respiration.

Litter production and rhizodeposition

Fluxes entering the litter pool correspond to the senescence of plant organs. The carbon and nitrogen contained in plant tissues are transferred to the pools of litter contained in the soil profile. The above-ground dead biomass enters the litter pool of the first soil layer while root dead materials remain as litter in their corresponding soil layer. For winter wheat, only leaf senescence is considered for the above-ground organs, as stems generally remain until maturity. For ryegrass, on the contrary, all the shoot material is subject to senescence and returns to the litter pool after a given lifetime. Note that the lifetime of each leaf or stem is not modelled in TADA, but a continuous flux of C and N due to senescence is computed according to:

$$lit_{X,C} = \frac{X_C * f(T_{air})}{\tau_X * f_\theta} \quad \text{and} \quad lit_{X,N} = \frac{X_N * f(T_{air})}{\tau_X * f_\theta} \tag{2.53}$$

where X_C and X_N represent the carbon or nitrogen content of the leaves reservoir for croplands (X=*leaf*) or the shoot reservoir for grasslands (X=*shoot*) [gC or gN m^{-2}], τ_X is the lifespan of leaves or shoot [days], $f(\theta)$ and $f(T_{air})$ are the water and air temperature factors affecting plant organs turnover. These factors are based on Lazzarotto

et al. (2009). The air temperature factor is the same as in equation 2.44 and the water factor is calculated as:

$$f(\theta) = \begin{cases} f_{\text{anaerob}} & \text{if } \theta = \theta_{\text{sat}} \\ 1 - (1 - f_{\text{anaerob}}) \frac{\theta - \theta_{\text{anaerob}}}{\theta_{\text{sat}} - \theta_{\text{anaerob}}} & \text{if } \theta_{\text{anaerob}} < \theta < \theta_{\text{sat}} \\ 1 & \text{if } \theta_{\text{ws}} < \theta \leq \theta_{\text{anaerob}} \\ \frac{\theta - \theta_{\text{wp}}}{\theta_{\text{ws}} - \theta_{\text{wp}}} & \text{if } \theta_{\text{wp}} < \theta \leq \theta_{\text{ws}} \\ f_{min} & \text{if } \theta \leq \theta_{\text{wp}} \end{cases} \tag{2.54}$$

with θ_{ws} the soil water content at scarcity, which corresponds to the SWC at incipient water stress for plant, before reaching the wilting point, θ_{anaerob} the soil water content in anaerobic condition, which takes into account the oxygen deficiency that induces shoot and root stress. $f_{anaerob}$ and f_{min} are parameters equal to 0.7 and 0.1 respectively. The water factor is calculated for each soil layer, and weighted averaged until the rooting depth. Equation 2.54 illustrates that between scarcity and anaerobic conditions, organs lifespan is higher, as f_θ is equal to 1. As SWC increases above the anaerobic condition or decreases below scarcity, f_θ decreases, and the litter fluxes given by equation 2.53 are enhanced.

For roots, the litter flux for soil layer i is given by:

$$lit_{root,C,i} = \frac{root_{C,i} * f(T_{soil})}{\tau_{root} * f_\theta} \quad \text{and} \quad lit_{root,N,i} = \frac{root_{N,i} * f(T_{soil})}{\tau_{root} * f_\theta} \tag{2.55}$$

with $root_{C,i}$ and $root_{N,i}$ the root carbon or nitrogen content in layer i, $f(T_{soil})$ the temperature factor computed with equation 2.44, where the averaged soil temperature along the soil profile is used, τ_{root} the roots lifespan and f_θ the water factor, calculated with equation 2.54.

Rhizodeposition from root segments leads to fluxes of C and N leaving the roots reservoirs, and fueling the soil litter pools. The term *rhizodeposition* covers exudates, mucillage, secretion and emission of gases. This flux is calculated considering that 13.5% of the increase of roots C and N content is lost by rhizodeposition, according to the results of Newman (1978).

2.2.4 Grazing

In order to take the effect of grazing on plant growth , on soil N cycle and on GHG emissions into account, a new grazing module was added in TADA (figure 2.5). This grazing module is quite basic compared to other grazing models, but could be improved if some weaknesses are noted during future model tests.

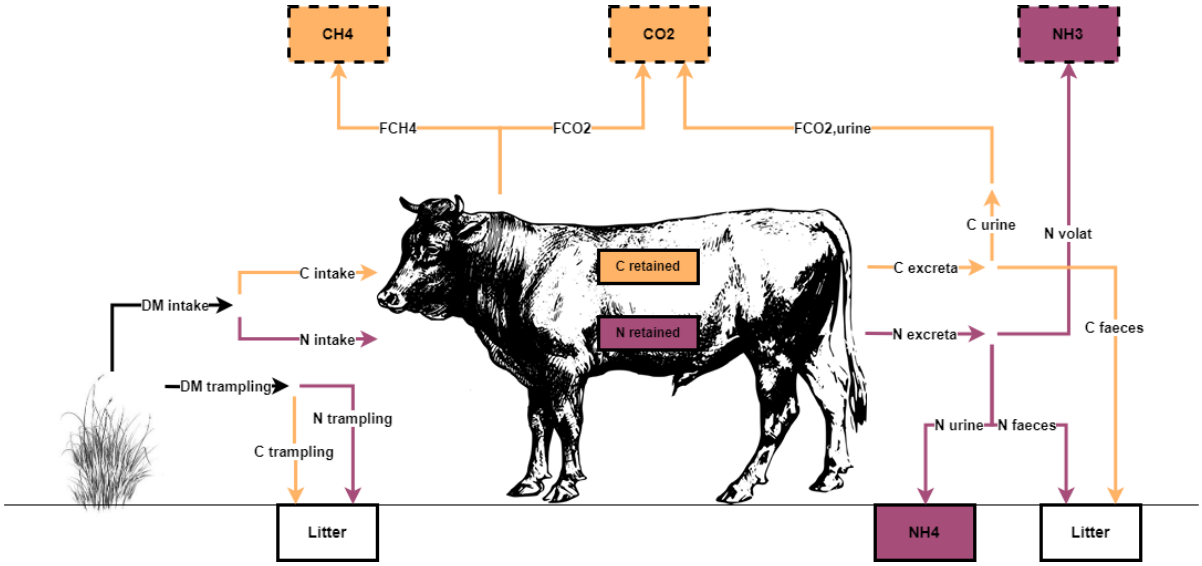

Figure 2.5: Diagram of carbon and nitrogen fluxes in the grazing module (orange stands for carbon, purple stands for nitrogen and black stands for both carbon and nitrogen).

Cattle dry matter intake DM_{intake} is computed as a trade-off between the animals intake capacity, i.e. the maximum dry matter intake in optimal conditions, and the available dry matter. Thanks to an allometric relationship between shoot height and shoot DM, grass height can be computed at any moment of the simulation. If shoot height falls below a limit grass height under which cows can no more graze, the intake is null and the modeller is warned that the pasture is overgrazed. As a default value, a limit grass height of 3cm can be used. If grass is high enough, the maximum DM intake [gDM m^{-2} day^{-1}] is then computed as follows:

$$DM_{intake,max} = DM_{cap} * n_{cattle} \tag{2.56}$$

where DM_{cap} is the animals DM intake capacity set by default at 1500 gDM LU^{-1} day^{-1}, considering that one LU of 600 kg consumes on average a DM quantity of 2.5% of its weight per day (Singhal et al., 2005). The same estimation was made by Zeeman et al. (2010). Specified by the user as an input, n_{cattle} is the number of LU per m^2. The actual DM intake is computed as follows:

$$DM_{intake} = \begin{cases} DM_{intake,max} & \text{if} \quad DM_{available} \geq DM_{intake,max} \\ DM_{available} & \text{if} \quad DM_{available} < DM_{intake,max} \end{cases} \tag{2.57}$$

where $DM_{available}$ is the available DM, computed as the difference between the actual grass DM content and the DM corresponding to the limit grass height of 3cm. Note that in this first version of TADA grazing module, livestock is only consuming standing biomass and no concentrate feed is considered.

The C and N intakes are directly evaluated from the DM intake, considering a constant C and N content per g of DM:

$$C_{intake} = dm_c * DM_{intake} \quad \text{and} \quad N_{intake} = dm_n * DM_{intake} \tag{2.58}$$

where C_{intake} and N_{intake} are expressed in gC m^{-2} day^{-1} and in gN m^{-2} day^{-1} respectively and dm_c and dm_n are the carbon and nitrogen contents of dry matter [gC gDM^{-1}], [gN gDM^{-1}], taken as constant values of 42.71 and 2.75% (measured in Dorinne grassland site). These fluxes of C and N intake are two additional fluxes leaving the shoot carbon and shoot nitrogen reservoirs during grazing periods.

The nitrogen intake has different fates: a part of it is retained for milk or meat production and the rest returns the soil as excreta, under the form of urine or faeces. The percentage of retained nitrogen is hard to evaluate, and mainly depends on the type of cow (milking or suckler cow) and on its development stage. As a first approximation, the hypothesis is made that a very small quantity of nitrogen and carbon is retained by suckler cows, compared to other fluxes. This hypothesis was also made by Gourlez et al. (2019) when estimating the carbon budget of cows. However, in the TADA model, the user still has the choice to modify $f_{ret,N}$ and $f_{ret,C}$, the percentages of N and C retained for milk or meat production. Once N retention has been computed, the remaining part is considered to be ejected as excreta, of which a fixed percentage is volatilized as ammonia (Menzi et al., 1997 cited by Riedo et al., 2000):

$$N_{volat} = f_{volat} N_{intake} (1 - f_{ret,N}) \tag{2.59}$$

where f_{volat} is the percentage of excreta N volatilized as NH_3, and N_{volat} is expressed in gN m^{-2} day^{-1}. After having deduced the volatilized N, the remaining excreta is divided into faeces and urine forms, according to a constant fraction, f_{urine}:

$$N_{urine} = f_{urine}(1 - f_{volat}) N_{intake}(1 - f_{ret,N}) \quad \text{and} \quad N_{faeces} = (1 - f_{urine})(1 - f_{volat}) N_{intake}(1 - f_{ret,N}) \tag{2.60}$$

where N_{urine} and N_{faeces} are expressed in gN m^{-2} day^{-1}. A value of 0.6 was chosen for f_{urine}, according to Oenema et al. (1997). Nitrogen excreted as faeces enters the surface litter pool, where its fate is considered similar to the one of dead biomass. Nitrogen under the form of urine is assumed to be directly hydrolyzed by urease, and enters the NH_4 pool, according to Riedo et al. (2000).

As for nitrogen, the carbon intake may follow different paths: some of it may be used for milk or meat production, some carbon is emitted to the atmosphere as CO_2 by cattle respiration or as CH_4 by enteric fermentation. The remaining part is lost as urine of faeces. Fixed percentages of carbon intake are considered to be emitted as CO_2 and CH_4:

$$F_{CO2} = f_{resp}\, C_{intake} \quad \text{and} \quad F_{CH4} = f_{meth}\, C_{intake} \tag{2.61}$$

where F_{CO2} and F_{CH4} are expressed in gC m^{-2} day^{-1}. A value of 0.03 is assigned to f_{meth} as a first approximation. Values ranging between 3 and 5% were reported by Crush et al. (1992), Vuichard et al. (2007) and Martin et al. (2010). The value of f_{resp} was based on Gourlez de la Motte et al. (2016) who estimated this proportion at around 0.73 from measurements of organic matter digestibility on a grazed pasture.

The carbon lost as urine is computed from the urine N flux, considering a constant C/N ratio in urea of 12:28:

$$C_{urine} = (C/N)_{urea} * N_{urine} \tag{2.62}$$

where C_{urine} is expressed in gC m^{-2} day^{-1}. The carbon contained in urine is assumed to be directly lost by respiration. Finally, the lost of C in the form of faeces is deducted from a mass balance:

$$C_{faeces} = C_{intake}(1 - f_{ret,C}) - F_{CO2} - F_{CH4} - C_{urine} \tag{2.63}$$

where C_{faeces} is a carbon flux in gC m^{-2} day^{-1}, entering the surface litter pool.

One last phenomenon taken into account in the grazing module is the shoot trampling by cattle. The herd does not only defoliates grass during biomass consumption. It also runs over grass, degrading it and leading to a flux of dead biomass. This phenomenon is taken into account in an improved version of PaSim by Vuichard et al. (2007). It is estimated that, with a stocking rate of 1 LU ha^{-1}, 0.8% of the herbage biomass is returned each day to a litter pool. The exports of C and N due to trampling may be computed as:

$$C_{trampling} = f_{remove} * 10,000 n_{cattle} * shoot_C \quad \text{and} \quad N_{trampling} = f_{remove} * 10,000 n_{cattle} * shoot_N \tag{2.64}$$

where $shoot_C$ and $shoot_N$ are the shoot C and N reservoirs in gC and gN, and $C_{trampling}$ and $N_{trampling}$ are expressed in gC m^{-2} day^{-1} and gN m^{-2} day^{-1}. The stocking density n_{cattle} is multiplied by 10,000 to obtain a number of LU per ha, as f_{remove} is expressed as a percentage of exported biomass per LU per ha.

In TADA, no attention is paid to the nutritional status of the animals themselves. Note that even if the C and N retained by animals for milk or meat production are represented by boxes in figure 2.5, cows are not considered as reservoirs, and the temporal evolution of their mass is not assessed. Also, this module uses a rough estimation of the intake capacity, while more precise estimations should take the type of cow, its age, its liveweight, its physiological status, its environment, the feed characteristics, etc. into account (Graux et al., 2011). This approach is rather developed in zootechnics models, but could be implemented in TADA, depending on the results provided by the grazing module.

2.2.5 Management

The management routine covers the different human operations that take place on a grassland or a cropland. The date, the type of operation and some additional information have to be entered in the model by the user (see section 2.1.3).

Tillage During tillage, the disturbed soil layers are mixed, affecting the soil bulk density, the soil microorganisms and different soil reservoirs. This operation is interpreted in the model as a homogenization over several layers (number of layers depending on tillage depth) for which variable values are set to the average computed over the tillage depth. The disturbed reservoirs are the carbon and nitrogen content of litter, the carbon and nitrogen content of SOM, the NO_3 and NH_4 concentrations, the soil water content and the soil temperature.

Fertilisation Regarding the fertilisation, only the nitrogen and carbon composition of fertilisers, composts and the manure are taken into account. The effect of phosphorus, potassium or other chemical compounds are not modelled in TADA. Nitrogen fertilisation can be liquid or solid, but for solid fertilisation, N is incorporated into the first soil layer only with the first precipitation greater than 0.1 mm 30 min^{-1}. Nitrogen can be found in three forms in fertilisers: nitrate, ammonium and urea. The percentage of these different forms in a fertiliser must be specified by the user, as these molecules can follow different processes before being incorporated into the soil. NO_3 and NH_4 directly enter their respective pool in the first soil layer. Urea first has to be hydrolyzed, a chemical reaction which will change one molecule of urea into two molecules of NH_4 and one of HCO_3. This process is assumed to be immediate in the model. A part of the the urea can leave the system by volatilization (around 7% of the urea according to Schjoerring & Mattson, 2001). The composition of compost or manure (C and N contents) is entered by the user, and the C and N contained in it are directly incorporated into the litter pool of the first soil horizon.

Sowing The sowing operation is defined by the user, with the day, density and depth specified as inputs. When the simulation reaches that day, it enters in a new phenological stage starting from the sowing to the seed germination. Moreover, the carbon and nitrogen content of the grain are estimated based on measurements made at Lonzée experimental site for winter wheat grain (41.7% of carbon and 1.53% of nitrogen). The carbon and nitrogen content of the grain is distributed into the different organs using the same coefficients as for the stage 3 (see table 2.2).

Winter wheat harvest During the harvest, a part of the above-ground material is removed from the system, but the rest of the plant organs enters the litter pool. The remaining above-ground materials reach the first soil horizon while dead roots move to the litter pool in the corresponding layer. The proportion of the above-ground biomass left on the field is calculated from measurement done at Lonzée experimental site. At harvest, it is assumed that all the reproductive organ is harvested.

Grass harvest When grass is harvested, the height left after the cutting must be specified by the user. An allometric equation fitted to field data is used to calculate the amount of C and N left in the above-ground vegetation. The difference between the remaining biomass and the previous content of the shoot reservoirs is assumed to be harvested. The impact of the harvest on the shoot and root senescence rates is not considered in the model.

2.3 Computer programming

This section aims to be a simplified user guide, making the TADA model easy to pick up. TADA is composed of three different types of files: the *.f90* files which correspond to the code divided into program units according to the different modules presented in the section 2.2, the *.txt* files which are the model inputs presented in section 2.1.3 and the *.blk* files which list the global variables and parameters, i.e. the shared values among the program units.

The *.f90* files are program units or groups of program units written in Fortran 90, as their file extension indicates. In this language, the program units are called subroutines. Each of them refers to a process or a module, such as the "pheno_wheat.f90" file which corresponds to the crop phenology module or the "can_hydro.f90" file which refers to the water interception process. For a simple usage of the model, without any intention of modifying the processes, the *.f90* files must be kept untouched. All the parameters that can be adapted or calibrated are defined outside these files.

As the different processes are interconnected, and so are the different subroutines, the value of a variable computed in one subroutine might be required in other subroutines. It is one of the roles of the *.blk* files. The *common* function makes the mentioned variables "global" and, at the same time, the dimensions of these variables are declared. The second role of these files is the declaration of parameters input, thanks to the *parameter* function. This function assigns a constant value to an expression that can also be shared among the program units. Only two of these files, containing the parameters assignment, need adjustment from the user: *species.blk* and *parameter.blk*. The first file consists of a list of parameters that depend on the studied species and ecosystem. These parameters, detailed in Appendix C (table C.1), come from the literature or have been calibrated. The second file contains general parameters essential to the model, such as the name of the input files, the beginning year, the number of meteorological data per day, etc (see the complete list in Appendix C, table C.2). Note that all the file names might be chosen in *parameter.blk* except for the meteorological data file which must have the following form: *weatheryear.txt*. The meteorological data for 2015, for example, is written *weather2015.txt*. If the simulation covers several years, there must be as many meteorological files as the number of years simulated.

The *.txt* files contain the meteorological data, the soil data, the initial reservoirs content and the management information. The meteorological data file does not accept any undefined value (i.e. NaN values) and must be established according to the following pattern:

Day [$JulianDays$]	Global radiation [W/m^2]	Air temperature [$°C$]	Precipitation [mm]	Relative humidity [$-$]	Wind velocity [m/s]	Atm pressure [hPa]
...	...	...	...	...	...	...

The soil data file contains general soil characteristics, such as the average slope and the length to the outlet, and then characteristics related to each soil layer (soil texture, bulk density, etc.). The number of lines describing these last characteristics must coincide with the parameter *nhz* which defines the number of soil layers in *parameter.blk*. In the initial reservoirs content file, the user must fill in the starting phenological stage in addition to the initial values of the reservoirs. The values for grasslands and croplands with the way they are obtained are presented in tables C.4 and C.3 (Appendix C). The three other variables next to the phenological stage (nspec, rt_{dpt}, stand_{age}) are exclusively for forests so the entered value has no impact. As for the meteorological data file, these files must not contain any undefined values. Regarding the management file, the way to complete it is described at the end of the concerned file. This chronological list might cover several years and includes the Julian days, the type of operation and some supplementary information.

Chapter 3

Experimental sites

The calibration and validation of the model presented beforehand will require GHG, biomass and meteorological data acquired in instrumented sites. We have the opportunity to benefit from the data collected in two major Belgian experimental sites that are under the responsibility of Gembloux Agro-Bio Tech: a cropland in Lonzée and an intensive pasture (grassland) in Dorinne. Lonzée has been labeled ICOS (Integrated Carbon Observation System) since 2017 whereas Dorinne is in the process of being labeled. ICOS is a European Research Infrastructure Consortium (ERIC) which is a legal entity corresponding to a network of stations measuring the concentration and fluxes of GHG. This research infrastructure promotes a better understanding of carbon cycle and GHG emissions over the Earth (terrestrial ecosystems, atmosphere and oceans) through long-term observations. This label guarantees the quality and the continuity of the data series.

3.1 Lonzée

Lonzée terrestrial observatory is a four year rotation crop field (sugar beet, winter wheat, seed potato, winter wheat) located 3.5km from Gembloux Agro-Bio Tech. This 12-ha crop has been cultivated by a local farmer for more than 80 years (Lognoul et al., 2019). The climate is oceanic temperate with an annual average temperature of 10°C and an annual precipitation near 800 mm. The soil texture is classified as silt or silty loam according to the USDA textural triangle, with nearly 15% of clay, 78% of silt and 7% of sand.

Located in a region reputed for agriculture, this experimental site follows a quite intensive crop management. Before every sowing, two steps are followed: the stubble breaking and the ploughing/tillage which can be either conventional (30cm) or superficial (8-10cm). Regarding the amendments, the farmer frequently applies insecticides, fungicides, herbicides as well as liquid nitrogen, following the usual procedure in the region. The field shows a high productivity with a dry grain yield around 9t/ha for winter wheat and around 20t/ha of exported biomass for sugar beets.

The site is equipped with an eddy covariance system and a meteorological station in the center of the field (Figure 3.1). The EC system is composed of a sonic anemometer (Solent Research HS-50, Gill Instruments Lymington, UK), allowing the measurement of the three components of wind speed and the temperature at high frequency (10-20 Hz), combined with an infrared gas analyser (LI-7200, LI-COR, Lincoln, NE, US) which measures the CO_2 and H_2O concentration at the same frequency. These devices allow to measure CO_2, water vapour, momentum and sensible heat fluxes at a half-hourly scale (Aubinet et al., 2009; Moureaux et al., 2006). In addition, a N_2O fluxes measuring campaign was held from April 2016 to November 2016 when a N_2O gas analyser was coupled with the existing EC system. Even if Lonzée integrated ICOS in 2017 as a level-2 station, fluxes and meteorological data have been measured since 2004.

As mentioned above, a meteorological station is also established on the experimental site with data sampled at 0.1Hz rate and averaged every 30 min. Radiation sensors measure incoming/outgoing longwave (far infrared) and shortwave (solar) radiation. Photo-receptor cells also determine the incoming, outgoing and diffuse photosynthetic

photon flux density (PPFD). Air temperature is measured at two different heights as well as relative humidity, while canopy temperature is measured with a thermal camera. Along with these sensors, there are a rain gauge, a barometer, a NDVI (Normalized difference vegetation index) sensor and a sonic ranging sensor (quantifying snow depth). Soil temperature and soil water content are measured at five distinct depths (5, 15, 25, 55, 85cm below-ground) but soil heat flux is only known at 5cm below-ground.

Figure 3.1: Lonzée terrestrial observatory in 2018

As a precaution against the lack of meteorological data, a back-up station has been set up next to the primary one. Moreover, since 2018, additional measurements of soil temperature and soil water content profiles have been implemented a few meters away from the main station.

Aside from these fluxes and meteorological data, biomass measurements are also carried out during field campaigns and samplings. Canopy height, leaf area index (LAI), above-ground biomass are assessed at least six times per growing season. In addition, leaf area to mass ratio, carbon and nitrogen mass fraction, remaining above-ground biomass after harvest are measured once a year. Phenology stages are determined during every growing season according to the BBCH scale. Finally, the vertical profile of soil carbon content is quantified every 10 years with a motor corer (100 cores in the first meter soil layer).

Based on biomass measurements, an allometric relationship was established for winter wheat crops in Lonzée. This relationship is based on eight measurements of plant above-ground dry mass (stem, leaves, grain, etc.) coupled with measurements of vegetation height. From emergence to anthesis, plant height is linked to its dry mass according to ($R^2 = 0.996$):

$$h = 0.09175\, W_{up,tot} - 2.139 * 10^{-5}\, (W_{up,tot})^2 \tag{3.1}$$

where h is the vegetation height [cm] and $W_{up,tot}$ is the total above-ground dry mass [gDM m^{-2}]. From height measurements, it can be noted that plant height tends to decrease at the end of the crop cycle. This occurs approximately at anthesis, and plant height is assumed to remain constant after that moment.

In 2017, a campaign of soil sampling was carried out in Lonzée. In total, 100 soil cores of 1m depth were collected on the field. These cores were divided into 5 soil horizons: 0-5cm, 5-15cm, 15-30cm, 30-60cm and 60-100cm. These samples were analysed in 2017 to determine the C, N and OM contents by the « INRA- Laboratoire d'Analyse des Sols » in Arras, France. The rest was sent in 2019 to the « Centre provincial de l'Agriculture et de la ruralité » in La Hulpe, Belgium, to measure soil texture and soil pH, except for the first horizon which was no longer available. Aside from these measurements, soil bulk density was assessed on these samples. In 2018, during another

campaign, 3 soil samples were collected with cylindrical cores at 3 locations on Lonzée site, at 3 distinct depths (0-25cm, 25-55cm, 55-85cm). Afterwards, pF curves were established for each sample by the « Laboratoire de Mécanique et Physique du sol » , Gembloux, Belgium, with a pressure plate apparatus. With these curves, mean values of SWC at field capacity and wilting point were calculated among the 9 replicates per soil horizon.

3.2 Dorinne

Dorinne terrestrial observatory is located in the Condroz region of Belgium, in the village of Dorinne, 18km away from Namur. The description of the experimental site given hereafter is based on Gourlez de la Motte et al. (2016) and Gourlez de la Motte (2019). The site consists of two adjacent permanent pastures of 4.22 ha and 4.04 ha for pasture 1 and pasture 2 respectively (figure 3.2), intensively grazed by Belgian Blue cattle. The grasslands are composed of grasses (66%), legumes (16%) and other species (18%), with perennial ryegrass (Lolium perenne L.) and white clover (Trifolium repens L.) being the dominant species. The site has been a permanent grassland for probably more than a century, and organic and inorganic fertilisers have been applied regularly for about 40 years (mean N fertilisation rate of 120 kg N ha^{-1} $year^{-1}$). A grassland renovation (ploughing and resowing) occurred in spring 2018 in pasture 2. This had not been done for more than 50 years. The site is dominated by a large colluvial depression exposed south-west/north-east, based on a loamy plateau. The dominant soils are colluvic regosols, according to the FAO classification, characterized by calcareous and clay substrates. Soil texture is characterized as silt loam according to the USDA classification, with 69, 17 and 14% of silt, clay and sand textures respectively. The climate is temperate oceanic, with mean annual temperature of 9.4°C and mean annual precipitation of 905 mm (IRM, 2018).

Figure 3.2: Aerial image of Dorinne experimental site, divided into two pastures.

The farm includes a herd composed of 235 Belgian Blue heads, with on average 95 calvings a year. During the grazing season, feed is rarely supplied to the cattle, only during potential grass shortage. The average stocking density is around 2.3 livestock units (LU) per ha and per year, cows being almost continuously on the pasture from March to mid-November. In winter, cattle is fed at the barn with wheat straw, maize and grass silage, winter cover forage, beet pulps, and ProtiWanze®, a byproduct of bioethanol production from wheat.

At the experimental site, both eddy covariance and meteorological data have been acquired since 2010 in pasture 1, and since 2015 in pasture 2 (figure 3.3). For the EC technique, a sonic anemometer (CSAT3, Campbell Scientific Ltd, UK) is installed on a mast of 2.6 m above-ground in pasture 1 and 1.92 m in pasture 2, both coupled with CO_2-H_2O infrared gas analysers (LI-7000, LI-COR Inc., Lincoln, NE, USA). These systems allow measuring carbon dioxide, latent heat, sensible heat and momentum fluxes every 30 min, through 10 Hz sampling. The CH_4 fluxes have been measured in pasture 1 with the same anemometer, coupled with a CH_4 gas analyser (PICARRO G2311-f, PICARRO Inc, USA) since 2012. Finally, quantum cascade lasers (Aerodyne Research Inc, USA) were installed in 2018 in pasture 1 and pasture 2, allowing continuous sampling of N_2O, H_2O and CH_4 fluxes. The figure 3.3 gives an overview of the gas analysers installed on both masts, along with the data of GHG fluxes available for given periods. Note that in 2016 and 2017, in pasture 2, as the LI-7000 analyser did not provide the expected accuracy, these data are not to take into account.

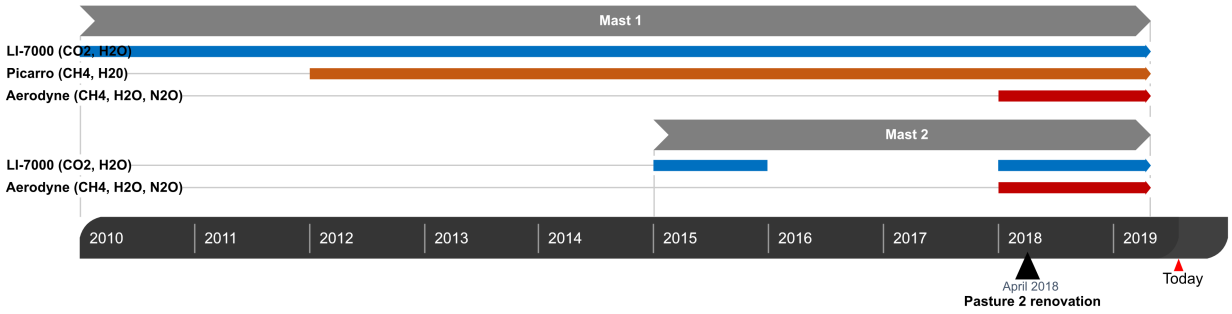

Figure 3.3: Timeline of the installation of gas analysers on pasture 1 and pasture 2.

In both pastures, at the same location as the EC systems, meteorological stations acquire the following data: air temperature, relative humidity, rainfall, atmospheric pressure, soil temperature at 2, 5, 10, 25 and 50cm below-ground, soil moisture at 5, 25 and 50cm below-ground, and different radiation variables (incoming/outgoing longwave and shortwave radiations, incoming and diffuse PPFD). Meteorological data are sampled at a rate of 0.1 Hz and averaged every 30 min.

To complete the continuous EC and meteorological data, punctual biomass measurements are done. The herbage mass is deduced in the field from the herbage height measured on average once a week with a rising plate meter, using allometric relationships fitted to Dorinne station. The allometric equation was created with the relation between harvested grass height and its measured dry biomass (Gourlez de la Motte et al., 2016). In order to express the above-ground biomass as a function of the total vegetation height, this equation was adapted as follows:

$$W_{sh} = \frac{-3.7781 * h^2}{2} + 219.98 * h \tag{3.2}$$

with W_{sh} the shoot dry matter [kg ha^{-1}] and h the total plant height [cm]. The methodology to obtain this equation is detailed in Vandewattyne (2019).

During the grazing periods, grass growth is evaluated with secured enclosures. This method is fully described in Gourlez de la Motte et al. (2016). Three enclosures from which cattle are excluded are installed on pasture 1. Each enclosure is made of five strips (0.5 x 2m), which are successively cut every week in order to simulate grazing. As 5 strips are present, measurements must be conducted during 5 weeks. On week 1, strip 1 is cut, its initial and final heights are measured, and the herbage biomass is deducted from the allometric relationship. On week 2, strips 1 and 2 are mowed, on week 3, strips 1 and 3, until cutting strips 1 and 5 on week 5. With that method, a weekly grass growth can be obtained from the means between strips and secured enclosures. Evaluating grass growth under grazing can also be useful to determine cattle grass intake, which is taken equal to the variation of grass height between the beginning and the end of a stocking period, plus the estimation of grass growth (Gourlez de la Motte et al., 2016).

In 2019, a soil sampling was carried out. Twenty samples were randomly collected on pasture 1, at three distinct depths: 0-10cm, 10-35cm, 35-70cm. Soil texture, soil pH, soil N and soil C contents were measured on these samples by the « Centre provincial de l'Agriculture et de la ruralité » in La Hulpe, Belgium. Soil bulk density was measured near the EC mast at the three depths of interest by means of soil samples collected in a pit with metallic cylinders of known volume.

3.3 Gap filling of meteorological data

As one of the goals of this thesis is to adjust the TADA model to simulate the behaviour of the vegetation of these experimental sites, some series of continuous data corresponding to the inputs (presented in section 2.1.3) have to be established specifically to each experimental site. Input variables, such as meteorological conditions, are normally recorded but some technical problems and regular maintenance of measurement devices sometimes lead to missing data. Unfortunately, TADA does not accept any undefined values as inputs and data gap filling is necessary. As a reminder, the required meteorological data for the TADA model are the global radiation, the precipitation, the air temperature, the relative humidity and the atmospheric pressure.

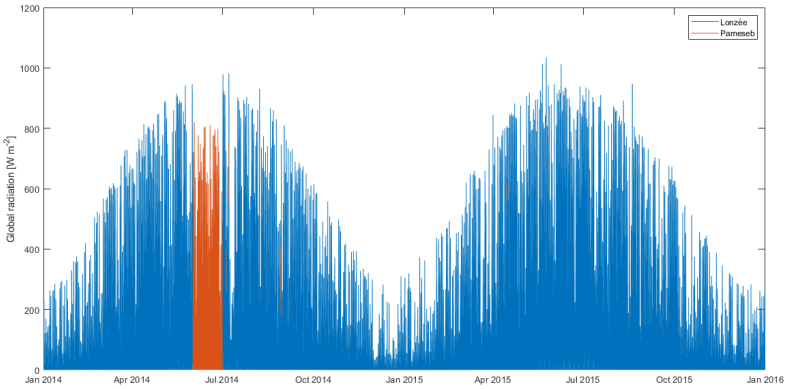

Figure 3.4: Global radiation in Lonzée (blue) completed with Pameseb measures (orange)

Stations from the CRA-W/Pameseb network could be used as a substitute to the Lonzée and Dorinne experimental sites and provide hourly data of these meteorological variables, except for the atmospheric pressure: Sombreffe, 10.6km from the Lonzée site and Haut-le-Wastia located 8.9km from the Dorinne site. In order to gap fill the 30-min meteorological datasets, the hourly records were interpolated linearly. Consequently, the air temperature at 1.30pm is the arithmetic mean of the air temperature at 1pm and 2pm. As the global radiation seemed inconsistent

with the measured radiation in Lonzée (see figure 3.4), the missing values of global radiation were rather estimated from the measured PPFD. The relation between these two variables was considered linear with a slope of PPFD as a function of global radiation equal to 1.8135.

Regarding the atmospheric pressure, data were gap filled with the pressure measurements of the gas analyser in Lonzée. As this information was not available for Dorinne and this site is not located far from Lonzée (approximately 30km), the missing values were filled with the atmospheric pressure at the Lonzée site, corrected for the difference in altitude.

Chapter 4

Calibration of the water cycle

The implementation of an ecosystem model to simulate a forest, crop or grassland dynamics requires a certain accuracy in the model outputs. As presented in section 2.2, most of the processes running the ecosystem are expressed by means of empirical equations including various species or site-dependent parameters which must be specified for the experimental site that is simulated before running the TADA model. Some of the parameters values can be found in the literature (optimal temperatures for root growth, photoperiod required for plant development, reference temperatures for leaf senescence, etc.), especially when they seem to be generic (independent on site conditions). Most of the time, a limited number of parameters values is directly available from on-site measures (the specific leaf area, the carbon content of dry matter) (Zhu & Zhuang, 2014). Finally, many parameters can not be directly measured in the field, or taken from the literature, as their value is highly dependent on the site conditions and on the modelled species. As a consequence, calibrating these unknown parameters by comparing experimental and modelled data remains a widely-used method in ecosystem modelling (Rasse et al., 2001; Graux et al., 2011; Kröbel et al., 2011; Puche et al., 2019). The quality of parameters calibration is critical for ecosystem models, as the uncertainty of model parameters is a major source of simulation errors (Medlyn et al., 2005). Consequently, the reliability of models is tightly linked to the quantity and quality of the data used for model calibration (Baldocchi & Wilson, 2001). In this chapter, the parameters involved in the water cycle will be separately calibrated for three main processes: soil evaporation, canopy transpiration and water infiltration and percolation. A brief methodology will first be given and some results will be presented and then discussed.

4.1 Methodology

4.1.1 General procedure

Tuning parameter values is done by comparing modelled and measured data. As a model aims at reproducing reality, the goal of parameters calibration, also called *parametrization*, is to stick predictions to measures as closely as possible, by making parameters vary. Model parametrization may be conducted by manual or automatic calibration, the first one requiring less computing power, and the second one often providing more accurate results for the same working time. In both cases, model calibration is based on an optimization criterion, expressed as a function of model residues, i.e. the difference between measured and modelled data. By modifying one or more parameters at a time, the evolution of that function of model residues is studied. While manual calibration usually consists in testing different parameter values within a predefined range, and choosing the ones that minimize the residues function, automatic calibration relies on more complex linear, nonlinear, heuristic or probabilistic methods (Obropta & Kardos, 2007) such as the Gauss-Marquardt-Levenberg method or the Monte Carlo Markov chain algorithm. Automatic calibration will be preferred when the number of parameters that must be tuned increases. However, in this work, a manual calibration was chosen, firstly for the sake of simplicity and considering the time available to perform a Master thesis, and secondly to get a precise understanding of how parameters separately affect the processes of interest.

The method chosen for the manual parametrization of the water cycle is displayed in figure 4.1. This procedure is used separately for each process that has to be calibrated, and is reiterated for each parameter. As all the parameters can not be calibrated simultaneously, a sensitivity analysis must first be performed in order to know in which order parameters should be calibrated. Afterwards, the TADA model is run with various values for parameter i (first one in the list provided by the sensitivity analysis), and the value that minimizes the residues is chosen through an optimization criterion. Then, the procedure is repeated with a new parameter j (second in the list) but using the new fixed value for the parameter i, until calibrating all the parameters of interest. Once model parametrization done, the calibrated process may be validated with a new dataset. The aim is to evaluate to which extent the model error increases in conditions that could be slightly different from the ones used for model calibration. This step is important to spot model overfitting, i.e. the elaboration of a model that reproduces so precisely the conditions on which it was developed that it can not be extrapolated to new conditions.

Figure 4.1: Procedure of manual model parametrization

Sensitivity analysis The sensitivity analysis is the first step of the methodology presented in figure 4.1. It is used to list in which order parameters will be calibrated. The method used for this first step is the constant fraction analysis: one upper and one lower bound value for each parameter (+10% and -10% of a reference value) are defined, the model is run with these configurations, and the variation of one output variable chosen as target variable is assessed. For example, the sensitivity analysis of soil evaporation will consider the cumulative evaporation during a fortnight as target variable. When both bounds are tested in the model, the sensitivity index of parameter i is computed as:

$$s_i = \left| \frac{out_{up} - out_{low}}{out_0} \right| / \left| \frac{p_{i,up} - p_{i,low}}{p_{i,0}} \right| \tag{4.1}$$

where $p_{i,0}$, $p_{i,up}$, $p_{i,low}$ are the reference, upper and lower values of parameter i and out_0, out_{up} out_{low} are the output variables corresponding to the different parameter values. The most sensitive parameter will be the one with the highest s_i. It must be noted that some parameters will be weakly sensitive, or even insensitive. Calibrating these parameters will not be possible, as their effect can not be perceived on the target ouput.

TADA model When an order of parameters is established for a given module of the model, different values are tested for parameter i and one is chosen following the optimization procedure, then for parameter j, etc.. Note that all the TADA model is not optimized in one procedure, and that each module is calibrated separately. This requires the isolation of the module of interest, to avoid the interference with the other ones, which in turn depend on their own parameters values. For example, to calibrate canopy transpiration, net carbon assimilation must be known at every time step (because the stomatal resistance, needed to compute transpiration, is dependent on GPP). In this

case, measured GPP data will be preferred to carbon assimilation model outputs in order to avoid the propagation of the error already present in the photosynthetical module. The way to isolate each module will be discussed later.

Optimization When the model is run with a given parameter value, observations (i.e. measured data) and predictions (i.e. model output) are compared through various optimization criteria. The statistical parameter R^2 may express the correlation between observations and predictions. However, model bias are not accounted by R^2 (Mitchell, 1997), and several alternatives are available, such as the root mean squared error (RMSE) which measures the mean deviation of model predictions from the observations:

$$RMSE = \sqrt{\sum_{i}^{N} \frac{(x_i - \widehat{x}_i)^2}{N}} \tag{4.2}$$

where x_i and $\widehat{x}_i$ are the observed and predicted variables at a given time step i and N is the size of the dataset used for calibration. The optimization index chosen here is based on half-hourly data, instead of daily- or weekly-averaged estimates, in order to focus on the intra-day variability of fluxes that must be calibrated. Note that the RMSE does not consider whether a phenomenon is over- or underestimated, as the difference is squared. As the aim of model calibration is to minimize the RMSE, parameters values are tested over an interval covering the realistic range, until finding a range where the minimum of RMSE can be encountered. The procedure is then repeated on this interval until reaching a certain level of precision in parameter estimation (generally, few percents). This procedure is then applied to the second parameter, etc., until having calibrated all the sensitive parameters. Besides the RMSE, a mean bias error (MBE) can be computed for each parameter value as:

$$MBE = \frac{1}{N} \sum_{i=1}^{N} (x_i - \widehat{x}_i) \tag{4.3}$$

This MBE indicates whether the variable of interest is on average over- or underestimated by the model. One last statistical coefficient that was computed is the Theil's inequality coefficient (TIC), introduced by Henri Theil in 1958:

$$TIC = \frac{\sqrt{\sum_{i=1}^{N} (x_i - \widehat{x}_i)^2}}{\sqrt{\sum_{i=1}^{N} x_i^2} + \sqrt{\sum_{i=1}^{N} \widehat{x}_i^2}} \tag{4.4}$$

The main advantage of this coefficient is that it is bounded between 0 and 1, and allows comparisons between parametrizations of different models or modules. A value of 0 corresponds to a perfect prediction, while a value of 1 indicates a total inequality between observations and predictions (Leuthold, 1975).

4.1.2 Evaporation

In TADA, three sources of water vapour are considered: snow sublimation E_{sn}, soil water evaporation E_{soil} and canopy transpiration TR (figure 2.1). The total flux of water vapour E_{tot} may be measured with the EC technique, and may be set equal to the sum of three contributions:

$$E_{tot} = E_{sn} + E_{soil} + TR \tag{4.5}$$

These fluxes occur in distinct conditions, so that E_{tot} corresponds to its evaporation or transpiration components for some specific periods. First, snow periods are rare and most of the time, $E_{tot} = E_{soil} + TR$. Secondly, E_{tot} sometimes corresponds to E_{soil} when no vegetation is present ($TR = 0$). This corresponds to inter-cropping periods for Lonzée, when the ground is naked, and to the beginning of the renovation of pasture 2 in Dorinne, when the soil was ploughed. Therefore, soil evaporation was calibrated against E_{tot} measurements acquired during these bare soil periods. To obtain an estimation of total water vapour exchange, the air canopy storage (computed from the variation of the air water vapour concentration in the canopy) was added to the EC flux E_{flux}, expressed in mm day^{-1} and obtained from LE_{flux} expressed in Wm^{-2} (transformation with the latent heat of water vaporization). In Lonzée, E_{flux} was measured with a LI-7200 analyser during the period of interest and with the Aerodyne analyser in pasture 2 in Dorinne, which was assumed to be the most precise analyser for E_{flux} measurements during the period of bare soil. Note that only positive values of E_{tot} were kept, as evapotranspiration fluxes are assumed to leave from the ecosystem.

Table 4.1: Parametrization of the water cycle

		Evaporation	**Transpiration**	**Infiltration and percolation**
	Parameters	λ_{ae},λ_{bl},ϵ_{cst},ϵ_{water},z_0	a_1,vpd_0,z_0	C_i,m_i
	Measured	E_{tot}	trans	SWC
	Modelled	E_{soil}	TR	θ
	Model inputs	SWC	GAI, h, SWC, GPP	E_{soil}
Lonzée	*Time range calibration*	01.09.14 - 27.10.14	14.04.14 - 14.07.14	01.09.14 - 27.10.14
	Time range validation	07.04.14 - 10.05.14	14.04.14 - 14.07.14	-
Dorinne	*Time range calibration*	02.05.18 - 16.05.18	01.09.13 - 31.12.13	29.04.18 - 16.05.18
	Time range validation	02.05.18 - 16.05.18	01.09.13 - 31.12.13	-

Additional information regarding the calibration of the evaporation process is given in table 4.1. The parameters that could be adjusted are listed in the first line. As a reminder, these parameters and the equations in which they are involved are detailed in section 2.2.1. Five parameters were considered potentially influential for soil evaporation: λ_{ae} and λ_{bl}, the weighting coefficients of the aerodynamical and soil surface boundary layer resistance, ϵ_{cst} and ϵ_{water}, two parameters involved in the expression of soil pore resistance and z_0 the roughness length, used to compute u^*, which in turn impacts the soil surface boundary layer and aerodynamical resistance.

As presented beforehand, the calibration of a given module is performed by isolating it from the other ones. For soil evaporation, the values of the soil water content (SWC), which influences soil pore resistance, were not the outputs of the TADA model, but measured values.

In Lonzée, the calibration of soil evaporation was performed in 2014 from the 1^{st} of September (stubble breaking after harvest) to the 27^{th} of October (seed emergence). The validation was done on a shorter period of 33 days in 2014, from the 7^{th} of April (soil preparation and planting) to the 10^{th} of May (first visible shoots). Before shoots were visible on field images, it is estimated that no water is transpired by plants and that E_{tot} remains equal to the evaporation flux. In Dorinne, only one period of bare soil occurred in the available dataset. In 2018, during the grassland renovation on pasture 2, some glyphosate was first applied on the field in March, the soil was tilled on the 13^{th} of April and grass was sowed on the 23^{th} of April. On images, grass is estimated to have emerged around the 16^{th} of May. However, during that pasture renovation, SWC sensors had to be removed and then re-installed, which leads to a big gap in SWC data. The only remaining period which corresponds to a bare soil and when SWC data were available ranges from the 2^d of May to the 16^{th} of May. As no other period was available for model validation, even days were used for calibration and odd days for validation.

4.1.3 Transpiration

Once the evaporation process calibrated for bare soil conditions, the hypothesis is made that the parameters obtained for bare soil can be used for soils covered by vegetation. As a consequence, canopy transpiration can be computed, when no snow is present ($E_{sn} = 0$), as:

$$trans = E_{tot} - E_{soil} \tag{4.6}$$

where E_{tot} must be expressed in mm day^{-1} and is computed with the same methodology than for the parametrization of soil evaporation. For Lonzée, E_{flux} is measured with the LI-7200 gas analyser and with the Picarro gas analyser in Dorinne, which was assumed to be the most precise one for E_{flux} measurements. In equation 4.6, E_{soil} is modelled with the parameters previously calibrated for Dorinne and Lonzée datasets respectively.

To parametrize canopy transpiration, the estimated transpiration $trans$ is compared to the modelled one TR. Three parameters were identified as influent for this parametrization: a_1 which is a stomatal resistance factor, vpd_0 which is an empirical coefficient required to compute the dependence of this resistance to the vapour pressure deficit (equation 2.25), and z_0 the roughness length. All three parameters are involved in plant transpiration through the regulation of the total conductance for water vapour transfer.

Besides these parameters, the values of some variables must be known to compute plant transpiration. Once more, in order to reduce the potential bias in this parametrization, these values where not the TADA model outputs, but those estimated from measurements. First of all, the GAI must be provided at every time step in order to weight the boundary layer resistance, as well as plant height h which impacts the aerodynamical and boudary layer resistance. In Lonzée, h and GAI were estimated from, respectively, biomass measurements introduced in an allometric relationship (equation 3.1), and specific leaf area SLA to tranform a mass into a surface. In Dorinne, plant height was directly available from weekly measurements, and GAI was obtained by estimating the biomass corresponding to h (equation 3.2), multiplied by grass SLA (value coming from Lazzarotto et al., 2009). As sometimes only punctual measurements of GAI and h are available, a linear temporal interpolation was done to fill the gaps and obtain values for each half-hour (see Delhez (2019)). Measured values of SWC at 5cm and gross carbon assimilation were also used to compute canopy transpiration. For gross assimilation values, GPP estimations were used. They come from gap filled NEE (EC measurements), partitioned into GPP and R_{eco}. The partitioning was performed by the *REddyProc* package of *R* software (`https://cran.r-project.org/web/packages/REddyProc`). For more information, the partitioning algorithm is described in Reichstein et al. (2005).

The time range used for the adjustment and the verification of the transpiration module in Dorinne is the whole year 2013, which is characterized by a nearly continuous EC dataset, by frequent biomass measurements and by a regular management. This year was divided into two datasets: a calibration one (even days) and a validation one (odd days). In Lonzée, the period of vegetation when biomass data were available ranges from the 14^{th} of April 2014 to the 14^{th} of July 2014. As for Dorinne, this time range was divided into even and odd days for model calibration and validation.

4.1.4 Infiltration and percolation

Initially, model SWC had to be compared with measurements in each soil horizon in order to parametrize both water infiltration and water percolation. Unfortunately, the simulations showed important discrepancies between predicted and observed SWC. As it was hazardous to determine whether this divergence was due to an inaccurate description in the model, to a shift in the sensors signal or to both, water infiltration and percolation was not calibrated. Instead of focusing on absolute values of SWC, more attention was paid to its variability, i.e. to the dynamics of water transfer.

This dynamics was described and compared for observations and predictions at Lonzée and Dorinne. For this last site, in addition, some parameters were tuned to obtain the same shape for the stabilization of soil moisture after a rain event. These parameters are C_i and m_i both used in the expression of the saturated hydraulic conductivity (equation 2.17). Quantitatively, the SWC stabilization was described by the number of days required after the beginning of a given precipitation to reach an equilibrium. For both sites, the periods considered during the adjustment were the bare soil periods, similar to the ones used for the parametrization of soil evaporation. Also, more attention was paid to the SWC at 5cm, as its variation is more easily detectable than in deeper soil horizons.

4.2 Results

4.2.1 Sensitivity analysis

The results of the sensitivity analysis performed for the three processes of interest are displayed in table 4.2. As a reminder, these values indicate how the output varies when the parameters are separately modified around a reference value. For the evaporation process, the three most influential parameters are λ_{ae}, z_0 and λ_{bl}. This implies that soil evaporation is mostly controlled by the aerodynamical and boundary layer resistance, as these three parameters are involved in their computation. The other variable that could potentially control soil evaporation is the soil pore resistance, which depends on SWC of the first soil layer. However, this resistance seems to be less influential as the parameters involved in its computation, ϵ_{water} and ϵ_{cst}, are the least sensitive parameters. This could partially be explained by the fact that the time ranges used for this sensitivity analysis (the same ones as for the calibration) did not cover high variations of SWC, leading to a narrow range of r_{soil} values. Indeed, soil pore resistance stays very low as long as the SWC is close to the field capacity as it is the case for the sensitivity analysis period. Consequently, this resistance and the evaporation are nearly not affected by any variation of ϵ_{water} and ϵ_{cst} during this period. This hypothesis is consolidated by the fact that the sensitivity of ϵ_{water} and ϵ_{cst} is much lower for Dorinne than for Lonzée, as the dataset covers 14 days with a variation coefficient of 2.82% for SWC at Dorinne vs. 56 days with a coefficient of variation of 6.78% at Lonzée. As a consequence, ϵ_{water} and ϵ_{cst} will not be calibrated hereafter, and their default values provided by Passerat (1986, cited in Mahfouf Noilhan, 1991) will be used.

Table 4.2: Sensitivity of evaporation, transpiration, infiltration and percolation parameters.

		Sensitivity (%)	
		Lonzée	Dorinne
Evaporation	λ_{ae}	69.67	96.85
	z_0	18.68	26.14
	λ_{bl}	3.25	4.00
	ϵ_{water}	3.56	0.71
	ϵ_{cst}	1.31	0.05
Transpiration	a_1	-	48.64
	vpd_0	-	21.66
	z_0	-	0.00
Infiltration and percolation	m_i	-	619.06
	C_i	-	85.72

No sensitivity analysis was performed on Lonzée data, because the measures of canopy transpiration seemed inaccurate. This will be discussed and illustrated in section 4.2.3. For Dorinne, a_1 was the most influential parameter of canopy transpiration, followed by vpd_0. Plant transpiration showed no sensitivity to the roughness coefficient z_0. This illustrates that unlike soil evaporation, the boundary and aerodynamical resistances are not so important in the transpiration process, and more influence comes from the stomatal conductance.

As explained before, the variable of interest for the infiltration and percolation process is the time required to stabilize soil moisture at 5cm after a precipitation. This time directly depends on K_{sat} representing the velocity of water transfer from one soil layer to the adjacent one, and which is highly sensitive to m_i and C_i. Considering the high influence of these two parameters, no other parameter will be considered to calibrate the stabilization of SWC. The results show that m_i is the most influential parameter.

4.2.2 Evaporation

4.2.2.1 Lonzée

Figure 4.2 illustrates the comparison of measured and modelled evaporation computed with calibrated parameters of Lonzée site, from the 10^{th} of September 2014 to the 1^{st} of October 2014. At first sight, TADA seems to accurately reproduce the dynamics of soil evaporation during the eight first days. However, on the 19^{th} of September, precipitation occurs, and important disagreements between TADA outputs and measurements can be observed after that date. The residues (corresponding to the difference between outputs and measurements) were plot against potential driving variables, but not relationship could be derived. The most likely explanation is that, after a precipitation, the assumption that E_{tot} corresponds to E_{soil} for bare soil is not correct. Some of the water reaching the ground surface probably directly evaporates, which is why E_{tot} increases right after the precipitation and does not correspond to the modelled soil pores evaporation. This observation reveals a default in the representation of the water cycle in TADA. An evaporative flux from the intercepted rain should be added from a reservoir of surface water. Neglecting this additional flux also leads to an overestimation of water infiltration. This implementation was not realised in the frame of this Master thesis for a matter of time. Instead, a new calibration was performed after having removed the days after rainfall (from the 18^{th} to the 23^{d} of September). If a larger dataset was available with several dry and rainy periods, a statistical analysis could have been carried out in order to evaluate, on average, how many days after a precipitation should be removed from the dataset of calibration.

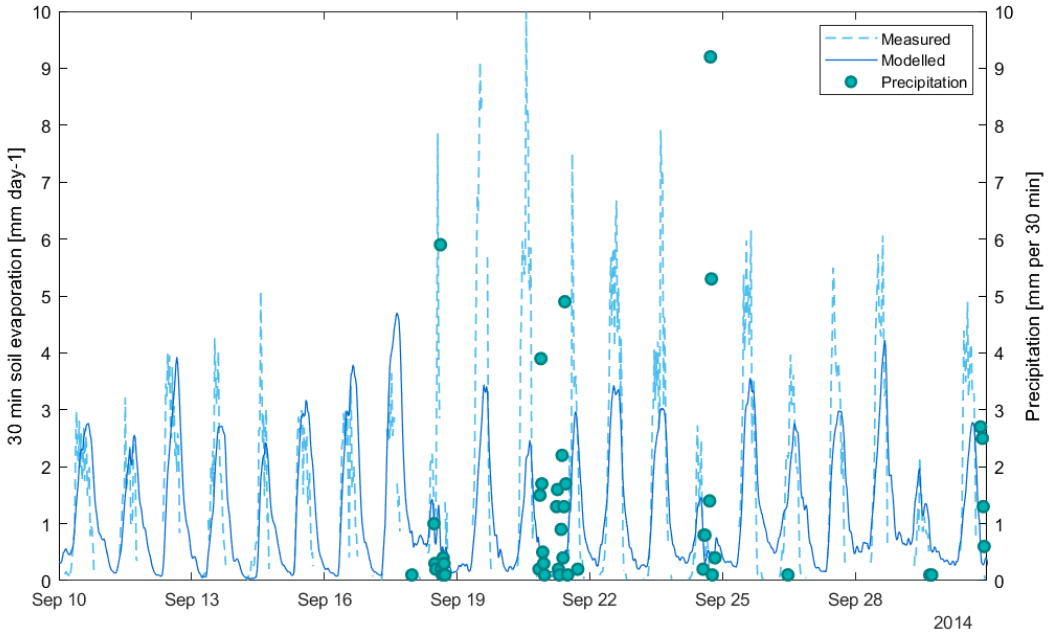

Figure 4.2: First calibration of soil evaporation in Lonzée (2014).

The results and statistics of the second calibration (after having removed rainy periods) and associated validation are listed in table 4.3. Starting from the reference parameter values, the largest reduction of RMSE and TIC is obtained after the tuning of λ_{ae}, which is the most sensitive parameter, the second one being z_0. During the calibration tests, the adjusted value of z_0 was identical to the reference one, which is why RMSE could not be reduced. This consolidates the choice of 0.0015 m for z_0 provided for bare soil by Jones (1992). The two last parameters ϵ_{cst} and ϵ_{water} were not changed, as their modification did not lead to substantial reductions of RMSE, and because default values were preferred, as the dataset of calibration did not cover wide variations of SWC.

Table 4.3: RMSE, MBE and TIC parameters computed with the uncalibrated evaporation model, with the calibrated one, and with the validation dataset (Lonzée, 2014).

	Parameter	**Value**	**RMSE** [mm day^{-1}]	**MBE**	**TIC** [-]
Uncalibrated	-	-	1.9789	1.1652	0.5975
Calibration	λ_{ae}	1.55	1.3737	0.1661	0.3196
	z_0	0.0015	1.3737	0.1661	0.3196
	λ_{bl}	1.26	1.3725	0.2080	0.3235
	ϵ_{cst}	3.8113	1.3725	0.2080	0.3235
	ϵ_{water}	-13.515	1.3725	0.2080	0.3235
Validation	-	-	1.8172	0.2439	0.4097

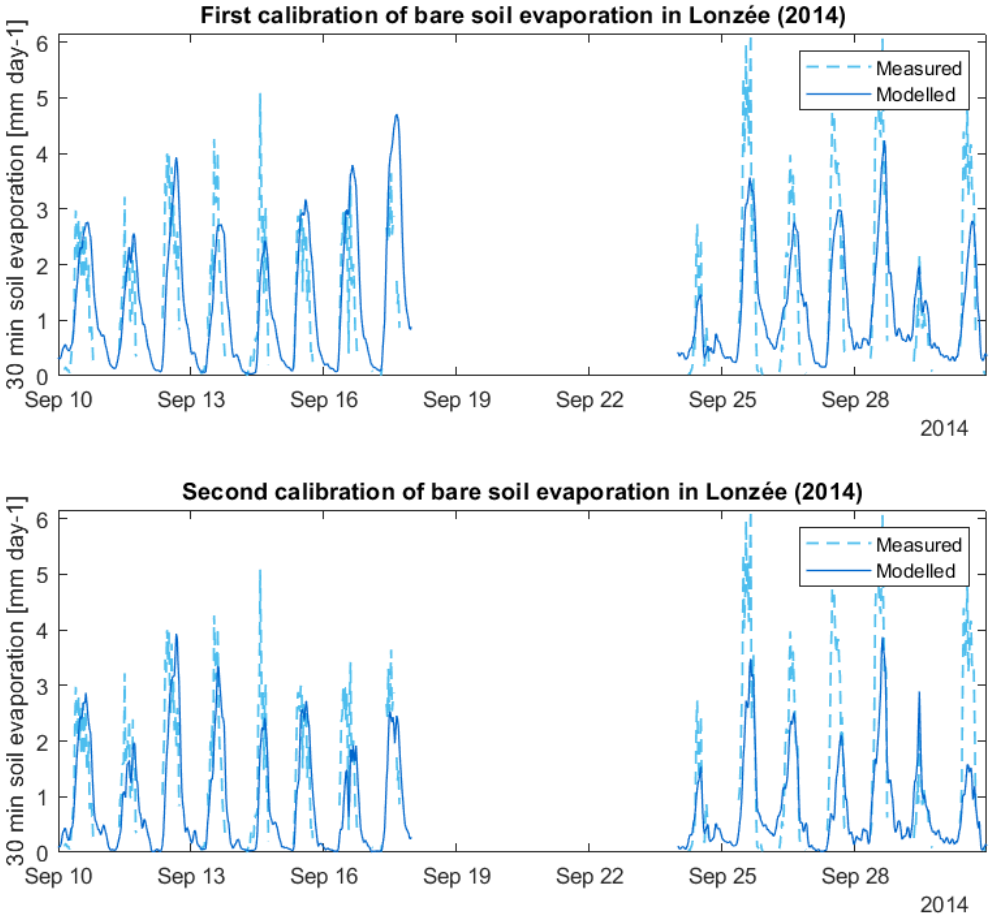

Figure 4.3: Comparison of first and second calibration of bare soil evaporation in Lonzée (2014).

The remaining RMSE after the parametrization of bare soil evaporation is 1.3725. It means that, on average, an error of 1.38 mm day^{-1} is made when estimating soil evaporation. The TIC indicates a rather good predictability. As a comparison, Maes et al. (2019) reached a RMSE of 0.56 mm day^{-1} when comparing predictions of evapotranspiration computed with a radiation-driven approach of evapotranspiration. With another model of ecosystem evapotranspiration, Hssaine et al. (2018) obtained RMSE from 49 to 128 W m^{-2}, i.e. 1.73 to 4.53 mm day^{-1}, depending on the conditions of the modelled field.

The effect of removing the periods following a precipitation is illustrated in figure 4.3. On average, there still are some underestimations of E_{tot} as indicated by the MBE in table 4.3. This is probably due to the fact that all the rainy periods were not completely removed in the calibration dataset (for example, after a short and slight precipitation). As no period was removed from the validation dataset, the RMSE, MBE and TIC are larger comparing to those obtained for calibration. As a comparison, Merlin et al. (2018) tested the calibration of soil evaporation from eddy covariance measurements during a continuous period of nine month on the one hand and over separate drying periods bounded by significant rainfall events on the other hand. When comparing both methodologies, removing the precipitation events resulted in a better correlation between measured and predicted soil evaporation.

4.2.2.2 Dorinne

The results of the parametrization of soil evaporation for Dorinne experimental site are given in table 4.4. Compared to the calibration for Lonzée site, λ_{ae} and λ_{bl} are smaller, indicating that less weight is given to r_{ae} and r_{bl} in the total resistance to soil evaporation. This is why ϵ_{cst} is set at a higher value, providing more influence to the soil pore resistance. However, it must be noted that for Dorinne as for Lonzée, λ_{ae} was reduced to a value close to 1 instead of its reference value of 4 in the ASPECTS version, which would indicate better estimations of r_{ae} and r_{bl} by equations 2.9 and 2.10 (no need of the weighting factors λ_{ae} and λ_{bl}). In their review of evaporation rates measured in different grassland sites, Kelliher et al. (1993) compared aerodynamical resistances estimated for grassland sites. The mean value of r_{ae} across the 7 grassland sites listed in Kelliher et al. (1993) is about 40 s m^{-1} while the mean half-hourly value of r_{ae} during the calibration reaches 427 s m^{-1}, which is more than ten times higher. Kelliher et al. (1993) expressed aerodynamical resistance for sites with vegetation, while the value of 427 is obtained for bare soil. This difference can partly be explained by the fact that aerodynamical resistance decreases with increasing vegetation height (Bonan, 2008a).

A possible source of error in the estimation of r_{ae} and r_{bl} in TADA is the hypothesis that neutral stability conditions are always met, which is necessary to express these resistances only as a function of u and u^* (equations 2.9 and 2.10). In unstable or stable conditions, r_{ae} and r_{bl} are assumed to change, and some formulations were proposed in these conditions, taking the stability parameter into account (Bonan, 2008a). However, the sensible heat fluxes must be known to evaluate the stability parameter at every time step, which is not the case for the TADA model, as no energy cycle is modelled. According to Camillo & Gurney (1986), aerodynamical resistance is higher for neutral stability conditions than for unstable conditions. As unstable conditions tend to occur during the day, when most of the soil evaporation takes place, r_{ae} and r_{bl} might be overestimated with the hypothesis of neutral stability conditions and r_{soil} would consequently be underestimated. This would explain the divergence with the values of Kelliher et al. (1993).

Table 4.4: RMSE, MBE and TIC parameters computed with the uncalibrated evaporation model, with the calibrated one, and with the validation dataset (Dorinne, 2018).

	Parameter	**Value**	**RMSE** [mm day^{-1}]	**MBE**	**TIC** [-]
Uncalibrated	-	-	3.7071	2.2964	0.7145
Calibration	λ_{ae}	0.78	2.5699	0.2176	0.3088
	z_0	0.0015	2.5699	0.2176	0.3088
	λ_{bl}	0.93	2.5695	0.1836	0.3069
	ϵ_{cst}	55.3	2.5666	0.2605	0.3108
	ϵ_{water}	-13.515	2.5666	0.2605	0.3108
Validation	-	-	2.7501	0.0014	0.3483

Although this calibration allowed reducing the error compared to the reference situation (ASPECT), the RMSE remains relatively high. A part of this error comes from a divergence between measures and predictions during the first days of calibration (after the 2^{nd} of May) as 31mm of rain fell from the 29^{th} of April to the 1^{st} of May, leading to higher E_{tot} fluxes. However, the TIC remains in the same order as for Lonzée, because the magnitude of soil evaporation is higher in Dorinne (figure 4.4), thus reducing the relative error. As for Lonzée, there is on average an underestimation of evaporation fluxes by the TADA model, among others due to the precipitation that occurs before the period of calibration. After the 5^{th} of May, evaporation fluxes are quite satisfactorily reproduced, as well for the calibration dataset as for the validation one. However, the results of this parametrization being established for a very short time range (16 days), their extrapolation to other periods has to be carefully verified in the following steps.

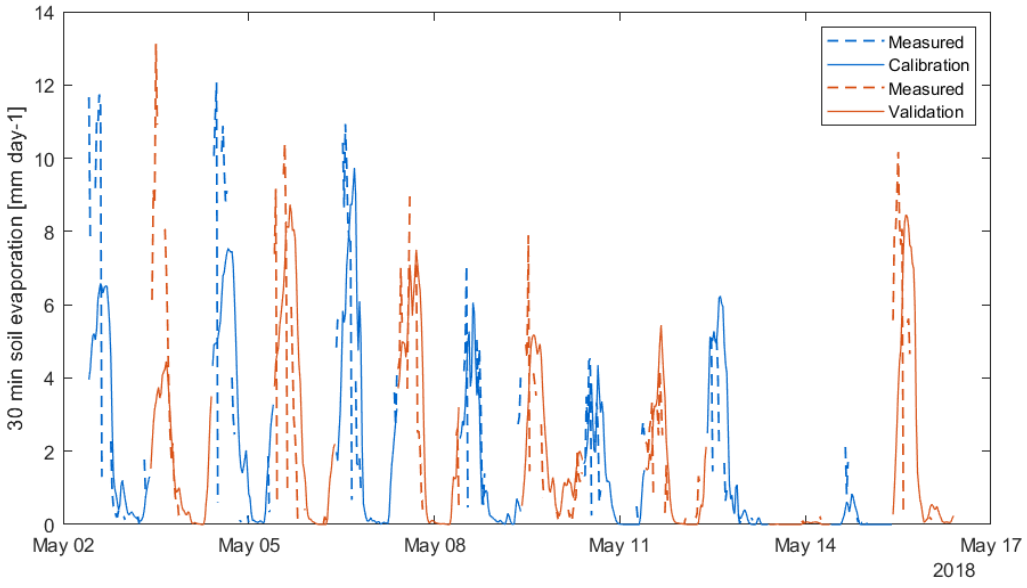

Figure 4.4: Calibration and validation of bare soil evaporation in Dorinne (2018).

4.2.3 Transpiration

4.2.3.1 Lonzée

Canopy transpiration could not be calibrated with the dataset acquired in Lonzée. As presented in section 4.1.3, the observed value for canopy transpiration *trans* was computed as the difference between the evapotranspiration flux E_{tot} and the modelled soil evaporation E_{soil}. However, as illustrated in figure 4.5, E_{soil} often overshoots the E_{tot} measurements with the adjusted parameters, leading to negative estimates of *trans*. Besides making plant transpiration impossible to calibrate for every time step when E_{soil} is higher than E_{tot}, this observation questions the transposition of parameters values obtained during the E_{soil} adjustment performed on bare soil to soils covered with vegetation. Indeed, while evaporation fluxes were underestimated for bare soil conditions, E_{soil} is overestimated during the rest of the year. This involves that the adjustments from bare soil evaporation can not be extrapolated to other conditions. This may be caused by a narrow range of environmental conditions encountered during the naked ground periods, such as the weak variations of SWC, that lead to a wrong calibration of ϵ_{cst} and ϵ_{water}. Ideally, the evaporation of bare soil should be calibrated on a full year of bare soil conditions, hoping that contrasted climatic periods will be met. As no such dataset is available for Lonzée, the best option remains the use of default parameters provided in the ASPECTS model. An alternative to the distinct parametrization of evaporation and transpiration will also be discussed in section 4.2.5.

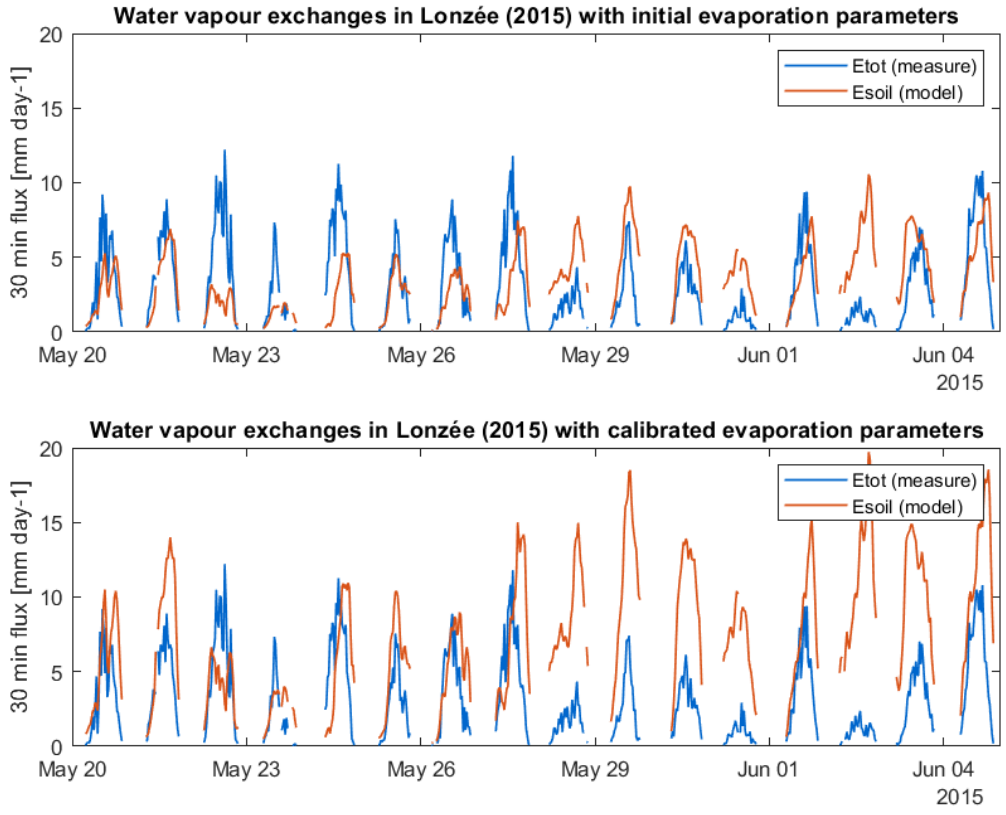

Figure 4.5: Comparison of water vapour exchanges in Lonzée (2015) with initial and calibrated soil evaporation parameters.

In addition to the difficulty of obtaining a calibration dataset with a large panel of environmental conditions, the idea of extrapolating parameters calibrated on bare soil to soils covered with vegetation can bring some bias when

the model is not mechanistic enough. As stated in Bonan (2008a), aerodynamical resistance decreases with higher vegetation height, as the roughness length increases. The impact of this decrease might not be well reproduced on r_{ae} with equation 2.9 because of a too empirical approach. Therefore, this decrease of r_{ae} for higher vegetation can only be taken into account by the diminution of the weighting coefficient λ_{ae} that multiplied r_{ae} and values obtained under bare soil conditions are not adequate for vegetated fields.

4.2.3.2 Dorinne

The issue encountered in Lonzée dataset was also present in Dorinne. An additional hypothesis to the ones already presented for Lonzée can be suggested to explain that phenomenon. The calibration of bare soil evaporation was performed for pasture 2, with the 2018 dataset, which is the only bare soil period for Dorinne experimental site. Afterwards, the calibration of canopy transpiration was performed for pasture 1. The parameters obtained for soil evaporation might be highly plot-specific and might not be transferable from one pasture to another, potentially because of a difference in soil composition or structure. Besides the distinct site conditions, the calibration carried out on pasture 2 used EC data obtained with the Aerodyne gas analyser, while the calibration of transpiration conducted on pasture 1 relied on those acquired with the Picarro gas analyser. As a reminder, distinct analysers were used because they were the ones expected to provide the most accurate measurements for the chosen periods. However, some bias may arise from the use of two different devices.

Table 4.5: RMSE, MBE and TIC parameters computed with the uncalibrated evaporation model, with the calibrated one, and with the validation dataset (Dorinne, 2013).

	Parameter	**Value**	**RMSE** [mm day^{-1}]	**MBE**	**TIC** [-]
Uncalibrated	-	-	1.7270	0.0988	0.4290
Calibration	a_1	3.1	1.5813	0.4612	0.4750
	vpd_0	740	1.5766	0.5097	0.4895
	z_0	0.0015	1.5766	0.5097	0.4895
Validation	-	-	1.5884	0.4607	0.4805

Although E_{soil} was sometimes overestimated and overshot E_{tot}, this did not happen as much as for Lonzée dataset, and a calibration procedure was tested through the removal of the periods when E_{soil} exceeded E_{tot}. As shown in table 4.5, the parameters adjustment in the transpiration module reduced the RMSE in a very low proportion, and even increased the TIC. As a_1 and vpd_0 are two parameters also involved in the photosynthetic modules, modifying theses parameters values based on this calibration is not advised, as it would bring a potential bias in the estimation of the ecosystem GPP. Therefore, the values of a_1 and vpd_0 derived from the parametrization of the ecosystem GPP (Delhez, 2019) will be recommended.

4.2.4 Infiltration and percolation

4.2.4.1 Dorinne

As presented in section 4.1.4, the parameters adjustment for water infiltration and percolation does not focus on absolute values of SWC, but rather on their temporal evolution, i.e. on the dynamics of water transfer. Indeed, as illustrated in figure 4.6, there is an offset of about 4% between the stabilized values of predicted and observed SWC. Considering the accuracy of the SWC probes, it is difficult to charge this difference to sensors or model errors. Despite the presence of this offset, the comparison of SWC variability can still be analysed.

Figure 4.6 shows the evolution of the modelled SWC (θ) in the first soil layer, compared to SWC measured at 5cm below ground. Note that soil moisture probes tend to be sensitive to variations of temperature, which explain the oscillation of SWC in figure 4.6. In order to precisely spot the number of days that SWC needed to flatten out, the mean daily values of SWC are also displayed. It took approximately 10 days to reach an equilibrium after the end of the precipitation displayed on the left of figure 4.6. With the reference values of C_i and m_i, K_{sat} was estimated at 3.37 mm h^{-1} for the first soil layer and θ stabilized only 2 days after the end of the precipitation, indicating too high infiltration rates.

As m_i was the most influential parameter for the dynamics of water transfer, it was first adjusted within its acceptable range before adjusting C_i. This procedure gives a $m_i = 3.3$ and a $C_i = 1400$, providing a saturated hydraulic conductivity of 1.22 mm h^{-1}. This value seems coherent for silt loam texture, as Rawls et al. (1998) measured 25% and 75% percentile values for K_{sat} of 1.0 and 9.9 mm h^{-1} with a database of 1,508 soil samples. The corresponding temporal evolution of θ is displayed in dark blue in figure 4.6 and fits relatively well to the measured one. As the infiltration rate was reduced to correspond to observations, the magnitude of the peak after the precipitation increases, as more water is accumulated in the first soil layer.

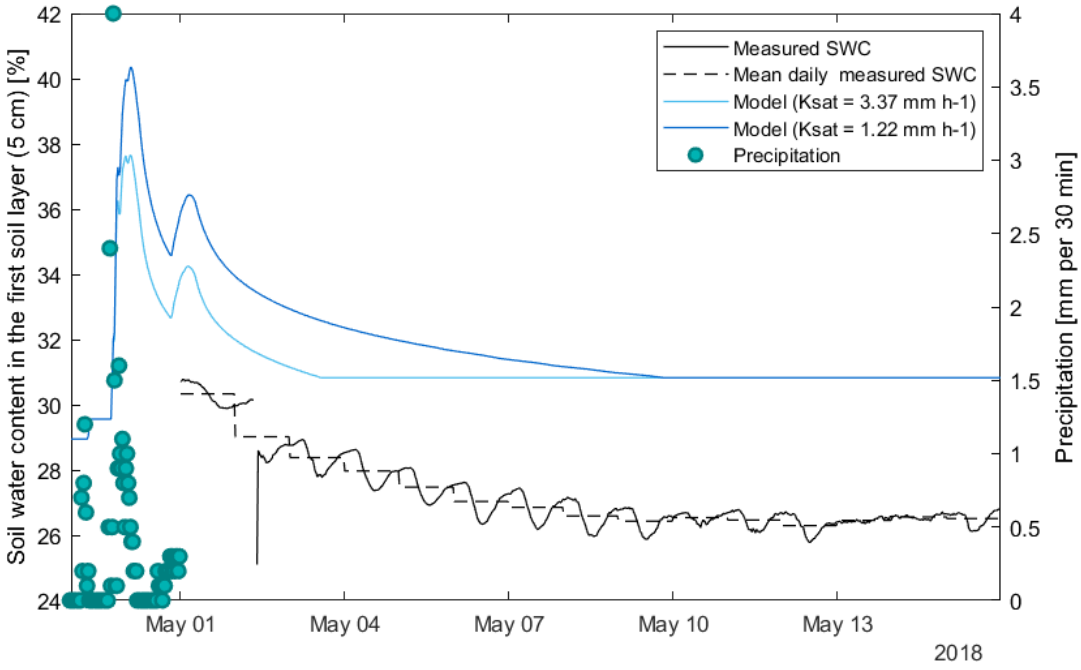

Figure 4.6: Dynamics of water transfer after a precipitation in Dorinne (2018).

Another interesting observation is that after rainfall, θ exactly stabilizes at the field capacity in the first soil layer. This is due to the fact that in ASPECTS, no vertical transfer of water was assumed to occur under the field capacity θ_{fc} (see section 2.2.1). However, according to the equation of Darcy, vertical fluxes of water are proportional to a gradient of hydraulic head H which is the sum of gravitational, pressure and osmotic potentials (Marshall & Holmes, 1988). Although the osmotic potential can often be neglected for water movements in soils, the pressure potential h, or matric potential, that arises from the interactions between water and soil particles is an important component of water movements in unsaturated soils. This component is taken into account in TADA model (by the water diffusivity which multiplies a vertical gradient of θ (equations 2.15 and 2.19)), but only above the field capacity. Under this value, fluxes due to a gradient of matric potential should still be accounted for in the TADA model, to represent phenomena such as capillary rise.

4.2.4.2 Lonzée

Even though no parametrization of water infiltration and percolation was performed for Lonzée experimental site (too high divergence between measurements and model outputs), the comparison of measured and modelled SWC during the period of bare soil highlights some limits of the model (figure 4.7). An important offset of SWC can be observed between observations (dashed lines) and predictions (solid lines) which sometimes reaches values of around 0.1 m^3 m^{-3}. It is difficult to determine whether this difference must be imputed to errors from the soil moisture probes, to soil parameters values that could have been poorly estimated by the model, or to both.

Table 4.6: Measured and modelled soil water contents at field capacity and wilting point for Lonzée.

		θ_{fc} [%]		θ_{wp} [%]	
	Depth [cm]	**Measured**	**Modelled**	**Measured**	**Modelled**
Layer 1	0 - 25	29.65 ± 1.3	29.60	14.30 ± 1.2	7.83
Layer 2	25 - 55	32.2 ± 0.5	31.27	17.6 ± 2.0	10.16
Layer 3	55 - 85	36.8 ± 1.0	32.69	22.7 ± 1.8	12.12

Table 4.6 summarizes the comparison of measured and modelled SWC at field capacity θ_{fc} and wilting point θ_{wp} for Lonzée experimental site. As a reminder, θ_{fc} and θ_{wp} were measured with a pressure plate apparatus, as detailed in section 3.1. Although TADA seems to predict θ_{fc} with a high accuracy, especially in the two first soil layers, an important bias is brought by the model when estimating θ_{wp} with Saxton & Rawls (2006) equations. However, this variable does not strongly impacts water fluxes, unless the SWC falls below θ_{wp} which did not occur during the simulation displayed in figure 4.7. Therefore, the accuracy of soil moisture probes must be questioned and some quality checks should be carried out in the future.

Although the absolute values of measured SWC can be biased, the variation of these variables is illustrated in figure 4.7. An important precipitation occurs before the 1^{st} of September, after which no rain falls during a fortnight, leading to a continuous decrease of SWC. The rate of this decrement is distinct between observations and predictions. While the modelled SWC at 5, 15 and 25cm decline at a quite similar rate relatively coherent with those of the 15 and 25cm probes, the decline of the measured SWC at 5cm is steeper. This difference is in part explained by the fact that θ in the first soil horizon (5cm) was modelled with the texture of the second horizon (15cm) as no soil data was available for horizon 1. Figure 4.7 highlights the importance of a precise estimation of soil properties when modelling water transfer, as the equations of the water module are quite sensitive to soil texture. A soil property that was not taken into account in this simulation is the soil bulk density. Although it was measured for Lonzée and Dorinne experimental sites, the bulk density can not be introduced into TADA model equations without providing the volume fraction of gravel. Measuring this quantity and precisely assessing soil properties in the first soil horizon could maybe improve the dynamics of water infiltration and percolation in the first soil horizon.

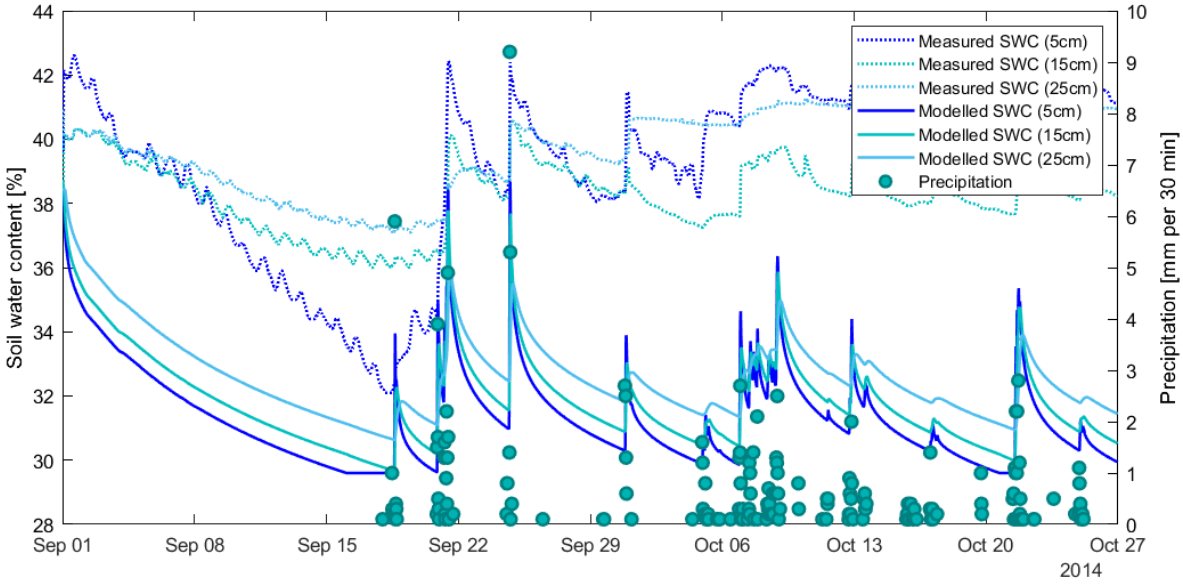

Figure 4.7: Dynamics of water transfer in Lonzée (2014).

4.2.5 Overall analysis

In this section, a general discussion of the calibration of the water cycle is provided and some paths of improvement are suggested. An important conclusion drawn from the calibration of the evaporation and transpiration modules is that, with the available datasets, these phenomena could not be parametrized with sufficient accuracy. The chosen methodology was based on a partitioning of E_{tot} fluxes between their evaporation and transpiration components. However, the periods of bare soil are so restrictive in terms of variation of environmental conditions that the results of the parametrization of soil evaporation are not representative for all the year. The approach chosen in this work could maybe have provided better results with a larger dataset collected during a whole year of naked ground, which is quite unlikely to happen. What is more, as discussed in section 4.2.3, the estimations of aerodynamical and boundary layer resistance differ from bare soil to vegetated periods. Their calculation could be improved with a more mechanistic approach, taking the presence of vegetation into account.

Faced with this reality, alternatives must be considered. Massman (1992) provided a new method to partition evapotranspiration measurements into soil and plant contributions, i.e. evaporation and transpiration. This algorithm is based on micrometeorological data, and surface energy balance measurements which are available for the instrumented sites of Lonzée and Dorinne. Using Massman's (1992) methodology would allow calibrating both evaporation and transpiration modules on a whole year of E_{tot} measurements, thus providing a wider range of soil and atmospheric conditions. Another option to parametrize the ecosystem evapotranspiration would be to consider both modules simultaneously. One calibration would be performed on a whole year (or more) of E_{tot} fluxes, by gathering the parameters present in E_{soil} and TR equations. All parameters could be calibrated in their order of sensitivity so as to match E_{tot} fluxes and the sum $E_{soil} + TR$. The underlying risk of this method is that a good calibration in terms of RMSE could be obtained with high values of E_{soil} and low values of TR or inversely. Therefore, this parametrization should define a range of limit values that E_{soil} and TR can not exceed. The importance of precisely estimating the contribution of evaporation and transpiration in water vapour emissions depends on the objective pursued by the modeller. If more attention is paid to vegetation growth, the assessment of ecosystem evapotranspiration mainly aims at estimating the amount of water that is lost by the soil system and with it the water contained in the soil profile, which in turn impacts plant growth through hydric stress. Knowing whether this water is lost by transpiration or evaporation is not a major concern for the TADA model user. Indeed, estimating the transpiration rate could be necessary to evaluate plant growth if the transfer of sugar and nutrients through

the plant system was modelled according to a flow of water from the roots to the stomata. However, this is not the case in the TADA model.

Some other users could be interested in studying the ecosystem water cycle, and more precisely the evolution of SWC in the different soil layers. If so, an exact evaluation of E_{soil} and TR is critical as the water lost by the soil profile is not extracted at the same location for evaporation and transpiration fluxes. In the calibration performed in this work, only the total transpiration was considered. However, as explained in section 2.2.1, TADA computes the total plant transpiration and then partitions an equivalent plant uptake between soil layers, thus reducing their SWC with different magnitudes. Once plant transpiration parametrized, calibrating the partitioning of plant uptake could be interesting to improve the estimation of SWC in each soil horizon. This parametrization requires an estimation of the fine root surface (or total root biomass as a proxy) in each layer, which should rather be measured, as the calibration of the root growth module has not been performed yet.

Another module that should be parametrized for a precise estimation of SWC is the interception module. Although the amount of intercepted water is smaller for winter wheat or ryegrass than for tree species, water interception can result in a time lag between the precipitation and the increase of SWC in the first soil horizons. Some tests taking or not water interception into account should be carried out to determine if the inclusion of this phenomenon results in an important delay in the dynamics of SWC. If so, this module should be considered and calibrated against measured SWC.

Overall, the calibration of the water cycle revealed the importance of wide and variate datasets in calibrating phenomena that are tightly linked to environmental conditions. When calibrating a bioechemically based model of carbon exchange, Schulz et al. (2001) found that an EC dataset of several weeks was insufficient to obtain accurate results. According to Rauch et al. (2002), lack of data may be a greater hindrance to models than lack of suitable algorithms. Besides the availability of datasets, the accuracy of the measures used for calibration is a major concern (Medlyn et al., 2005), as larger uncertainty in the measurements implies larger uncertainty in parameter estimates (Hollinger & Richardson, 2005). However, the estimation of errors in the data is challenging, due to the lack of spatially replicated measures (Medlyn et al., 2005). As described by Baldocchi (2003) and Hollinger & Richardson (2005), EC fluxes are affected by both random and systematic errors, mainly due to the random character of turbulence and to the post-processing of these data. Hollinger & Richardson (2005) found out that fluxes uncertainties tend to increase with flux magnitude, which can be a major problem when calibrating fluxes modelled at an intra-day time step, as the reproduction of biased peaks by the model might lead to a poor parametrization. Therefore, along with EC data, an uncertainty assessment might be of great interest to express the reliability of measurements. By comparing results from two EC towers measuring similar vegetation at close locations, uncertainty can be estimated, as done by Hollinger & Richardson (2005). Alternatively, uncertainty assessment can be realized by taking four types of uncertainties into account (a random one, one associated to the gap filling procedure, one to the u^* threshold selection, and a last one due to frequency corrections) as done by Gourlez de la Motte et al. (2016) for carbon fluxes measurements. The average uncertainty over a 5-year carbon budget was estimated between +26 gC m^{-2} yr^{-1} and -17 gC m^{-2} yr^{-1} compared to a 5-year mean NEE of -141 gC m^{-2} yr^{-1}. In a multi-site analysis of random error in EC sites, Richardson et al. (2006) evaluated this error, i.e. the standard deviation of E_{tot} measurements, between 3.4 W m^{-2} (0.12 mm day^{-1}) and 38.1 W m^{-2} (1.35 mm day^{-1}) for a grassland site and between 11 W m^{-2} (0.39 mm day^{-1}) and 33.1 W m^{-2} (1.17 mm day^{-1}) for a cropland one. These errors could potentially account for a part of the RMSE computed during model calibration. According to Moorhead et al. (2019), the errors around half-hourly estimates of evapotranspiration would be higher than for daily-averaged values. This also explains why the calibrations performed with the TADA model may be more erratic than other adjustments based on daily estimations of soil evaporation and plant transpiration.

As described in Hollinger & Richardson (2005) and Richardson et al. (2006), assessing the uncertainty around flux data is important to compare and determine parameters derived by fitting models to measured fluxes. This assessment is part of the maximum likelihood methods taking random errors into account and that have been tested to provide unbiased estimates of model parameters (Schulz et al., 2001). Another problem inherent to model parametrization that can be tackled by uncertainty assessment is the equifinality in the parameter sets (Schulz et al., 2001). Equifinality implies that there may be many sets of parameters values that allow a quite good and

similar fit between measures and model predictions. With an estimation of flux uncertainty, confidence intervals can be associated with parameters estimates, as well as more precise parameters estimations, reducing the number of possible sets of parameters (Hollinger & Richardson, 2005). For more information, Hollinger & Richardson (2005) illustrate how to use the maximum likelihood analysis and Monte Carlo simulation based on flux uncertainty to estimate parameters of a big-leaf model. Such methods could be used in a future calibration of the TADA model to reduce the uncertainty around parameters estimates.

Chapter 5

Test of the grazing module

This chapter aims at evaluating, at first glance, how the grazing module implemented in the TADA model helps to fairly reproduce the dynamics of grazed pastures. The target variable considered here is the grass height. First because it was frequently measured in Dorinne (on average every week from March/April to November), and secondly because the evolution of grass height is the result of various processes, such as carbon allocation, shoot senescence, and animal grazing. Both measured and modelled grass heights will be compared and some ways to calibrate the processes running grass growth will be considered. This procedure is also an opportunity to evaluate the influence of some parameters that were adjusted during the carbon and nitrogen cycles calibration performed in Delhez (2019) and Vandewattyne (2019).

5.1 Modelling of grass height

Grass height can be deduced from the shoot dry matter content by using the allometric relationship designed for Dorinne (equation 3.2). As the shoot dry matter is obtained from the aerial carbon reservoir (with a constant ratio of gC per gDM), dealing with the dynamics of grass growth means to study the temporal evolution of the shoot carbon reservoir. This evolution depends on five distinct fluxes according to:

$$\frac{dC_{sh}}{dt} = sh_{growth} - lit_{sh,C} - harv_{sh,C} - C_{intake} - C_{trampling} \tag{5.1}$$

where sh_{growth} is the net assimilated carbon that is allocated to the shoot compartment, $lit_{sh,C}$ is the carbon flux from the shoot transferred into the litter pool due to plant senescence, $harv_{sh,C}$ is the carbon exported when the pasture is mowed, C_{intake} is the carbon consumed by cow ingestion and $C_{trampling}$ is the carbon lost due to the degradation of shoot material consecutive to animal trampling. Note that all these flux densities are expressed in gC $m^{-2}day^{-1}$.

sh_{growth} is directly proportional to the plant gross photosynthesis that was calibrated by Delhez (2019) for Dorinne experimental site. However, this calibration relied on measured values of shoot nitrogen content. As the module of nitrogen uptake by plants has not been calibrated yet, it was preferred to use the GPP values estimated from measurements instead of modelled ones, in order to reduce the potential bias inherent to GPP modelling. Besides this, the estimation of the fluxes present in equation 5.1 depends on different variables and parameters, such as the shoot/root allocation coefficients for sh_{growth}, the shoot lifespan for $lit_{sh,C}$, the DM intake capacity of cattle for C_{intake} and the coefficient of trampling for $C_{trampling}$. For a first trial, these parameters were given values found in the literature rather than based on measurements, as a way to test their effect before adjusting them. As a year without mowing was chosen for this simulation, $harv_{sh,C}$ can be neglected in equation 5.1, but the uncertainty around other fluxes will be discussed in the results.

The year chosen for the modelling of grass height dynamics is 2013, characterized by a discontinuous grazing on pasture 1. The grazing season ranges from the 25^{th} of April to the 6^{th} of October. TADA model was run during the whole year with a gap filled climatic dataset. Carbon assimilation values were forced with estimates of GPP,

obtained from NEE measurements and partitioned with the *REddyProc* package of *R* software. A management file was also completed for this year, with two types of information: the stocking densities, expressed in LU ha^{-1} and solid fertilisations, that occurred on the 2^d of April (40kg N ha^{-1}) and 11^{th} of July (54kg N ha^{-1}).

During that year, grass height was measured on average every week from the 8^{th} of April to the 26^{th} of November. Between these punctual measures, a linear interpolation was made to obtain a continuous estimation of grass height. Before the first measure of grass height, and after the last one, as no estimation of grass height was available, it was estimated that grass height remained stable, which is very likely as grass barely grows in winter.

To run the TADA model for Dorinne site, reservoirs contents must be initialised. When possible, some values were estimated from measurements and others from the literature when no site-specific estimation could be made. The resulting values are summarized in Appendix B, table C.4. The shoot N and C content on the $1st$ of January 2013 were estimated from the grass height at the beginning of the simulation, from the allometric relationship 3.2, and from the grass C and N concentration measured in Dorinne (gC gDM^{-1}, gN gDM^{-1}). As no measures of root C and root N content were carried out in Dorinne, an initial value of total root dry matter for temperate grasslands was taken from Jackson et al. (1996). This DM was partitioned between soil layers according to the density profile proposed by Arora & Boer (2003) (equation B.9). Once partitioned, C and N content per soil layer were obtained by using the same C and N concentration as for shoot material. In 2019, the total soil carbon content was measured for pasture 1 in the three soil layers. It was assumed that this C content had not substantially changed in six years, so that this value could be used in 2013. This hypothesis is often valid for grasslands which tend to see their C sequestration stabilize after many years of regular and constant management practices (Smith, 2014). This carbon content had to be partitioned between a carbon litter pool and a carbon SOM pool. This was carried out by Vandewattyne (2019) with a steady-state simulation made on Dorinne experimental site. The total N content in each soil layer was also measured in 2019, and was assumed to be the same as in 2013. This nitrogen was partitioned between the NO_3, NH_4 and organic pools according to coefficients of Sharpley & Smith (1995). Afterwards, the organic N was split into the SOM and litter N pools based on their C content and their C/N ratios, taken from ASPECTS.

5.2 Results and discussion

Figure 5.1 illustrates the evolution of observed and predicted grass height throughout the year 2013 in Dorinne experimental site. To interpret this evolution, the stocking density, expressed in livestock units (LU) per ha is also displayed in dashed line. Modelled and measured dynamics are quite similar, as illustrated by the simultaneous rises, peaks and decreases in figure 5.1, but the amplitude of the variations is overestimated by the model. This is probably due to different rates of increments and decrements, which are the result of distinct processes (carbon allocation, shoot senescence, cattle intake, etc.), all controlled by more or less empirical parameters.

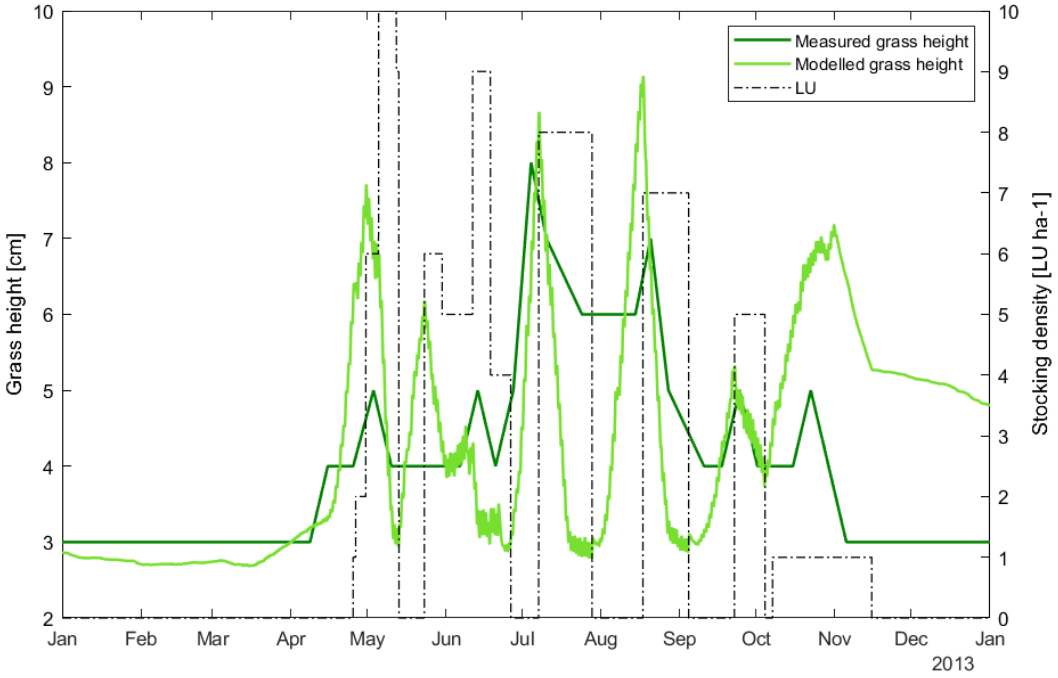

Figure 5.1: Evolution of grass height in Dorinne (2013).

From March to April, modelled grass height remains quite stable, but can not be really compared to measurements which began on the 8^{th} of April. After that date, the measured GPP is boosted and leads to an increase of both measured and modelled grass height. The distinct rates of that increase must be questioned. If it is assumed that measures of GPP are correct, the quantity of carbon that is allocated to the shoot reservoir first depends on the maintenance and growth respiration that are removed from the GPP to obtain the net assimilated carbon, and secondly on the shoot/root allocation coefficient. As explained in section 2.2.3, the maintenance respiration mainly depends on various parameters, among which the reference respiration rate, the shoot and root dry matter content and the dependence on air and soil temperature (equation 2.43). As the temperature dependence is expressed with a $Q10$-like relationship (equation 2.44), up to seven parameters can be spotted to calibrate maintenance respiration. The balance of GPP and maintenance respiration is partitioned between a net carbon assimilation and a growth respiration according to a species-dependent coefficient of assimilation efficiency. This net C assimilate must then be allocated to the above- or below-ground material, depending on a shoot/root allocation coefficient, which depends on the phenological stage, on the shoot and root DM content, and on partitioning parameters. On the 13^{th} of April, vegetation switches to its reproductive phase, and more carbon is allocated to the shoot organs. This modification boosts the shoot grass production in conjunction with the increase of GPP.

It is difficult to determine whether the overestimation of grass height increment is due to a wrong parametrization of maintenance and/or growth respiration or to a poor estimation of the phenological stages and/or their allocation coefficients. As explained before, a real calibration should be performed, considering the high number of parameters involved in the estimation of grass growth. To do so, a sensitivity analysis should be carried out, and modelled grass height could be compared with measures from secured enclosures, described in section 3.2, which enable to neglect the effect of grazing in the estimates of the evolution of grass height.

A potential bias of this calibration could arise from the use of a constant carbon concentration in the shoot, and from the allometric relationship used to transform DM content into plant height. Indeed, it is possible that shoot carbon content is better estimated than the grass height if the transformation of shoot carbon content to grass height brings some bias. Therefore, continuous measures of above-ground carbon content in the secured enclosures could be useful for a precise calibration of grass growth.

On the 25^{th} of April, the first cows arrive on the pasture, but grass height does not start to decrease yet. The peak of shoot height is reached quite simultaneously for the measurements and the simulation, and shoot carbon content only starts falling with higher stocking densities (6 LU ha^{-1} on the 30^{d} of April and 10 LU ha^{-1} on the 5^{th} of May). The rate of this decrease is not similar between observations and predictions. Considering that grass growth is already overestimated, the exports of shoot material due to grass intake and animal trampling are too high. To square with the expected rate of decrease, grass growth should first be calibrated against data from secured enclosures. Afterwards, the reduction of the grass export should arise from a trade-off between the two processes of grass export, controlled by DM_{cap} (equation 2.56) and f_{remove} (equation 2.64).

To do so, different options are possible. Attempts can be made of precisely estimating the intake capacity of Belgian Blue Beef. For Dorinne experimental site, Gourlez de la Motte et al. (2019) estimated the mean intake capacity between 2010 and 2014 at 8.9 kg of DM LU^{-1} day^{-1}. This estimation is based on measures of grass growth both in the pasture and in secured enclosures (to determine grass growth without grazing). Note that this value only considers the grass intake, and not the supplementary feeds given to cattle, so that estimates of grass intake range from 6.8 kg DM in 2013 to 11.9 kg DM in 2011, depending on the amount of feed provided to the herd. The high variability of estimates obtained by Gourlez de la Motte et al. (2019) highlights the strong dependence of intake capacity on environment and management practices. Many other ways of estimating cattle voluntary intake of dry matter are presented in Decruyenaere et al. (2015). The quality of the ingested biomass and the quantity and composition of excreted faeces can be measured and used to estimate cattle intake, but this requires housing the animals in digestibility crates which is not representative of natural conditions encountered in the pasture. Other methods linking *in vivo* intake to laboratory measurements were developed (Decruyenaere et al., 2015) but they are labour intensive and generally present poor repeatability. The alternative tested by Decruyenaere et al. (2015) relies on near infrared reflectance spectroscopy (FNIRS) applied to faeces in order to predict the composition of forage and to deduce from it the cattle voluntary intake. This method could be considered for a precise estimation of intake capacities of BBB in Dorinne, but it requires a continuous sampling of animal faeces. In order to improve the accuracy of the TADA model, the different classes of animals should also be considered through distinct estimations of intake capacities. What is more, estimations of grass intake are very likely to change with environmental conditions and management practices, and these effects should be taken into account with long-term measurements to face various situations.

Another way to estimate animals intake capacity is to follow the methodology proposed in an enhanced version of the PaSim model (Graux et al., 2011). In their new model of grass intake, Graux et al. (2011) distinguish three classes of animals: (1) suckler cows and their claves, (2) dairy cows, (3) beef and dairy heifers. The intake capacity of dairy heifers and beef is computed according to the type of production (milk, meat) and to the animal liveweight. For dairy cows, many variables are considered when estimating the intake capacity: the potential milk production, the liveweight, the body condition scores, the age and the physiological status of the cow. For every category of animal, the real herbage dry matter intake is computed from the intake capacity which can be limited according to the herbage organic matter digestibility (OMD), its nitrogen content, and its availability. To include this module in the TADA model, some improvements are required like the introduction of a new fibre pool, as OMD depends on the fractions of fibres in the ingested shoot compartments, and on their digestibility. Finally, the effect of

temperature is taken into account through a decrease of herbage digestibility above 15°C, and through a limitation of herbage intake at high temperatures, accounting for heat stress. Another approach to predict voluntary intake was developed by Illius & Gordon (1991) with a dynamic mechanistic model simulating rumen processes. However, this level of complexity is too high for a model such as TADA which focuses more on the whole ecosystem dynamics.

A potential error that could arise from the use of a one vertical dimension model is the horizontal heterogeneity of grass consumption. As a matter of fact, cows are generally not evenly distributed over the whole pasture, and some spots of preferential grass consumption may exist. This disparity can lead to over- and underestimations of cattle intake, and with it of grass height. Gourlez de la Motte et al. (2019) tested the hypothesis of a homogeneous cattle distribution on Dorinne pasture, by tracking cows position with GPS devices. This hypothesis is often stated for EC systems, in order to average NEE estimated over the whole pasture. They found out that cattle visited the whole pasture during the day, with a preferential spot in the south-west direction, but tended to cluster near the water trough and near an adjacent pasture in the north-west during the night. This could lead to a biased estimation of grass consumption in some areas of the pasture, especially since the longest and most intense grazing events normally occur at dusk (Gregorini et al., 2006) when the animals tend to gather near the water spot. However, in Dorinne experimental site, where grass height measurements collected on the whole pasture are averaged, the problem of heterogeneity may be reduced. On the one hand, cattle intake could be calibrated against these data, thus balancing the zones of preferential and reduced grass consumption, and on the other hand, the modelled grass height obtained with the hypothesis of a homogeneous field could be compared to the measured and averaged plant height.

The last flux present in equation 5.1 is the dead shoot material entering the litter pool. This flux is directly proportionate to the shoot lifespan, which depends on temperature and water through functions presented in equation 2.53. The reference lifespan of shoot material is difficult to determine, as it depends on the grass species, on grass age and on environmental conditions. Two approaches may be considered. First, shoot lifespan can be calibrated along with other parameters involved in grass growth and grass exports. Alternatively, repeated measures of grass litter could be carried out so as to estimate the death of standing biomass, and its corresponding lifetime.

Conclusion

In order to better understand the dynamics of cropland and grassland ecosystems in a changing environmental context, and facing some new management practices, this work consisted in developing a grassland and cropland model. This conception relied on an existing forest model, which was enhanced in this thesis in order to consider two additional types of ecosystems, namely croplands and grasslands. The resulting model (TADA) has been widely described in this manuscript.

One of the main goals of this thesis was to calibrate some processes or modules present in the TADA model. The model was divided according to its main cycles, and separately calibrated. While this thesis focuses on the water cycle, Delhez (2019) and Vandewattyne (2019) calibrated different carbon and nitrogen modules. The calibration and the validation of soil evaporation relied on the hypothesis that soil evaporation was equal to total evapotranspiration (E_{tot}) during bare soil periods. After a sensitivity analysis identifying the most influential parameters, their values were adjusted by comparing modelled soil evaporation to measures of E_{tot} acquired in a grassland and a cropland sites. Although observations and predictions of bare soil evaporation did not significantly differ when the calibrated parameters were used, modelled soil evaporation was overestimated for soils covered with vegetation. This flux was sometimes higher than E_{tot}, while it should be much lower as plant transpiration is an important component of E_{tot} fluxes. Considering this issue, canopy transpiration could not be calibrated. The unrealistic outputs of soil evaporation module are probably either due to a narrow range of environmental conditions in the dataset of calibration (short periods of bare soil for managed ecosystems) or to a parameterization of the canopy aerodynamic resistance not mechanistic enough. As a conclusion, soil evaporation and plant transpiration should be calibrated simultaneously against E_{tot} measures, or separately but over the same period if the algorithm of Massman (1992) provides a reasonable partitioning of E_{tot} into soil evaporation and plant transpiration.

The infiltration and percolation of water could not be accurately calibrated, as it was difficult to detect whether dissimilarities between modelled and measured SWC were due to a wrong simulation of water transfer or to a data offset inherent to soil moisture probes. So far, only the simulated dynamics of water transfer could be compared to observations. This comparison highlighted the necessity of, firstly, modifying TADA equations in order to consider phenomena such as capillary rise, and secondly to acquire a good estimation of the soil bulk density together with the gravel fraction in order to improve estimates of field capacity and wilting point.

Overall, for any calibration, uncertainties around the dataset should be assessed in order to provide standard deviations around adjusted parameters values, and also to improve the estimation of these parameters. Different methods are presented in Hollinger & Richardson (2005) and Richardson et al. (2006), and should be considered in a future calibration of the TADA model.

Finally, the grazing model was tested by comparing both measured and modelled grass height in a grazed pasture. Improving this module would require adjustments of the maintenance and growth respiration parameters, the shoot/root partitioning coefficient and shoot lifespan during ungrazed periods. Besides that, a better estimation of cattle grass intake should be made, and different ways of doing it are considered.

So far, the TADA model did not prove much of its utility in modelling ecosystems. Many processes, besides the ones already calibrated by Delhez (2019) and Vandewattyne (2019) remain to be calibrated, and some frequent biomass and soil measurements campaigns should be established. Nevertheless, this work was an important part

of the modification of a forest model into a grassland and a cropland one, which is a considerable task. It also illustrates how ecosystem models can be modulated in order to test different practices and environments. Hence, the use of such tools to anticipate the effects of global warming on agricultural ecosystems remains relevant.

Bibliography

AbdElgawad, H., Peshev, D., Zinta, G., Van den Ende, W., Janssens, I. A. & Asard, H. (2014), 'Climate Extreme Effects on the Chemical Composition of Temperate Grassland Species under Ambient and Elevated CO2: A Comparison of Fructan and Non-Fructan Accumulators', *PLoS ONE* **9**(3).

Allard, V., Soussana, J. F., Falcimagne, R., Berbigier, P., Bonnefond, J. M., Ceschia, E., D'hour, P., Hénault, C., Laville, P., Martin, C. & Pinarès-Patino, C. (2007), 'The role of grazing management for the net biome productivity and greenhouse gas budget (CO2, N2O and CH4) of semi-natural grassland', *Agriculture, Ecosystems and Environment* **121**(1-2), 47–58.

Allen, R. G., Pereira, L. S., Raes, D. & Smith, M. (1998), 'Crop evapotranspiration - Guidelines for computing crop water requirements', *FAO irrigation and drainage* **56**, 15.

Amthor, J. S. (1984), 'The role of maintenance respiration in plant growth.', *Plant, Cell and Environment* **7**(8), 561–569.

Andrew, I. K. & Storkey, J. (2016), 'Using simulation models to investigate the cumulative effects of sowing rate, sowing date and cultivar choice on weed competition', *Crop Protection* **95**, 109–115.

Arora, V. K. & Boer, G. J. (2003), 'A Representation of Variable Root Distribution in Dynamic Vegetation Models', *Earth Interactions* **7**, 1–19.

Arora, V. K. & Gajri, P. R. (1998), 'Evaluation of a crop growth-water balance model for analysing wheat responses to climate- and water-limited environments', *Field Crops Research* **59**(3), 213–224.

Arrouays, D., Saby, N. P., Boukir, H., Jolivet, C., Ratié, C., Schrumpf, M., Merbold, L., Gielen, B., Gogo, S., Delpierre, N., Vincent, G., Klumpp, K. & Loustau, D. (2017), 'Soil sampling and preparation for monitoring soil carbon', *International Agrophysics* **32**(4), 633–643.

Asseng, S., Cao, W., Zhang, W. & Ludwig, F. (2009), Crop Physiology, Modelling and Climate Change: Impact and Adaptation Strategies, *in* 'Crop Physiology', Elsevier, pp. 511–543.

Asseng, S., Richter, C. & Wessolek, G. (1997), 'Modelling root growth of wheat as the linkage between crop and soil', *Plant and Soil* **190**, 267–277.

Aubinet, M. ., Grelle, A. ., Ibrom, A. ., Rannik, U. ., Moncrieff, J. ., Foken, T. ., Kowalski, A., Martin, P., Berbigier, P. ., Bernhofer, C. ., Clement, R. ., Elbers, J. ., Granier, A. ., Grunwald, T. ., Morgenstern, K. ., Pilegaard, K. ., Rebmann, C. ., Snijders, W. ., Valentini, R. . & Vesala, T. . (2000), Estimates of the Annual Net Carbon and Water Exchange of Forests: The EUROFLUX Methodology, *in* 'Advances in Ecological Research', Vol. 30, pp. 114–175.

Aubinet, M., Moureaux, C., Bodson, B., Dufranne, D., Heinesch, B., Suleau, M., Vancutsem, F. & Vilret, A. (2009), 'Carbon sequestration by a crop over a 4-year sugar beet / winter wheat / seed potato / winter wheat rotation cycle', *Agricultural and Forest Meteorology* **149**, 407–418.

Aulakh, M. S., Wassmann, R., Bueno, C. & Rennenberg, H. (2001), 'Impact of root exudates of different cultivars and plant development stages of rice (Oryza sativa L.) on methane production in a paddy soil', *Plant and Soil* **230**(1), 77–86.

Bahn, M., Knapp, M., Garajova, Z., Pfahringer, N. & Cernusca, A. (2006), 'Root respiration in temperate mountain grasslands differing in land use', *Global Change Biology* **12**, 995–1006.

Bajželj, B., Richards, K. S., Allwood, J. M., Smith, P., Dennis, J. S., Curmi, E. & Gilligan, C. A. (2014), 'Importance of food-demand management for climate mitigation', *Nature Climate Change* **4**(10), 924–929.

Baldocchi, D. D. (2003), 'Assessing the eddy covariance technique for evaluating carbon dioxide exchange rates of ecosystems: past, present and future', *Global Change Biology* **9**(4), 479–492.

Baldocchi, D. D., Hincks, B. B. & Meyers, T. P. (1988), 'Measuring Biosphere-Atmosphere Exchanges of Biologically Related Gases with Micrometeorological Methods', *Ecology* **69**(5), 1331–1340.

Baldocchi, D. D. & Wilson, K. B. (2001), 'Modeling CO2 and water vapor exchange of a temperate broadleaved forest across hourly to decadal time scales', *Ecological Modelling* **142**(1-2), 155–184.

Baldocchi, D., Detto, M., Sonnentag, O., Verfaillie, J., Teh, Y. A., Silver, W. & Kelly, N. M. (2012), 'The challenges of measuring methane fluxes and concentrations over a peatland pasture', *Agricultural and Forest Meteorology* **153**, 177–187.

Barraclough, P. & Leigh, R. (1984), 'The growth and activity of winter wheat roots in the field: the effect of sowing data and soil type on root growth of high-yielding crops', *The Journal of Agricultural Science* **103**, 59–74.

Bastidas, L. A., Hogue, T. S., Sorooshian, S., Gupta, H. V. & Shuttleworth, W. J. (2006), 'Parameter sensitivity analysis for different complexity land surface models using multicriteria methods', *Journal of Geophysical Research Atmospheres* **111**(20), 1–19.

Beauchemin, K. A., Kreuzer, M., O'Mara, F. & McAllister, T. A. (2008), 'Nutritional management for enteric methane abatement: a review', *Australian Journal of Experimental Agriculture* **48**(2), 21–27.

Beaujouan, V., Durand, P. & Ruiz, L. (2001), 'Modelling the effect of the spatial distribution of agricultural practices on nitrogen fluxes in rural catchments', *Ecological Modelling* **137**(1), 93–105.

Best, M. J., Pryor, M., Clark, D. B., Rooney, G. G., Essery, R. L. H., Ménard, C. B., Edwards, J. M., Hendry, M. A., Porson, A., Gedney, N., Mercado, L. M., Sitch, S., Blyth, E., Boucher, O., Cox, P. M., Grimmond, C. S. B. & Harding, R. J. (2011), 'The Joint UK Land Environment Simulator (JULES), model description – Part 1: Energy and water fluxes', *Geoscientific Model Development* **4**(3), 677–699.

Bhandral, R., Saggar, S., Bolan, N. S. & Hedley, M. J. (2007), 'Transformation of nitrogen and nitrous oxide emission from grassland soils as affected by compaction', *Soil and Tillage Research* **94**(2), 482–492.

Bonan, G. (2008*a*), *Ecological Climatology: Concepts and Applications*, second edn, Cambridge University Press.

Bonan, G. B. (2008*b*), 'Forests and Climate Change: Forcings, Feedbacks, and the Climate Benefits of Forests', *Science* **320**, 1444–1449.

Bond-Lamberty, B. & Thomson, A. (2010), 'Temperature-associated increases in the global soil respiration record', *Nature* **464**(25), 579–582.

Bosello, F. & Zhang, J. (2005), 'Assessing Climate Change Impacts: Agriculture', *SSRN Electronic Journal* **94**(05), 21.

Box, G. & Draper, N. (1987), *Empirical model-building and response surfaces*, Wiley, New York.

Braker, G. & Conrad, R. (2011), *Diversity, structure, and size of N2O-producing microbial communities in soils: What matters for their functioning?*, Vol. 75.

Brasseur, G. P., Gupta, M., Anderson, B. E., Balasubramanian, S., Barrett, S., Duda, D., Fleming, G., Forster, P. M., Fuglestvedt, J., Gettelman, A., Halthore, R. N., Jacob, S. D., Jacobson, M. Z., Khodayari, A., Liou, K. N., Lund, M. T., Miake-Lye, R. C., Minnis, P., Olsen, S., Penner, J. E., Prinn, R., Schumann, U., Selkirk, H. B., Sokolov, A., Unger, N., Wolfe, P., Wong, H. W., Wuebbles, D. W., Yi, B., Yang, P. & Zhou, C. (2016), 'Impact of aviation on climate: FAA's Aviation Climate Change Research Initiative (ACCRI) phase II', *Bulletin of the American Meteorological Society* **97**(4), 561–583.

Brilli, L., Bechini, L., Bindi, M., Carozzi, M., Cavalli, D., Conant, R., Dorich, C. D., Doro, L., Ehrhardt, F., Farina, R., Ferrise, R., Fitton, N., Francaviglia, R., Grace, P., Iocola, I., Klumpp, K., Léonard, J., Martin, R., Massad, R. S., Recous, S., Seddaiu, G., Sharp, J., Smith, P., Smith, W. N., Soussana, J.-F. & Bellocchi, G. (2017), 'Review and analysis of strengths and weaknesses of agro-ecosystem models for simulating C and N fluxes', *Science of The Total Environment* **598**(March), 445–470.

Brisson, N., Gary, C., Justes, E., Roche, R., Mary, B., Ripoche, D., Zimmer, D., Sierra, J., Bertuzzi, P., Burger, P., Bussière, F., Cabidoche, Y. M., Cellier, P., Debaeke, P., Gaudillère, J. P., Hénault, C., Maraux, F., Seguin, B. & Sinoquet, H. (2003), 'An overview of the crop model STICS', *European Journal of Agronomy* **18**(3-4), 309–332.

Brisson, N., Launay, M., Mary, B. & Beaudoin, N. (2008), *Conceptual Basis, Formalisations and Parameterization of the Stics Crop Model*.

Brown, S. (2002), 'Measuring carbon in forests: current status and future challenges', *Environmental Pollution* **116**(3), 363–372.

Bureau, M. (n.d.), Modélisation hydro-géochimique du bassin supérieur de la Moselle, PhD thesis, Nancy-Université - Institut National Polytechnique de Lorraine.

Burney, J. A., Davis, S. J. & Lobell, D. B. (2010), 'Greenhouse gas mitigation by agricultural intensification', *Proceedings of the National Academy of Sciences* **107**(26), 12052–12057.

Butterbach-Bahl, K., Baggs, E. M., Dannenmann, M., Kiese, R. & Zechmeister-Boltenstern, S. (2013), 'Nitrous oxide emissions from soils: How well do we understand the processes and their controls?', *Philosophical Transactions of the Royal Society B: Biological Sciences* **368**.

Buysse, P., Bodson, B., Debacq, A., Ligne, A. D., Heinesch, B., Manise, T., Moureaux, C. & Aubinet, M. (2017), 'Agricultural and Forest Meteorology Carbon budget measurement over 12 years at a crop production site in the silty-loam region in Belgium', *Agricultural and Forest Meteorology* **246**(June), 241–255.

Camillo, P. J. & Gurney, R. J. (1986), 'A resistance parameter for bare-soil evaporation models', *Soil Science* **141**(2), 95–105.

Canadell, J. G. & Raupach, M. R. (2008), 'Managing forests for climate change mitigation', *Science* **320**(5882), 1456–1457.

Cao, G., Tang, Y., Mo, W., Wang, Y., Li, Y. & Zhao, X. (2004), 'Grazing intensity alters soil respiration in an alpine meadow on the Tibetan plateau', *Soil Biology and Biochemistry* **36**, 237–243.

Carlson, K. M., Gerber, J. S., Mueller, N. D., Herrero, M., MacDonald, G. K., Brauman, K. A., Havlik, P., O'Connell, C. S., Johnson, J. A., Saatchi, S. & West, P. C. (2017), 'Greenhouse gas emissions intensity of global croplands', *Nature Climate Change* **7**(1), 63–68.

Chapuis-lardy, L., Wrage, N., Metay, A., Chotte, J. L. & Bernoux, M. (2007), 'Soils, a sink for N2O? A review', *Global Change Biology* **13**(1), 1–17.

Charlson, R., Schwartz, S., Hales, J., Cess, R., Coakley, J., Hansen, J. & Hofmann, D. J. (1992), 'Climate forcing by anthropogenic aerosols', *Science* **255**(1981), 423–430.

Chidawanyika, F., Mudavanhu, P. & Nyamukondiwa, C. (2019), 'Global Climate Change as a Driver of Bottom-Up and Top-Down Factors in Agricultural Landscapes and the Fate of Host-Parasitoid Interactions', *Frontiers in Ecology and Evolution* **7**(March), 1–13.

Choudhury, B. J. (2000), 'A sensitivity analysis of the radiation use efficiency for gross photosynthesis and net carbon accumulation by wheat', **101**, 217–234.

Ciais, P., Reichstein, M., Viovy, N., Granier, A., Ogée, J., Allard, V., Aubinet, M., Buchmann, N., Bernhofer, C., Carrara, A., Chevallier, F., De Noblet, N., Friend, A. D., Friedlingstein, P., Grünwald, T., Heinesch, B., Keronen, P., Knohl, A., Krinner, G., Loustau, D., Manca, G., Matteucci, G., Miglietta, F., Ourcival, J. M., Papale, D., Pilegaard, K., Rambal, S., Seufert, G., Soussana, J. F., Sanz, M. J., Schulze, E. D., Vesala, T. & Valentini, R. (2005), 'Europe-wide reduction in primary productivity caused by the heat and drought in 2003', *Nature* **437**(7058), 529–533.

Ciais, P., Wattenbach, M., Vuichard, N., Smith, P., Piao, S. L., Don, A., Luyssaert, S., Janssens, I. A., Bondeau, A., Dechow, R., LEIP, A., SMITH, P., BEER, C., VAN DER WERF, G. R., GERVOIS, S., VAN OOST, K., TOMELLERI, E., FREIBAUER, A. & SCHULZE, E. D. (2010), 'The European carbon balance. Part 2: croplands', *Global Change Biology* **16**(5), 1409–1428.

Clark, D. B., Mercado, L. M., Sitch, S., Jones, C. D., Gedney, N., Best, M. J., Pryor, M., Rooney, G. G., Essery, R. L. H., Blyth, E., Boucher, O., Harding, R. J., Huntingford, C. & Cox, P. M. (2011), 'The Joint UK Land Environment Simulator (JULES), model description – Part 2: Carbon fluxes and vegetation dynamics', *Geoscientific Model Development* **4**(3), 701–722.

Coleman, K. & Jenkinson, D. S. (2014), 'RothC - A model for the turnover of carbon in soil: Model description and users guide', *Rothamsted Research* p. 44.

Confalonieri, R., Bregaglio, S., Cappelli, G., Francone, C., Carpani, M., Acutis, M., El Aydam, M., Niemeyer, S., Balaghi, R. & Dong, Q. (2013), 'Wheat modeling in Morocco unexpectedly reveals predominance of photosynthesis versus leaf area expansion plant traits', *Agronomy for Sustainable Development* **33**(2), 393–403.

Conrad, R. (1996), 'Soil Microorganisms as Controllers of Atmospheric Trace Gases (H2, CO, CH4, OCS, N2O, and NO)', *Microbiological Reviews* **60**(4), 609–640.

Conrad, R. (2009), 'The global methane cycle: Recent advances in understanding the microbial processes involved', *Environmental Microbiology Reports* **1**(5), 285–292.

Costa, M. H., Yanagi, S. N., Souza, P. J., Ribeiro, A. & Rocha, E. J. (2007), 'Climate change in Amazonia caused by soybean cropland expansion, as compared to caused by pastureland expansion', *Geophysical Research Letters* **34**(7), 2–5.

Crush, J. R., Waghorn, G. C. & Rolston, M. P. (1992), 'Greenhouse gas emissions from pasture and arable crops grown on a Kairanga soil in the Manawatu, North Island, New Zealand', *New Zealand Journal of Agricultural Research* **35**, 253–257.

de Klein, C. A., Smith, L. C. & Monaghan, R. M. (2006), 'Restricted autumn grazing to reduce nitrous oxide emissions from dairy pastures in Southland, New Zealand', *Agriculture, Ecosystems and Environment* **112**, 192–199.

de Noblet-Ducoudré, N., Gervois, S., Ciais, P., Viovy, N., Brisson, N., Seguin, B. & Perrier, A. (2004), 'Coupling the Soil-Vegetation-Atmopshere-Transfer Scheme ORCHIDEE to the agronomy model STICS to study the influence of croplands on the European carbon and water budgets', *Agronomie* **24**(June), 397–407.

de Pury, D. G. G. (1995), Scaling photosynthesis and water use from leaves to paddocks, PhD thesis, The Australian National University, Canberra.

de Pury, D. G. G. & Farquhar, G. D. (1997), 'Simple scaling of photosynthesis from leaves to canopies without the errors of big-leaf models', *Plant, Cell and Environment* **20**(5), 537–557.

Decruyenaere, V., Planchon, V., Dardenne, P. & Stilmant, D. (2015), 'Prediction error and repeatability of near infrared reflectance spectroscopy applied to faeces samples in order to predict voluntary intake and digestibility of forages by ruminants', *Animal Feed Science and Technology* **205**, 49–59.

Delhez, L. (2019), Mechanistic modelling of cropland and grassland ecosystems: focus on the carbon cycle and on plant phenology, Master's thesis, Université de Liège - Gembloux Agro-Bio Tech.

Dentener, F., Stevenson, D., Cofala, J., Mechler, R., Amann, M., Bergamaschi, P., Raes, F. & Derwent, R. (2005), 'The impact of air pollutant and methane emission controls on tropospheric ozone and radiative forcing: CTM calculations for the period 1990-2030', *Atmospheric Chemistry and Physics* **5**(7), 1731–1755.

Dlamini, P., Chivenge, P. & Chaplot, V. (2016), 'Overgrazing decreases soil organic carbon stocks the most under dry climates and low soil pH: A meta-analysis shows', *Agriculture, Ecosystems and Environment* **221**, 258–269.

Downing, T. & Gamroth, M. (2007), Non structural Carbohydrates in Cool-season Grasses, Technical Report November, Oregon State University.

Drewer, J., Anderson, M., Levy, P. E., Scholtes, B., Helfter, C., Parker, J., Rees, R. & Skiba, U. (2017), 'The impact of ploughing intensively managed temperate grasslands on N2O, CH4 and CO2 fluxes', *Plant and Soil* **411**, 193–208.

Dumortier, P., Aubinet, M., Beckers, Y., Chopin, H., Debacq, A., Motte, L. G. D., Jérôme, E., Wilmus, F. & Heinesch, B. (2017), 'Methane balance of an intensively grazed pasture and estimation of the enteric methane emissions from cattle', *Agricultural and Forest Meteorology* **232**, 527–535.

Duursma, R. A. (2015), 'Plantecophys - An R package for analysing and modelling leaf gas exchange data', *PLoS ONE* **10**(11), 1–13.

Ebi, K. L. & McGregor, G. (2008), 'Climate Change, Tropospheric Ozone and Particulate Matter, and Health Impacts', *Environmental Health Perspectives* **116**(11), 1449–1455.

Ehdaie, B., Alloush, G. A., Madore, M. A. & Waines, J. G. (2006), 'Genotypic Variation for Stem Reserves and Mobilization in Wheat', *Crop Science* **46**(5), 2093.

Ehdaie, B., Alloush, G. & Waines, J. (2008), 'Genotypic variation in linear rate of grain growth and contribution of stem reserves to grain yield in wheat', *Field Crops Research* **106**(1), 34–43.

Eurostat (2017), 'Agri-environmental indicator: greenhouse gas emissions'.
URL: *https://ec.europa.eu/eurostat/statistics-explained/index.php?title=Agri-environmental_indicator_-_greenhouse_gas_emissions*

Faivre, R., Leenhardt, D., Voltz, M., Benoît, M., Papy, F., Dedieu, G. & Wallach, D. (2004), 'Spatialising crop models', *Agronomie* **24**, 205–217.

Falge, E., Baldocchi, D., Olson, R., Anthoni, P., Aubinet, M., Bernhofer, C., Burba, G., Ceulemans, R., Clement, R., Dolman, H., Granier, A., Gross, P., Grünwald, T., Hollinger, D., Jensen, N.-O., Katul, G., Keronen, P., Kowalski, A., Lai, C. T., Law, B. E., Meyers, T., Moncrieff, J., Moors, E., Munger, J., Pilegaard, K., Rannik, Ü., Rebmann, C., Suyker, A., Tenhunen, J., Tu, K., Verma, S., Vesala, T., Wilson, K. & Wofsy, S. (2001), 'Gap filling strategies for defensible annual sums of net ecosystem exchange', *Agricultural and Forest Meteorology* **107**(1), 43–69.

Falkowski, P. (2000), 'The Global Carbon Cycle: A Test of Our Knowledge of Earth as a System', *Science* **290**(5490), 291–296.

Falloon, P.; Smith, P.; Betts, R.; Jones, C.D.; Smith, J.; Hemming, D.; Challinor, A. (2009), Carbon Sequestration and Greenhouse Gas Fluxes from Cropland Soils – Climate Opportunities and Threats, *in* S. Singh, ed., 'Climate change and crops', Springer-Verlag Berlin Heidelberg, pp. 81–111.

Fang, C. & Moncrieff, J. B. (1999), 'A model for soil CO2 production and transport 1: Model development', *Agricultural and Forest Meteorology* **95**(4), 225–236.

FAO (2016), 'FAOSTAT Land Use domain'.
URL: *http://www.fao.org/faostat/en/#data/RL*

Farquhar, G. D., von Caemmerer, S. & Berry, J. A. (1980), 'A biochemical model of photosynthetic CO2 assimilation in leaves of C3 species', *Planta* **149**(1), 78–90.

Fischer, R. A. & Maurer, R. (1978), 'Drought resistance in spring wheat cultivars. I. Grain yield responses', *Australian Journal of Agricultural Research* **29**(5), 897–912.

Föhse, D., Claassen, N. & Jungk, A. (1991), 'Phosphorus efficiency of plants - II. Significance of root radius, root hairs and cation-anion balance for phosphorus influx in seven plant species', *Plant and Soil* **132**(2), 261–272.

Frankenberg, C., Meirink, J. F., Van Weele, M., Platt, U. & Wagner, T. (2005), 'Assessing methane emissions from global space-borne observations', *Science* **308**(5724), 1010–1014.

Gabrielle, B., Laville, P., Duval, O., Nicoullaud, B., Germon, J. C. & Hénault, C. (2006), 'Process-based modeling of nitrous oxide emissions from wheat-cropped soils at the subregional scale', *Global Biogeochemical Cycles* **20**(4), 1–11.

Gabrielle, B., Menasseri, S. & Houot, S. (1995), 'Analysis and Field Evaluation of the Ceres Models Water Balance Component', *Soil Science Society of America Journal* **59**(5), 1403.

Gégo, E. (1993), Développement d'un modèle de simulation pour l'étude de l'évolution de l'azote minéral du sol sous une culture de froment d'hiver (Triticum aestivum L.)., PhD thesis, Faculté Universitaire des Sciences Agronomiques de Gembloux.

Gibbs, R. J. & Reid, J. B. (1992), 'Comparison between net and gross root production by winter wheat and by perennial ryegrass', *New Zealand Journal of Crop and Horticultural Science* **20**(4), 483–487.

Goidts, E. & van Wesemael, B. (2007), 'Regional assessment of soil organic carbon changes under agriculture in Southern Belgium (1955–2005)', *Geoderma* **141**(3-4), 341–354.

Gollany, H. T., Follett, R. F. & Liang, Y. (2012), CQESTR Simulations of Soil Organic Carbon Dynamics, *in* 'Managing Agricultural Greenhouse Gases', Elsevier, pp. 271–292.

Gomez-Casanovas, N., Hudiburg, T. W., Bernacchi, C. J., Parton, W. J. & Delucia, E. H. (2016), 'Nitrogen deposition and greenhouse gas emissions from grasslands: Uncertainties and future directions', *Global Change Biology* **22**(4), 1348–1360.

Gourlez de la Motte, L. (2019), Carbon balance of an intensively managed pasture: methodology, evaluation and impacts of weather conditions and grazing strategy, PhD thesis, Université de Liège - Gembloux Agro-Bio Tech.

Gourlez de la Motte, L., Dumortier, P., Beckers, Y., Bodson, B., Heinesch, B. & Aubinet, M. (2019), 'Herd position habits can bias net CO2 ecosystem exchange estimates in free range grazed pastures', *Agricultural and Forest Meteorology* **268**, 156–168.

Gourlez de la Motte, L., Jérôme, E., Mamadou, O., Beckers, Y., Bodson, B., Heinesch, B. & Aubinet, M. (2016), 'Carbon balance of an intensively grazed permanent grassland in southern Belgium', *Agricultural and Forest Meteorology* **228-229**, 370–383.

Graux, A.-I., Gaurut, M., Agabriel, J., Baumont, R., Delagarde, R., Delaby, L. & Soussana, J.-F. (2011), 'Development of the Pasture Simulation Model for assessing livestock production under climate change', *Agriculture, Ecosystems & Environment* **144**(1), 69–91.

Graux, A.-I., Lardy, R., Gaurut, M., Duclos, E. & Klump, K. (2012), PaSim User's guide, Technical Report December, Grassland Ecosystem Research Unit, French National Institute for Agricultural Research.

Gregorini, P., Tamminga, S. & Gunter, S. (2006), 'Behavior and Daily Grazing Patterns of Cattle', *The Professional Animal Scientist* **22**(3), 201–209.

Gregory, P. J., McGowan, M., Biscoe, P. V. & Hunter, B. (1978), 'Water relations of winter wheat. 1. Growth of the root system', *The Journal of Agricultural Science* **91**, 91–102.

Guo, L. & Gifford, R. (2002), 'Soil carbon stocks and land use change: a meta analysis', *Glob Change Biology* **8**, 345–360.

Hannaway, D., Fransen, S., Cropper, J., Consortium, N. P. & Griggs, T. (1999), 'Perennial ryegrass (Lolium perenne L.)', (March 2014).

Hashimoto, S., Wattenbach, M. & Smith, P. (2011), 'A new scheme for initializing process-based ecosystem models by scaling soil carbon pools', *Ecological Modelling* **222**(19), 3598–3602.

Heady, E. O. (1957), 'An Econometric Investigation of the Technology of Agricultural Production Functions', *Econometrica* **25**(2), 249.

Hiller, R. V., Bretscher, D., Delsontro, T., Diem, T., Eugster, W., Henneberger, R., Hobi, S., Hodson, E., Imer, D., Kreuzer, M., Künzle, T., Merbold, L., Niklaus, P. A., Rihm, B., Schellenberger, A., Schroth, M. H., Schubert, C. J., Siegrist, H., Stieger, J., Buchmann, N. & Brunner, D. (2014), 'Anthropogenic and natural methane fluxes in Switzerland synthesized within a spatially explicit inventory', *Biogeosciences* **11**(7), 1941–1960.

Hindrichsen, I. K., Wettstein, H. R., Machmüller, A. & Kreuzer, M. (2006), 'Methane emission, nutrient degradation and nitrogen turnover in dairy cows and their slurry at different milk production scenarios with and without concentrate supplementation', *Agriculture, Ecosystems and Environment* **113**(1-4), 150–161.

Hirasawa, T. & Hsiao, T. C. (1999), 'Some characteristics of reduced leaf photosynthesis at midday in maize growing in the field', *Field Crops Research* **62**(1), 53–62.

Hoad, S., Russel, G., Kettlewell, P. & Belshaw, M. (2004), Root system management in winter wheat : practices to increase water and nitrogen use, Technical Report 351, Home-Grown Cereals Authority, Home-Grown Cereals Authority (UK).

Hodgkinson, L., Dodd, I. C., Binley, A., Ashton, R. W., White, R. P., Watts, C. W. & Whalley, W. R. (2017), 'Root growth in field-grown winter wheat : Some effects of soil conditions, season and genotype', *European Journal of Agronomy* **91**(October), 74–83.

Hofmann, D. J., Butler, J. H., Dlugokencky, E. J., Elkins, J. W., Masarie, K., Montzka, S. A. & Tans, P. (2006), 'The role of carbon dioxide in climate forcing from 1979 to 2004: Introduction of the Annual Greenhouse Gas Index', *Tellus, Series B: Chemical and Physical Meteorology* **58**(5), 614–619.

Hogue, T. S., Bastidas, L. A., Gupta, H. V. & Sorooshian, S. (2006), 'Evaluating model performance and parameter behavior for varying levels of land surface model complexity', *Water Resources Research* **42**(8), 1–17.

Hollinger, D. Y. & Richardson, A. D. (2005), 'Uncertainty in eddy covariance measurements and its application to physiological models', *Tree Physiology* **25**(7), 873–885.

Hoogenboom, G. (2000), 'Contribution of agrometeorology to the simulation of crop production and its applications', *Agricultural and Forest Meteorology* **103**, 137–157.

Hörtnagl, L., Barthel, M., Buchmann, N., Eugster, W., Butterbach-Bahl, K., Díaz-Pinés, E., Zeeman, M., Klumpp, K., Kiese, R., Bahn, M., Hammerle, A., Lu, H., Ladreiter-Knauss, T., Burri, S. & Merbold, L. (2018), 'Greenhouse gas fluxes over managed grasslands in Central Europe', *Global Change Biology* **24**(5), 1843–1872.

Houghton, R. A., House, J. I., Pongratz, J., Van Der Werf, G. R., Defries, R. S., Hansen, M. C., Le Quéré, C. & Ramankutty, N. (2012), 'Carbon emissions from land use and land-cover change', *Biogeosciences* **9**(12), 5125–5142.

Hssaine, B. A., Merlin, O., Rafi, Z., Ezzahar, J., Jarlan, L., Khabba, S. & Er-Raki, S. (2018), 'Calibrating an evapotranspiration model using radiometric surface temperature, vegetation cover fraction and near-surface soil moisture data', *Agricultural and Forest Meteorology* **256-257**, 104–115.

Hutchings, N. & Gordon, I. (2001), 'A dynamic model of herbivore - plant interactions on grasslands', *Ecological Modelling* **136**, 209–222.

Illius, A. W. & Gordon, I. J. (1991), 'Prediction of intake and digestion in ruminants by a model of rumen kinetics integrating animal size and plant characteristics', *The Journal of Agricultural Science* **116**(1), 145–157.

IPCC (1990), 'IPCC Reoprt: Policymakers Summary'.

IPCC (2007), *Climate Change 2007: The Physical Science Basis*, Cambridge University Press, Cambridge.

IPCC (2013), *Climate Change 2013: The Physical Science Basis*, Cambridge University Press, Cambridge.

IPCC (2014), *Climate Change 2014: Synthesis Report*, Geneva, Switzerland.

IRM (2018), Statistiques climatiques des communes belges. Yvoir., Technical report.
URL: *https://www.meteo.be/resources/climatology/climateCity/pdf/climate_INS91141_fr.pdf*

Izaurralde, R., Williams, J., McGill, W., Rosenberg, N. & Jakas, M. Q. (2006), 'Simulating soil C dynamics with EPIC: Model description and testing against long-term data', *Ecological Modelling* **192**(3-4), 362–384.

Jablonski, L. M., Wang, X. & Curtis, P. S. (2002), 'Plant reproduction under elevated CO2 conditions: a meta-analysis of reports on 79 crop and wild species', *New Phytologist* **156**(1), 9–26.

Jackson, R. B., Canadell, J., Ehleringer, J. R., Mooney, H. A., Sala, O. E. & Schulze, E. D. (1996), 'A global analysis of root distributions for terrestrial biomes', *Oecologia* **108**(3), 389–411.

Jensen, B. B. (1996), 'Methanogenesis in monogastric animals', *Environmental Monitoring and Assessment* **42**, 99–112.

Jérôme, E., Beckers, Y., Bodson, B., Heinesch, B., Moureaux, C. & Aubinet, M. (2014), 'Impact of grazing on carbon dioxide exchanges in an intensively managed Belgian grassland', *Agriculture, Ecosystems and Environment* **194**, 7–16.

Jiang, Y., Li, Y., Nie, G. & Liu, H. (2016), 'Leaf and Root Growth, Carbon and Nitrogen Contents, and Gene Expression of Perennial Ryegrass to Different Nitrogen Supplies', *Journal of the American Society for Horticultural Science* **141**(6), 555–562.

Johnson, R. D. (2011), 'Soil ph its relationship with crop biodiversity and production', (8), 1–14.

Jones, C. A., Bland, W. L., Ritchie, J. & Williams, J. R. (1991), Simulation of Root Growth, *in* 'Modeling Plant and Soil Systems', number January, Agronomy Monograph, pp. 91–123.

Jones, H. G. (1992), *Plants and Microclimate: a Quantitative Approach to Environmental Plant Physiology*, second edn, Cambridge University Press.

Jones, J., Hoogenboom, G., Porter, C., Boote, K., Batchelor, W., Hunt, L., Wilkens, P., Singh, U., Gijsman, A. & Ritchie, J. (2003), 'The DSSAT cropping system model', *European Journal of Agronomy* **18**(3-4), 235–265.

Jones, J. W., Antle, J. M., Basso, B., Boote, K. J., Conant, R. T., Foster, I., Godfray, H. C. J., Herrero, M., Howitt, R. E., Janssen, S., Keating, B. A., Munoz-Carpena, R., Porter, C. H., Rosenzweig, C. & Wheeler, T. R. (2016), 'Brief history of agricultural systems modeling', *Agricultural Systems* **155**, 240–254.

Jones, M. B. & Donnelly, A. (2004), 'Carbon sequestration in temperate grassland ecosytems and the influence of management, climate and elevated CO2', *New Phytologist* **164**, 423–439.

Jongen, M., Jones, M. B., Hebeisen, T., Blum, H. & Hendrey, G. (1995), 'The effects of elevated CO2 concentrations on the root growth of Lolium perenne and Trifolium repens grown in a FACE* system', *Global Change Biology* **1**(5), 361–371.

Jouven, M., Carrère, P. & Baumont, R. (2006), 'Model predicting dynamics of biomass , structure and digestibility of herbage in managed permanent pastures. 1. Model description', *Grass and Forage Sciences* **61**, 112–124.

Kammann, C., Grünhage, L., Jäger, H.-J. & Wachinger, G. (2001), 'Methane fluxes from differentially managed grassland study plots: the important role of CH4 oxidation in grassland with a high potential for CH4 production', *Environmental Pollution* **115**, 261–273.

Kelliher, F. M., Leuning, R. & Schulze, E. D. (1993), 'Evaporation and canopy characteristics of coniferous forests and grasslands', *Oecologia* **95**(2), 153–163.

Khalil, M. A. K. & Shearer, M. J. (2000), Sources of Methane: An Overview, *in* 'Atmospheric Methane', Springer Berlin Heidelberg, Berlin, Heidelberg, pp. 98–111.

Kimball, B., Kobayashi, K. & Bindi, M. (2002), Responses of Agricultural Crops to Free-Air CO2 Enrichment, *in* 'Advances in Agronomy', Vol. 77, Elsevier Inc., pp. 293–368.

Kiniry, J. R. (1993), 'Nonstructural Carbohydrate Utilization by Wheat Shaded during Grain Growth', *Agronomy Journal* **85**(4), 844–849.

Kirkegaard, J. & Lilley, J. (2007), 'Root penetration rate - A benchmark to identify soil and plant limitations to rooting depth in wheat', *Australian Journal of Experimental Agriculture* **47**(5), 590–602.

Kirschke, S., Bousquet, P., Ciais, P., Saunois, M., Canadell, J. G., Dlugokencky, E. J., Bergamaschi, P., Bergmann, D., Blake, D. R., Bruhwiler, L., Cameron-Smith, P., Castaldi, S., Chevallier, F., Feng, L., Fraser, A., Heimann, M., Hodson, E. L., Houweling, S., Josse, B., Fraser, P. J., Krummel, P. B., Lamarque, J. F., Langenfelds, R. L., Le Quéré, C., Naik, V., O'doherty, S., Palmer, P. I., Pison, I., Plummer, D., Poulter, B., Prinn, R. G., Rigby, M., Ringeval, B., Santini, M., Schmidt, M., Shindell, D. T., Simpson, I. J., Spahni, R., Steele, L. P., Strode, S. A., Sudo, K., Szopa, S., Van Der Werf, G. R., Voulgarakis, A., Van Weele, M., Weiss, R. F., Williams, J. E. & Zeng, G. (2013), 'Three decades of global methane sources and sinks', *Nature Geoscience* **6**(10), 813–823.

Knapp, J., Laur, G., Vadas, P., Weiss, W. & Tricarico, J. (2014), 'Invited review: Enteric methane in dairy cattle production: Quantifying the opportunities and impact of reducing emissions', *Journal of Dairy Science* **97**(6), 1–31.

Kon Kam King, J., Granjou, C., Fournil, J. & Cecillon, L. (2018), 'Soil sciences and the French 4 per 1000 Initiative—The promises of underground carbon', *Energy Research and Social Science* **45**(December 2017), 144–152.

Krinner, G., Viovy, N., de Noblet-Ducoudré, N., Ogée, J., Polcher, J., Friedlingstein, P., Ciais, P., Sitch, S. & Prentice, I. C. (2005), 'A dynamic global vegetation model for studies of the coupled atmosphere-biosphere system', *Global Biogeochemical Cycles* **19**(1), 1–33.

Kröbel, R., Smith, W., Grant, B., Desjardins, R., Campbell, C., Tremblay, N., Li, C., Zentner, R. & McConkey, B. (2011), 'Development and evaluation of a new Canadian spring wheat sub-model for DNDC', *Canadian Journal of Soil Science* **91**(4), 503–520.

Külling, D. R., Dohme, F., Menzi, H., Sutter, F., Lischer, P. & Kreuzer, M. (2002), 'Methane Emissions of Differently fed Dairy Cows and Corresponding Methane and Nitrogen Emissions From Their Manure During Storage', *Environmental Monitoring and Assessment* **79**, 129–150.

Lal, R. (2004), 'Soil Carbon Sequestration Impacts on Global climate change and food security', *Science* **304**, 1623–1628.

Lal, R. (2010), 'Managing Soils and Ecosystems for Mitigating Anthropogenic Carbon Emissions and Advancing Global Food Security', *BioScience* **60**(9), 708–721.

Lal, R. & Kimble, J. M. (1997), 'Conservation tillage for carbon sequestration', *Nutrient Cycling in Agroecosystems* **49**, 243–253.

Laville, P., Lehuger, S., Loubet, B., Chaumartin, F. & Cellier, P. (2011), 'Effect of management, climate and soil conditions on N2O and NO emissions from an arable crop rotation using high temporal resolution measurements', *Agricultural and Forest Meteorology* **151**(2), 228–240.

Lazzarotto, P., Calanca, P. & Fuhrer, J. (2009), 'Dynamics of grass-clover mixtures-An analysis of the response to management with the PROductive GRASsland Simulator (PROGRASS)', *Ecological Modelling* **220**(5), 703–724.

Leuning, R. (1995), 'A critical appraisal of a combined stomatal-photosynthesis model for C3 plants', *Plant, Cell and Environment* **18**(4), 339–355.

Leuthold, R. M. (1975), 'On the Use of Theil's Inequality Coefficients', *American Journal of Agricultural Economics* **57**(2), 344–346.

Li, C., Frolking, S. & Frolking, T. A. (1992), 'A model of nitrous oxide evolution from soil driven by rainfall events: 1. Model Structure and Sensitivity', *Journal of Geophysical Research* **97**(D9), 9759–9776.

Li, C., Frolking, S. & Harriss, R. (1994), 'Modeling carbon biogeochemistry in agricultural soils', *Global Biogeochemical Cycles* **8**(3), 237–254.

Li, C., Han, Q., Luo, G., Zhao, C., Li, S., Wang, Y. & Yu, D. (2018), 'Effects of cropland conversion and climate change on agrosystem carbon balance of China's Dryland: A typical watershed study', *Sustainability* **10**(12), 1–16.

Li, C., Salas, W., Zhang, R., Krauter, C., Rotz, A. & Mitloehner, F. (2012), 'Manure-DNDC: a biogeochemical process model for quantifying greenhouse gas and ammonia emissions from livestock manure systems', *Nutrient Cycling in Agroecosystems* **93**(2), 163–200.

Liang, S., Wang, K., Zhang, X. & Wild, M. (2010), 'Review on Estimation of Land Surface Radiation and Energy Budgets From Ground Measurement, Remote Sensing and Model Simulations', *IEEE Journal of Selected Topics in Applied Earth Observations and Remote Sensing* **3**(3), 225–240.

Lin, X., Zhang, Z., Wang, S., Hu, Y., Xu, G., Luo, C., Chang, X., Duan, J., Lin, Q., Xu, B., Wang, Y., Zhao, X. & Xie, Z. (2011), 'Response of ecosystem respiration to warming and grazing during the growing seasons in the alpine meadow on the Tibetan plateau', *Agricultural and Forest Meteorology* **151**(7), 792–802.

Lloyd, J. & Taylor, J. A. (1994), 'On the Temperature Dependence of Soil Respiration', *Functional Ecology* **8**(3), 315.

Loarie, S. R., Lobell, D. B., Asner, G. P. & Field, C. B. (2011), 'Land-Cover and surface water change drive large albedo increases in south america', *Earth Interactions* **15**(7), 1–16.

Lobell, D. B., Bala, G. & Duffy, P. B. (2006), 'Biogeophysical impacts of cropland management changes on climate', *Geophysical Research Letters* **33**(6), 4–7.

Lognoul, M., Debacq, A., Ligne, A. D., Dumont, B., Manise, T., Bodson, B., Heinesch, B. & Aubinet, M. (2019), 'Agricultural and Forest Meteorology N2O flux short-term response to temperature and topsoil disturbance in a fertilized crop: An eddy covariance campaign', *Agricultural and Forest Meteorology* **271**(October 2018), 193–206.

Lognoul, M., Theodorakopoulos, N., Hiel, M.-p., Regaert, D., Broux, F., Heinesch, B., Bodson, B., Vandenbol, M. & Aubinet, M. (2017), 'Impact of tillage on greenhouse gas emissions by an agricultural crop and dynamics of N2O fluxes : Insights from automated closed chamber measurements', *Soil & Tillage Research* **167**, 80–89.

Lohmann, U. & Feichter, J. (2005), 'Global indirect aerosol effects: a review', *Atmospheric Chemistry and Physics Discussions* **4**(6), 7561–7614.

Lokupitiya, E. & Paustian, K. (2006), 'Agricultural Soil Greenhouse Gas Emissions', *Journal of Environment Quality* **35**(4), 1413.

Longdoz, B., Yernaux, M. & Aubinet, M. (2000), 'Soil CO2 efflux measurements in a mixed forest: Impact of chamber disturbances, spatial variability and seasonal evolution', *Global Change Biology* **6**(8), 907–917.

Luo, Y., Wan, S., Hui, D. & Wallace, L. L. (2001), 'Acclimatization of soil respiration to warming in a tall grass prairie', *Nature* **413**(11), 622–625.

Lüscher, A., Mueller-Harvey, I., Soussana, J. F., Rees, R. M. & Peyraud, J. L. (2014), 'Potential of legume-based grassland-livestock systems in Europe: A review', *Grass and Forage Science* **69**(2), 206–228.

Ma, S., Churkina, G., Wieland, R. & Gessler, A. (2011), 'Optimization and evaluation of the ANTHRO-BGC model for winter crops in Europe', *Ecological Modelling* **222**(20-22), 3662–3679.

Ma, S., Lardy, R., Graux, A.-I., Ben Touhami, H., Klumpp, K., Martin, R. & Bellocchi, G. (2015), 'Regional-scale analysis of carbon and water cycles on managed grassland systems', *Environmental Modelling & Software* **72**, 356–371.

MacDonald, G. J. (1988), 'Scientific Basis for the Greenhouse Effect', *Journal of Policy Analysis and Management* **7**(3), 425.

Maes, W. H., Gentine, P., Verhoest, N. E. C. & Miralles, D. G. (2019), 'Potential evaporation at eddy-covariance sites across the globe', *Hydrology and Earth System Sciences* **23**(2), 925–948.

Mahfouf, J. & Noilhan, J. (1991), 'Comparative study of various formulations of evaporation from bare soil using in situ data', *Journal of Applied Meteorology* **30**, 1354–1364.

Marcelis, L. & Heuvelink, E. (2007), Concepts of Modelling Carbon Allocation Among Plant Organs, *in* J. Vos, J; Marcelis, LFM; de Visser, PHB; Struik, PC; Evers, ed., 'Functional-Structural Plant Modelling in Crop Production'.

Marshall, T. & Holmes, J. (1988), *Soil Physics*, second edn, Cambridge University Press.

Martin, C., Morgavi, D. P. & Doreau, M. (2010), 'Methane mitigation in ruminants: from microbe to the farm scale', *Animal* **4:3**(March), 351–365.

Massman, W. J. (1992), 'A surface energy balance method for partitioning evapotranspiration data into plant and soil components for a surface with partial canopy cover', *Water Resources Research* **28**(6), 1723–1732.

McCown, R., Hammer, G., Hargreaves, J., Holzworth, D. & Freebairn, D. (1996), 'APSIM: a novel software system for model development, model testing and simulation in agricultural systems research', *Agricultural Systems* **50**(3), 255–271.

McCree, K. (1970), An equation for the rate of respiration of white clover plants grown under controlled conditions, *in* I. Setlik, ed., 'Prediction and Measurement of Photosynthetic Productivity', PUDOC, Wageningen, pp. 221–229.

Medlyn, B. E., Robinson, A. P., Clement, R. & McMurtrie, R. E. (2005), 'On the validation of models of forest CO2 exchange using eddy covariance data: some perils and pitfalls', *Tree Physiology* **25**(7), 839–857.

Merbold, L., Werner, E., Jacqueline, S., Mark, Z., David, N. & Nina, B. (2014), 'Greenhouse gas budget (CO2,CH4 and N2O) of intensively managed grassland following restoration', *Glob Change Biology* **20**, 1913–1928.

Merino, A., Pérez-Batallón, P. & Macías, F. (2004), 'Responses of soil organic matter and greenhouse gas fluxes to soil management and land use changes in a humid temperate region of southern Europe', *Soil Biology and Biochemistry* **36**(6), 917–925.

Merlin, O., Olivera-Guerra, L., Hssaine, B. A., Amazirh, A., Rafi, Z., Ezzahar, J., Gentine, P., Khabba, S., Gascoin, S. & Er-Raki, S. (2018), 'A phenomenological model of soil evaporative efficiency using surface soil moisture and temperature data', *Agricultural and Forest Meteorology* **256-257**(May 2017), 501–515.

Mika, J., Horváth, S. & Makra, L. (2001), 'Impact of documented land use changes on the surface albedo and evapotranspiration in a plain watershed', *Physics and Chemistry of the Earth, Part B: Hydrology, Oceans and Atmosphere* **26**(7-8), 601–606.

Misson, L., Rasse, D. P., Vincke, C., Aubinet, M. & François, L. (2002), 'Predicting transpiration from forest stands in Belgium for the 21st century', *Agricultural and Forest Meteorology* **111**, 265–282.

Mitchell, P. (1997), 'Misuse of regression for empirical validation of models', *Agricultural Systems* **54**(3), 313–326.

Moffat, A. M., Papale, D., Reichstein, M., Hollinger, D. Y., Richardson, A. D., Barr, A. G., Beckstein, C., Braswell, B. H., Churkina, G., Desai, A. R., Falge, E., Gove, J. H., Heimann, M., Hui, D., Jarvis, A. J., Kattge, J., Noormets, A. & Stauch, V. J. (2007), 'Comprehensive comparison of gap-filling techniques for eddy covariance net carbon fluxes', *Agricultural and Forest Meteorology* **147**(3-4), 209–232.

Monteith, J. L. (1972), 'Solar Radiation and Productivity in Tropical Ecosystems', *The Journal of Applied Ecology* **9**(3), 747.

Monteith, J. L. & Moss, C. J. (1977), 'Climate and the Efficiency of Crop Production in Britain [and Discussion]', *Philosophical Transactions of the Royal Society B: Biological Sciences* **281**(980), 277–294.

Monteith, J. L. & Unsworth, M. (1990), *Principles of Environmental Physics*, second edn, Edward Arnold Publishers Ltd.

Moorhead, J., Marek, G., Gowda, P., Lin, X., Colaizzi, P., Evett, S. & Kutikoff, S. (2019), 'Evaluation of Evapotranspiration from Eddy Covariance Using Large Weighing Lysimeters', *Agronomy* **9**(2), 99.

Moureaux, C., Debacq, A., Bodson, B., Heinesch, B. & Aubinet, M. (2006), 'Annual net ecosystem carbon exchange by a sugar beet crop', *Agricultural and Forest Meteorology* .

Mulligan, F., Dillon, P., Callan, J., Rath, M. & O'Mara, F. (2004), 'Supplementary Concentrate Type Affects Nitrogen Excretion of Grazing Dairy Cows', *Journal of Dairy Science* **87**(10), 3451–3460.

Necpálová, M., Anex, R. P., Fienen, M. N., Del Grosso, S. J., Castellano, M. J., Sawyer, J. E., Iqbal, J., Pantoja, J. L. & Barker, D. W. (2015), 'Understanding the DayCent model: Calibration, sensitivity, and identifiability through inverse modeling', *Environmental Modelling and Software* **66**, 110–130.

Newman, E. I. (1978), 'Root microorganisms: their significance in the ecosystem', *biol. Rev.* **53**(11), 511–554.

Nieto, O. M., Castro, J., Fernández, E. & Smith, P. (2010), 'Simulation of soil organic carbon stocks in a Mediterranean olive grove under different soil-management systems using the RothC model', *Soil Use and Management* **26**(2), 118–125.

Nisbet, E. G., Dlugokencky, E. J. & Bousquet, P. (2014), 'Methane on the Rise–Again', *Science* **343**(6170), 493–495.

Nonhebel, S. (1994), 'Inaccuracies in weather data and their effects on crop growth simulation results. I. Potential production', *Climate Research* **4**(1), 47–60.

Obropta, C. C. & Kardos, J. S. (2007), 'Review of Urban Stormwater Quality Models: Deterministic, Stochastic, and Hybrid Approaches', *Journal of the American Water Resources Association* **43**(6), 1508–1523.

Oenema, O., Velthof, G., Yamulki, S. & Jarvis, S. (1997), 'Nitrous oxide emissions from grazed grassland', *Soil Use and Management* **13**, 288–295.

Ojima, D. S., Parton, W. J., Schimel, D. S., Scurlock, J. M. & Kittel, T. G. (1993), 'Modeling the effects of climatic and CO2 changes on grassland storage of soil C', *Water, Air, & Soil Pollution* **70**, 643–657.

Owensby, C. E., Ham, J. M. & Auen, L. M. (2006), 'Fluxes of CO2 From Grazed and Ungrazed Tallgrass Prairie', *Rangeland Ecology and Management* **59**(2), 111–127.

Palosuo, T., Kersebaum, K. C., Angulo, C., Hlavinka, P., Moriondo, M., Olesen, J. E., Patil, R. H., Ruget, F., Rumbaur, C., Takáč, J., Trnka, M., Bindi, M., Çaldağ, B., Ewert, F., Ferrise, R., Mirschel, W., Şaylan, L., Šiška, B. & Rötter, R. (2011), 'Simulation of winter wheat yield and its variability in different climates of Europe: A comparison of eight crop growth models', *European Journal of Agronomy* **35**(3), 103–114.

Papale, D., Reichstein, M., Aubinet, M., Canfora, E., Bernhofer, C., Kutsch, W., Longdoz, B., Rambal, S., Valentini, R., Vesala, T. & Yakir, D. (2006), 'Towards a standardized processing of Net Ecosystem Exchange measured with eddy covariance technique: algorithms and uncertainty estimation', *Biogeosciences* **3**(4), 571–583.

Parry, M., Arnell, N., McMichael, T., Nicholls, R., Martens, P., Kovats, S., Livermore, M., Rosenzweig, C., Iglesias, A. & Fischer, G. (2001), 'Millions at risk: defining critical climate change threats and targets', *Global Environmental Change* **11**(3), 181–183.

Parton, W. J., Hartman, M., Ojima, D. & Schimel, D. (1998), 'DAYCENT and its land surface submodel: description and testing', *Global and Planetary Change* **19**(1-4), 35–48.

Paterson, M. (1996), *Global Warming and Global Politics*, Routledge, London.

Peeters, A. (2009), 'Importance, evolution, environmental impact and future challenges of grasslands and grassland-based systems in Europe', *Grassland Science* **55**(3), 113–125.

Peichl, M., Carton, O. & Kiely, G. (2012), 'Management and climate effects on carbon dioxide and energy exchanges in a maritime grassland', *Agriculture, Ecosystems and Environment* **158**, 132–146.

Petit, R. J., Raynaud, D., Basile, I., Chappellaz, J., Ritz, C., Delmotte, M., Legrand, M., Lorius, C., Pe, L., Petit, J.-R., Jouzel, J., Raynaud, D., Barkov, N. I., Barnola, J.-M., Basile, I., Bender, M., Chappellaz, J., Davis, M. & Delaygue, G. (1999), 'Climate and atmospheric history of the past 420,000 years from the Vostok ice core, Antarctica', *Nature* **399**(6735), 429–436.

Pheloung, P. & Siddique, K. (1991), 'Contribution of Stem Dry Matter to Grain Yield in Wheat Cultivars', *Functional Plant Biology* **18**(1), 53.

Philip, J. (1957), 'Evaporation, and moisture and heat fields in the soil', *Journal Of Meteorology* **14**, 354–366.

Pitari, G., Iachetti, D., di Genova, G., de Luca, N., Søvde, O. A., Hodnebrog, O., Lee, D. S. & Lim, L. L. (2015), 'Impact of coupled NOx/aerosol aircraft emissions on ozone photochemistry and radiative forcing', *Atmosphere* **6**(6), 751–782.

Polley, H. W., Frank, A. B., Sanabria, J. & Phillips, R. L. (2008), 'Interannual variability in carbon dioxide fluxes and flux-climate relationships on grazed and ungrazed northern mixed-grass prairie', *Global Change Biology* **14**, 1620–1632.

Porter, J. & Gawith, M. (1999), 'Temperatures and the growth and development of wheat: a review', *European Journal of Agronomy* **10**, 23–36.

Price, S. J., Kelliher, F. M., Sherlock, R. R., Tate, K. R. & Condron, L. M. (2004), 'Environmental and chemical factors regulating methane oxidation in a New Zealand forest soil', *Australian Journal of Soil Research* **42**(7), 767–776.

Puche, N., Senapati, N., Flechard, C., Klumpp, K., Kirschbaum, M. & Chabbi, A. (2019), 'Modeling Carbon and Water Fluxes of Managed Grasslands: Comparing Flux Variability and Net Carbon Budgets between Grazed and Mowed Systems', *Agronomy* **9**(4), 183.

Puech-Suanzes, I., Hsiao, T., Fereres, E. & Henderson, D. (1989), 'Water-Stress Effect on the Carbon Exchange Rates of Three Upland Cotton (Gossypium hirsutum) Cultivars in the Field', *Field Crops Research* **21**, 239–255.

Raiesi, F. & Asadi, E. (2006), 'Soil microbial activity and litter turnover in native grazed and ungrazed rangelands in a semiarid ecosystem', *Biology and Fertility of Soils* **43**, 76–82.

Ramanathan, V. & Feng, Y. (2009), 'Air pollution, greenhouse gases and climate change: Global and regional perspectives', *Atmospheric Environment* **43**(1), 37–50.

Randerson, J. T., Chapin, F., Harden, J. C., Neff, J. C. & E., H. M. (2002), 'Net Ecosystem Production : a Comprehensive Measure of Net Carbon Accumulation By Ecosystems', *Ecological Applications* **12**(4), 937–947.

Rasse, D. P. (2002), 'Nitrogen deposition and atmospheric CO2 interactions on fine root dynamics in temperate forests: A theoretical model analysis', *Global Change Biology* **8**(5), 486–503.

Rasse, D. P., François, L., Aubinet, M., Kowalski, A. S., Vande Walle, I., Laitat, E. & Gérard, J.-C. (2001), 'Modelling short-term CO2 fluxes and long-term tree growth in temperate forests with ASPECTS', *Ecological Modelling* **141**(1-3), 35–52.

Rauch, W., Bertrand-Krajewski, J.-L., Krebs, P., Mark, O., Schilling, W., Schütze, M. & Vanrolleghem, P. (2002), 'Deterministic modelling of integrated urban drainage systems', *Water Science and Technology* **45**(3), 81–94.

Ravishankara, A. R., Daniel, J. S. & Portmann, R. W. (2009), 'Nitrous Oxide (N2O): The Dominant Ozone-Depleting Substance Emitted in the 21st Century', *Science* **326**(5949), 123–125.

Rawls, W. J., Gimenez, D. & Grossman, R. (1998), 'Use of Soil Texture, Bulk Density, and Slope of the Water Retention Curve to predict Saturated Hydraulic Conductivity', *Transactions of the American Society of Agricultural Engineers* **41**(4), 983–988.

Rees, R. M., Augustin, J., Alberti, G., Ball, B. C., Boeckx, P., Cantarel, A., Castaldi, S., Chirinda, N., Chojnicki, B., Giebels, M., Gordon, H., Grosz, B., Horvath, L., Juszczak, R., Kasimir Klemedtsson, Å., Klemedtsson, L., Medinets, S., Machon, A., Mapanda, F., Nyamangara, J., Olesen, J. E., Reay, D. S., Sanchez, L., Sanz Cobena, A., Smith, K. A., Sowerby, A., Sommer, M., Soussana, J. F., Stenberg, M., Topp, C. F., Van Cleemput, O., Vallejo, A., Watson, C. A. & Wuta, M. (2013), 'Nitrous oxide emissions from European agriculture: An analysis of variability and drivers of emissions from field experiments', *Biogeosciences* **10**(4), 2671–2682.

Reichstein, M., Bahn, M., Ciais, P., Frank, D., Mahecha, M. D., Seneviratne, S. I., Zscheischler, J., Beer, C., Buchmann, N., Frank, D. C., Papale, D., Rammig, A., Smith, P., Thonicke, K., van der Velde, M., Vicca, S., Walz, A. & Wattenbach, M. (2013), 'Climate extremes and the carbon cycle', *Nature* **500**, 287.

Reynolds, S., Batello, C., Baas, S. & Mack, S. (2005), Grasslands and forage to improve livelihoods and reduce poverty, *in* D. McGilloway, ed., 'Grassland: a Global Resource', Wageningen Academic Pulishers, pp. 323–338.

Rezaei, E. E., Siebert, S., Hüging, H. & Ewert, F. (2018), 'Climate change effect on wheat phenology depends on cultivar change', *Scientific Reports* **8**(1), 1–10.

Richardson, A. D., Hollinger, D. Y., Burba, G. G., Davis, K. J., Flanagan, L. B., Katul, G. G., William Munger, J., Ricciuto, D. M., Stoy, P. C., Suyker, A. E., Verma, S. B. & Wofsy, S. C. (2006), 'A multi-site analysis of random error in tower-based measurements of carbon and energy fluxes', *Agricultural and Forest Meteorology* **136**(1-2), 1–18.

Ridley, B., Boland, J. & Lauret, P. (2010), 'Modelling of diffuse solar fraction with multiple predictors', *Renewable Energy* **35**(2), 478–483.

Riedo, M., Grub, A., Rosset, M. & Fuhrer, J. (1998), 'A pasture simulation model for dry matter production, and fluxes of carbon, nitrogen, water and energy', *Ecological Modelling* **105**(2-3), 141–183.

Riedo, M., Gyalistras, D. & Fuhrer, J. (2000), 'Net primary production and carbon stocks in differently managed grasslands: Simulation of site-specific sensitivity to an increase in atmospheric CO2 and to climate change', *Ecological Modelling* **134**(2-3), 207–227.

Ritchie, J. T. & Otter, S. (1985), 'Description and performance of CERES-Wheat: a user-oriented wheat yield model', *ARS Wheat Yield Project* **38**, 159–175.

Robertson, G. & Groffman, P. (2007), Nitrogen Transformations, *in* E. Paul, ed., 'Soil Microbiology, Chemistry, and Ecology', New York, USA, pp. 341– 364.

Robertson, G. P. (2004), 'Abatement of nitrous oxide, methane, and the other non-CO2 greenhouse gases: the need for a systems approach', *The global carbon cycle* pp. 493–506.

Robertson, G. P. & Vitousek, P. (2009), 'Nitrogen in Agriculture: Balancing the Cost of an Essential Resource', *Annual Review of Environement and Resources* **34**(97-125).

Robinson, D., Linehan, D. & Caul, S. (1991), 'What limits nitrate uptake from soil?', *Plant, Cell & Environment* **14**(1), 77–85.

Roche, J., Turnbull, M. H., Guo, Q., Novák, O., Späth, J., Gieseg, S. P., Jameson, P. E. & Love, J. (2017), 'Coordinated nitrogen and carbon remobilization for nitrate assimilation in leaf, sheath and root and associated cytokinin signals during early regrowth of Lolium perenne', *Annals of Botany* **119**(8), 1353–1364.

Rochette, P. & Janzen, H. H. (2005), 'Towards a revised coefficient for estimating N2O emissions from legumes', *Nutrient Cycling in Agroecosystems* **73**(2-3), 171–179.

Rogiers, N., Eugster, W., Furger, M. & Siegwolf, R. (2005), 'Effect of land management on ecosystem carbon fluxes at a subalpine grassland site in the Swiss Alps', *Theoretical and Applied Climatology* **80**, 187–203.

Rosenzweig, C., Jones, J., Hatfield, J., Ruane, A., Boote, K., Thorburn, P., Antle, J., Nelson, G., Porter, C., Janssen, S., Asseng, S., Basso, B., Ewert, F., Wallach, D., Baigorria, G. & Winter, J. (2013), 'The Agricultural Model Intercomparison and Improvement Project (AgMIP): Protocols and pilot studies', *Agricultural and Forest Meteorology* **170**, 166–182.

Rutkowska, B., Szulc, W., Sosulski, T., Skowrońska, M. & Szczepaniak, J. (2018), 'Impact of reduced tillage on CO2 emission from soil under maize cultivation', *Soil and Tillage Research* **180**(August 2017), 21–28.

Ryan, M. G. (1991), 'Effects of Climate Change on Plant Respiration', *Ecological Applications* **1**(2), 157–167.

Saggar, S., Jha, N., Deslippe, J., Bolan, N. S., Luo, J., Giltrap, D. L., Kim, D. G., Zaman, M. & Tillman, R. W. (2013), 'Denitrification and N2O: N2 production in temperate grasslands: Processes, measurements, modelling and mitigating negative impacts', *Science of the Total Environment* **465**, 173–195.

Salazar-Gutierrez, M., Johnson, J. & Chaves-Cordoba, B. (2013), 'Relationship of base temperature to development of winter wheat', *International Journal of Plant Production* **7**(4).

Saxton, K. E. & Rawls, W. J. (2006), 'Soil Water Characteristic Estimates by Texture and Organic Matter for Hydrologic Solutions', *Soil Science Society of America journal* **70**, 1569–1578.

Schimel, D. S. (1995), 'Terrestrial ecosystems and the carbon cycle', *Global Change Biology* **1**(1), 77–91.

Schjoerring, J. K. & Mattsson, M. (2001), 'Quantification of ammonia exchange between agricultural cropland and the atmosphere: Measurements over two complete growth cycles of oilseed rape, wheat, barley and pea', *Plant and Soil* **228**(1), 105–115.

Schlesinger, W. H. (2013), 'An estimate of the global sink for nitrous oxide in soils', *Global Change Biology* **19**(10), 2929–2931.

Schroder, J. L., Zhang, H., Girma, K., Raun, W. R., Penn, C. J. & Payton, M. E. (2011), 'Soil Acidification from Long-Term Use of Nitrogen Fertilizers on Winter Wheat', *Soil Science Society of America Journal* **75**(3), 957.

Schulz, K., Jarvis, A. & Beven, K. (2001), 'The Predictive Uncertainty of Land Surface Fluxes in Response to Increasing Ambient Carbon Dioxide', *Journal of Climate* **14**, 2551–2562.

Schulze, E. D., Luyssaert, S., Ciais, P., Freibauer, A., Janssens, I. A., Soussana, J. F., Smith, P., Grace, J., Levin, I., Thiruchittampalam, B., Heimann, M., Dolman, A. J., Valentini, R., Bousquet, P., Peylin, P., Peters, W., Rödenbeck, C., Etiope, G., Vuichard, N., Wattenbach, M., Nabuurs, G. J., Poussi, Z., Nieschulze, J. & Gash, J. H. (2009), 'Importance of methane and nitrous oxide for Europe's terrestrial greenhouse-gas balance', *Nature Geoscience* **2**(12), 842–850.

Sellers, P. J., Dickinson, R. E., Randall, D. A., Betts, A. K., Hall, F. G., Berry, J. A., Collatz, G. J., Denning, A. S., Mooney, H. A., Nobre, C. A., Sato, N., Field, C. B. & Henderson-Sellers, A. (1997), 'Modeling the Exchanges of Energy, Water, and Carbon Between Continents and the Atmosphere', *Science* **275**(5299), 502–509.

Sharpley, A. N. & Smith, S. J. (1995), 'Nitrogen and phosphorus forms in soils receiving manure', *Soil Science* **159**(4), 253–258.

Singhal, K. K., Mohini, M., Jha, A. K. & Gupta, P. K. (2005), 'Methane emission estimates from enteric fermentation in Indian livestock: Dry matter intake approach', *Current Science* **88**(1), 119–127.

Slafer, G. A. (2003), 'Genetic basis of yield as viewed from a crop physiologist's perspective', *Annals of Applied Biology* **142**(2), 117–128.

Smith, P. (2014), 'Do grasslands act as a perpetual sink for carbon?', *Global Change Biology* **20**(9), 2708–2711.

Smith, P., Martino, D., Cai, Z., Gwary, D., Janzen, H., Kumar, P., McCarl, B., Ogle, S., O'Mara, F., Rice, C., Scholes, B., Sirotenko, O., Howden, M., McAllister, T., Pan, G., Romanenkov, V., Schneider, U., Towprayoon, S., Wattenbach, M. & Smith, J. (2008), 'Greenhouse gas mitigation in agriculture', *Philosophical Transactions of the Royal Society B: Biological Sciences* **363**(1492), 789–813.

Smith, P., Powlson, D. S., Smith, J. U., Falloon, P. & Coleman, K. (2000), 'Meeting Europe's climate change commitments: Quantitative estimates of the potential for carbon mitigation by agriculture', *Global Change Biology* **6**(5), 525–539.

Soussana, J. F., Allard, V., Pilegaard, K., Ambus, P., Amman, C., Campbell, C., Ceschia, E., Clifton-Brown, J., Czobel, S., Domingues, R., Flechard, C., Fuhrer, J., Hensen, A., Horvath, L., Jones, M., Kasper, G., Martin, C., Nagy, Z., Neftel, A., Raschi, A., Baronti, S., Rees, R. M., Skiba, U., Stefani, P., Manca, G., Sutton, M., Tuba, Z. & Valentini, R. (2007), 'Full accounting of the greenhouse gas (CO2, N2O, CH4) budget of nine European grassland sites', *Agriculture, Ecosystems and Environment* **121**, 121–134.

Soussana, J. F. & Lemaire, G. (2014), 'Coupling carbon and nitrogen cycles for environmentally sustainable intensification of grasslands and crop-livestock systems', *Agriculture, Ecosystems and Environment* **190**, 9–17.

Spitters, C., van Keulen, H. & van Kraalingen, D. (1989), A simple and universal crop growth simulator: SUCROS87, *in* 'Simulation and systems management in crop protection', PUDOC, Wageningen, pp. 147–181.

Statbel (2018), 'Exploitations agricoles et horticoles'.
URL: *https://statbel.fgov.be/fr/themes/agriculture-peche/exploitations-agricoles-et-horticoles#figures*

Stavi, I. & Lal, R. (2013), 'Agriculture and greenhouse gases, a common tragedy. A review', *Agronomy for Sustainable Development* **33**(2), 275–289.

Stavi, I., Lal, R. & Owens, L. B. (2011), 'On-farm effects of no-till versus occasional tillage on soil quality and crop yields in eastern Ohio', *Agronomy for Sustainable Development* **31**(3), 475–482.

Steinfeld, H., J. Gerber, P., Wassenaar, T., Castel, V., Rosales, M. & De Haan, C. (2006), Livestock's long shadow: environmental issues and options. FAO., Technical report, FAO, Rome.

Suleau, M., Moureaux, C., Dufranne, D., Buysse, P., Bodson, B., Destain, J.-p., Heinesch, B., Debacq, A. & Aubinet, M. (2011), 'Respiration of three Belgian crops: Partitioning of total ecosystem respiration in its heterotrophic, above- and below-ground autotrophic components', *Agricultural and Forest Meteorology* **151**(5), 633–643.

Syakila, A. & Kroeze, C. (2011), 'The global nitrous oxide budget revisited', *Greenhouse Gas Measurement and Management* **1**(1), 17–26.

Tate, K. R. (2015), 'Soil methane oxidation and land-use change - from process to mitigation', *Soil Biology and Biochemistry* **80**, 260–272.

Thom, A. (1972), 'Momentum, mass and heat exchange of vegetation', *Quarterly Jounral of the Royal Meteorological Society* **98**, 124–134.

Thomson, A. J., Giannopoulos, G., Pretty, J., Baggs, E. M. & Richardson, D. J. (2012), 'Biological sources and sinks of nitrous oxide and strategies to mitigate emissions', *Philosophical Transactions of the Royal Society B: Biological Sciences* **367**(1593), 1157–1168.

Thornley, J. H. M. (1970), 'Respiration, Growth and Maintenance in Plants', *Nature* **227**(5255), 304–305.

Thornley, J. H. M. (1995), 'Shoot:Root allocation with respect to C, N and P: an investigation and comparison of resistance and teleonomic models', *Annals of Botany* **75**(4), 391–405.

Thornley, J. H. M. (1998), *Grassland dynamics: an ecosystem simulation model*, first edn, CAB International.

Thorup-Kristensen, K., Cortasa, M. S. & Loges, R. (2009), 'Winter wheat roots grow twice as deep as spring wheat roots, is this important for N uptake and N leaching losses?', *Plant and Soil* **322**(1), 101–114.

Tian, H., Lu, C., Ciais, P., Michalak, A. M., Canadell, J. G., Saikawa, E., Huntzinger, D. N., Gurney, K. R., Sitch, S., Zhang, B., Yang, J., Bousquet, P., Bruhwiler, L., Chen, G., Dlugokencky, E., Friedlingstein, P., Melillo, J., Pan, S., Poulter, B., Prinn, R., Saunois, M., Schwalm, C. R. & Wofsy, S. C. (2016), 'The terrestrial biosphere as a net source of greenhouse gases to the atmosphere', *Nature* **531**, 225–228.

Tsvetsinskaya, E. A., Mearns, L. O. & Easterling, W. E. (2001), 'Investigating the effect of seasonal plant growth and development in three-dimensional atmospheric simulations. Part I : Simulation of surface fluxes over the growing season', *Journal of climate* **14**(5), 692–709.

Tubiello, F. N. & Fischer, G. (2007), 'Reducing climate change impacts on agriculture: Global and regional effects of mitigation, 2000–2080', *Technological Forecasting and Social Change* **74**(7), 1030–1056.

UNFCC (2015), 'Adoption of the Paris Agreement', *Conference of the Parties on its twenty-first session* **4**(December), 32.

van der Meer, H. G. (2008), 'Optimising manure management for GHG outcomes', *Australian Journal of Experimental Agriculture* **48**(2), 38–45.

Van Heemst, H. D. J. (1988), 'Plant data values required for simple crop growth simulation models: review and bibliography', *Simulation Report CABO-TT* (17), 103.

van Keulen, H., Penning De Vries, F. W. T. & Drees, E. M. (1982), A summary model for crop growth As outlined in Section 1, *in* 'Simulation of plant growth and crop production', PUDOC, Wageningen, pp. 87–97.

van Wijk, M., Rufino, M., Enahoro, D., Parsons, D., Silvestri, S., Valdivia, R. & Herrero, M. (2014), 'Farm household models to analyse food security in a changing climate: A review', *Global Food Security* **3**(2), 77–84.

Vandewattyne, F. (2019), Mechanistic modelling of cropland and grassland ecosystems: focus on the nitrogen cycle, the soil carbon and the management practices, Master's thesis, Université de Liège - Gembloux Agro-Bio Tech.

Vergé, X. P., De Kimpe, C. & Desjardins, R. L. (2007), 'Agricultural production, greenhouse gas emissions and mitigation potential', *Agricultural and Forest Meteorology* **142**(2-4), 255–269.

Vuichard, N., Soussana, J.-F., Ciais, P., Viovy, N., Ammann, C., Calanca, P., Clifton-Brown, J., Fuhrer, J., Jones, M. & Martin, C. (2007), 'Estimating the greenhouse gas fluxes of European grasslands with a process-based model: 1 . Model evaluation from in situ measurements', *Global Biogeochemical Cycles* **21**, 1–14.

Wahlen, M. (1993), 'The Global Methane Cycle', *Annual Review of Earth and Planetary Sciences* **21**(1), 407–426.

Wallington, Timothy J; Srinivasan, J; Nielsen, O.J.; Highwood, E. (2004), Greenhouse gases and global warming, *in* A. Sabljic, ed., 'Encyclopedia of Life Support Systems (EOLSS)', EOLSS Publishers, Oxford.

Wallonie Agriculture SPW (2019*a*), Evolution de l'économie agricole et horticole de la Wallonie, Technical report, Wallonie Agriclture (SPW).

Wallonie Agriculture SPW (2019*b*), L'agriculture wallonne en chiffres, Technical report.

Wang, J., Yu, Q. & Lee, X. (2007), 'Simulation of crop growth and energy and carbon dioxide fluxes at different time steps from hourly to daily', *Hydrological Processes* **21**(18), 2474–2492.

Wang, L., Wang, J., Liu, W., Gan, Y. & Wu, Y. (2016), 'Biomass Allocation, Compensatory Growth and Internal C/N Balance of Lolium perenne in Response to Defoliation and Light Treatments', *Polish Journal of Ecology* **64**(4), 485–499.

Wang, W. & Dalal, R. C. (2015), 'Nitrogen management is the key for low-emission wheat production in Australia: A life cycle perspective', *European Journal of Agronomy* **66**, 74–82.

Wang, Y.-P. & Leuning, R. (1998), 'A two-leaf model for canopy conductance, photosynthesis and partitioning of available energy I:', *Agricultural and Forest Meteorology* **91**(1-2), 89–111.

Wardlaw, I. (1990), 'The control of carbon partitioning in plants', *New Phytologist* **116**(27), 341–381.

Wardlaw, I. F. & Willenbrink, J. (2000), 'Mobilization of fructan reserves and changes in enzyme activities in wheat stems correlate with water stress during kernel filling', *New Phytologist* **148**(3), 413–422.

Wattenbach, M., Sus, O., Vuichard, N., Lehuger, S., Gottschalk, P., Li, L., Leip, A., Williams, M., Tomelleri, E., Kutsch, W. L., Buchmann, N., Eugster, W., Dietiker, D., Aubinet, M., Ceschia, E., Béziat, P., Grünwald, T., Hastings, A., Osborne, B., Ciais, P., Cellier, P. & Smith, P. (2010), 'The carbon balance of European croplands: A cross-site comparison of simulation models', *Agriculture, Ecosystems and Environment* **139**(3), 419–453.

Weir, A. H., Bragg, P. L., Porter, J. R. & Rayner, J. H. (1984), 'A winter wheat crop simulation model without water or nutrient limitations', *The Journal of Agricultural Science* **102**(2), 371–382.

Whalen, S. C. (2005), 'Natural Wetlands and the Atmosphere', *Environmental Engineering Science* **22**(1), 73–94.

Williams, J. R., Jones, C. A., Kiniry, J. R. & Spanel, D. A. (1989), 'The EPIC Crop Growth Model', *Transactions of the ASAE* **32**(2), 0497–0511.

Williams, M., Rastetter, E., Fernandes, D., Goulden, M., Wofsy, S., Shaver, G., Melillo, J., Munger, J., Fan, S. & Nadelhoffer, K. (1996), 'Modelling the soil-plant-atmopshere continuum in a Quercus–Acer stand at Harvard Forest: the regulation of stomatal conductance by light, nitrogen and soil/plant hydraulic properties', *Plant, Cell and Environment* **19**, 911–927.

Xiao, J., Davis, K. J., Urban, N. M. & Keller, K. (2014), 'Uncertainty in model parameters and regional carbon fluxes: A model-data fusion approach', *Agricultural and Forest Meteorology* **189-190**, 175–186.

Xiong, Z.; Khalil, M. (2009), Greenhouse Gases from Crop Fields, *in* S. Singh, ed., 'Climate change and crops', Springer-Verlag Berlin Heidelberg, pp. 113–132.

Yanai, R. D., Vadeboncoeur, M. A., Hamburg, S. P., Arthur, M. A., Fuss, C. B., Groffman, P. M., Siccama, T. G. & Driscoll, C. T. (2013), 'From missing source to missing sink: Long-term changes in the nitrogen budget of a northern hardwood forest', *Environmental Science and Technology* **47**(20), 11440–11448.

Yilmaz, L. (2015), *Concepts and Methodologies for Modeling and Simulation*, Springer International Publishing.

Zabel, F., Putzenlechner, B. & Mauser, W. (2014), 'Global Agricultural Land Resources – A High Resolution Suitability Evaluation and Its Perspectives until 2100 under Climate Change Conditions', *PLoS ONE* **9**(9), e107522.

Zeeman, M. J., Hiller, R., Gilgen, A. K., Michna, P., Plüss, P., Buchmann, N. & Eugster, W. (2010), 'Management and climate impacts on net CO2 fluxes and carbon budgets of three grasslands along an elevational gradient in Switzerland', *Agricultural and Forest Meteorology* **150**(4), 519–530.

Zhang, H., Edwards, J., Carver, B. & Raun, B. (2004), 'Managing Acid Soils for Wheat Production', *Oklahoma Cooperative Extension Service* **F-2240**, 1–4.

Zhu, Q. & Zhuang, Q. (2014), 'Parameterization and sensitivity analysis of a process-based terrestrial ecosystem model using adjoint method', *Journal of Advances in Modeling Earth Systems* **6**(2), 315–331.

Appendices

Appendix A

Existing models

Table A.1: Models cited in this thesis with the meaning of the acronyms and the sources used.

Acronym	Meaning	Source
Anthro-BGC	Anthro BioGeochemical cycles	Ma et al. (2011)
APSIM	Agricultural Production Systems sIMulator	McCown et al. (1996)
ASPECTS	Atmosphere-Soil-Plant Exchanges of Carbon in Temperate Sylvae	Rasse et al. (2001)
CERES-EGC	Crop Environment Resource Synthesis - Environnement et Grande Cultures	Gabrielle et al. (2006)
CERES-Maize	Crop Environment Resource Synthesis - Maize	Ritchie & Otter (1985)
CERES-Wheat	Crop Environment Resource Synthesis - Wheat	Ritchie & Otter (1985)
ChinaAgrosys	China Agrosystems	Wang et al. (2007)
CQESTR	Pronounced as "sequester"	Gollany et al. (2012)
DayCent	-	Necpálová et al. (2015)
DNDC	DeNitrification DeComposition	Li et al. (1992)
DSSAT	Decision Support System for Agrotechnology Transfer	Jones et al. (2003)
EPIC	Environmental Policy Integrated Climate	Williams et al. (1989)
ORCHIDEE	Organising Carbon and Hydrology in Dynamic Ecosystems	Krinner et al. (2005)
ORCHIDEE-STICS	Asocition of ORCHIDEE and STICS	de Noblet-Ducoudré et al. (2004)
PaSim	Pasture Simulation	Riedo et al. (1998)
RothC	Rothamsted Carbon	Coleman & Jenkinson (2014)
SPA	Soil Plant Atmosphere	Williams et al. (1996)
STICS	Simulateur muLTIdisciplinaire pour les Cultures Standard	Brisson et al. (2003)

Appendix B

Additional modules of the TADA model

B.1 Soil temperature

Soil temperature is considered as a reservoir and is modelled in every soil layer. The evolution of this physical quantity is a result of heat conduction between soil layers:

$$c_{s,i}\Delta z_i \frac{dT_i}{dt} = F_{T,i-1} - F_{T,i} \tag{B.1}$$

where $c_{s,i}$ is the volumetric heat capacity [J m^{-3} kg^{-1}], depending on the proportion of solid and water phases in soil, T_i is the soil temperature in layer i and $F_{T,i-1}$ and $F_{T,i}$ are the heat fluxes due to conduction from layer *i-1* and to layer *i+1* respectively [K day^{-1}].

Heat conductive fluxes are obtained with the same soil discretization as for water fluxes:

$$F_{T,i} = D_{Tmoy,i,i+1} \frac{T_{i+1} - T_i}{\frac{1}{2}(\Delta z_i + \Delta z_{i+1})} \tag{B.2}$$

This flux is proportional to the gradient of temperature between two adjacent soil layers and to a mean soil heat conductivity $D_{Tmoy,i,i+1}$ taking into account both layers heat conductivities [J m^{-1} K^{-1} day^{-1}], which are expressed as an empirical function of soil water content.

The two boundary conditions regulating heat transfer in soil are the following ones:

- At the top of the soil profile, the soil temperature is equal to the air temperature as no energy balance is included in TADA;
- At the bottom of the soil profile, the temperature does not evolve with time, and is equal to the annual mean air temperature. This hypothesis is acceptable at a certain depth, the soil profile has a higher thermal inertia than the air.

B.2 Root development

In ASPECTS, two kinds of roots were considered: coarse roots and fine roots, which had different development patterns and different roles. In TADA, this distinction is not made as winter wheat and ryegrass do not produce roots as coarse as trees do. Therefore, only one type of root is considered, and its elongation is modelled through time. Root development is of great importance as the presence of roots in soil horizons defines the amount of nitrogen and water that can be consumed.

The development of **winter wheat** roots is based on Jones et al. (1991). Right after seeding, the depth of winter wheat roots is equal to the depth of planting dpt_{sow} [m]. After that, root depth is computed every time step, as the sum of the previous root depth and the potential increase in root depth, weighted by a stress factor:

$$dpt_t = dpt_{t-1} + pot_{incr} * strs_{rt} \tag{B.3}$$

where t stands for the time, pot_{incr} is the potential increase of root depth per time step [m] and $strs_{rt}$ is a stress factor, computed in the soil horizon where the root tip is growing. This factor ranges from 0 to 1, and is taken as the minimum value between a temperature stress, a soil strength stress, a soil aeration stress and an acidity stress, all ranging from 0 to 1 and computed according to Jones et al. (1991).

The potential increase of root depth pot_{incr} is calculated every time step, considering that roots grow from the sowing depth to the maximum root depth as a linear function of winter wheat development stage:

$$pot_{incr} = rt_{dpt,max} \frac{GS_t - GS_{t-1}}{GS_{dpt,max}}, \qquad GS < GS_{dpt,max} \tag{B.4}$$

where $rt_{dpt,max}$ is the maximum root depth [m] which is a genotype-dependent parameter and GS_t and GS_{t-1} are the growth stages of time steps t and *t-1*. The growth stage GS ranges from 0 (seed) to 1 (maturity) and is computed from the development units ($UPVT$) in the phenological module. $GS_{dpt,max}$ is the growth stage at which the root system ceases to increase in depth in soils without rooting constraints. Cereals usually stop developing their root system during grain filling ($GS_{dpt,max}$=0.6 to 0.9), and root depth does not increase any more after that stage.

Once the assimilated carbon has been allocated to the distinct plant organs, it is important to know which quantity is allocated to the roots present in the different soil horizons. The potential allocation of carbon to layer i is computed as:

$$pot_{alloc,i} = \frac{5 \frac{rt_{dens,i}}{0.025 + rt_{dens,i}} strs_{rt,i} * rt_{pres,i} * z_i}{LW_{ratio,i}} \tag{B.5}$$

where $rt_{dens,i}$ is the root length density [cm cm^{-3} of roots] for each soil layer (values gathered from Asseng, 1997; Hoad et al., 2004; Hodgkinson et al., 2017), $strs_{rt,i}$ is a stress factor to root development (the same as for root depth increase), $rt_{pres,i}$ is a factor describing the tendency of a plant to distribute its roots in layer i (computed according to a genotype-dependent factor), z_i is the depth of the middle of layer i and $LW_{ratio,i}$ is the length to weight ratio of roots in layer i [km kg^{-1}], expressed as a function of the growth stage, of the root depth and of a stress factor.

Once the potential carbon allocation has been computed for each soil layer, the real carbon allocation is computed as:

$$alloc_{C,rt,i} = alloc_{C,rt} \frac{pot_{alloc,i}}{\sum_{i=1}^{nhz} pot_{alloc,i}} \tag{B.6}$$

where $alloc_{C,rt,i}$ is the carbon allocated to roots in layer i [gC m^{-2} day^{-1}] and $alloc_{C,rt}$ is the assimilated carbon allocated to all roots, computed in the allocation module [gC m^{-2} day^{-1}].

Modelling the root system of **ryegrass** is different from winter wheat, in the way that at the beginning of the simulation, ryegrass already has developed its root system which is going to fluctuate along the year, according to environmental factors. The implemented new module of root development is based on Arora & Boer (2003) that improved the exponential root density profile proposed by Jackson et al. (1996). The potential root depth [m] is calculated at a given time t as:

$$dpt_{pot,t} = 3 \frac{(W_{rt})^{\alpha_{rt}}}{\beta_{rt}} \tag{B.7}$$

where W_{rt} is the total root biomass expressed in units of dry matter [gDM m^{-2}], and α_{rt} and β_{rt} are parameters depending on the type of vegetation. For α_{rt}=*0*, roots grow horizontally, as $dpt_{pot,n}$ does not change with an

increase of root biomass. For α_{rt}=*1*, roots mainly grow vertically. Therefore, the value of α_{rt}, between 0 and 1, defines whether roots grow preferentially horizontally or vertically. Similarly, β_{rt} determines if, for a given root dry matter content, the root system will rather be shallow or deep.

To take the effect of environmental factors into account, the actual root depth is not taken equal to the one computed with equation B.7, but a potential increase of root depth is computed every time step, which is then weighted by a stress factor, formulated in the same way as for winter wheat:

$$dpt_t = \begin{cases} dpt_{t-1} + strs_{rt}(dpt_{pot,t} - dpt_{t-1}) & \text{if} \quad dpt_{pot,t} - dpt_{t-1} > 0 \\ dpt_{t-1} + (dpt_{pot,t} - dpt_{t-1}) & \text{if} \quad dpt_{pot,t} - dpt_{t-1} \leq 0 \end{cases} \tag{B.8}$$

where dpt_t is the actual root depth a time t and dpt_{t-1} at the previous time step. If *(*$dpt_{pot,t}$*-*dpt_t*)* is positive, it means that roots should theoretically grow. Therefore, a stress factor is applied to make sure that root growth is limited under adverse conditions. On the contrary, if roots are supposed to shrink, mainly due to a decrease of root biomass, no stress factor is applied in equation B.8.

The root density profile proposed by Arora & Boer (2003) has an exponential form, as many root segments are expected to be encountered in soil surface and much fewer in deeper soil horizons. The root density [kg m^{-2}] at a given depth is given by:

$$\rho_i = \beta_{rt}(W_{rt})^{(1-\alpha_{rt})} e^{-z_i \frac{\beta_{rt}}{(W_{rt})^{\alpha_{rt}}}} \tag{B.9}$$

where z_i is the depth of the middle of soil layer i [m]. In order to maintain a certain root density profile, carbon is allocated to the roots of each soil layer proportionally to their theoretical root density:

$$alloc_{C,rt,i} = alloc_{C,rt} \frac{\rho_i}{\sum_{i=1}^{nhz} \rho_i} \tag{B.10}$$

where $alloc_{C,rt,i}$ is the carbon allocated to roots in layer i [gC m^{-2} day^{-1}] and $alloc_{C,rt}$ is the assimilated carbon allocated to all roots, computed in the allocation module [gC m^{-2} day^{-1}].

B.3 OM mineralization and humification

The mineralization encompasses the fluxes coming from soil litter and SOM to CO2 and NH4. The humification corresponds to the carbon and the nitrogen transfer from litter to SOM. Those fluxes are calculated with the same equations than in ASPECTS (see Bureau n.d.) except that woody litter is not represented for the grassland and cropland (because there are no woody materials in the vegetation). The carbon mineralization of litter or SOM (x) for an horizon i is calculated as:

$$miner_{C,x,i} = x_{c,i} * f_{\theta,i} * f_{T,i} * f_{aera,i} / lifespan_x \tag{B.11}$$

with $x_{c,i}$ the carbon content of the litter or SOM reservoir [gC m^{-2}], $lifespan_x$ the lifespan of the specific pool [day], $f_{\theta,i}$, $f_{T,i}$ and $f_{aera,i}$ the water, temperature and aeration factor, calculated with the following equations:

$$f_{water,i} = 0.5 + 0.5 * \cos(\pi + \frac{5.2358 * (\theta_i - \theta_{wp})}{\theta_{fc} - \theta_{wp}}) \tag{B.12}$$

$$f_{temp,i} = 2 * e^{\gamma_{temp} * (\frac{1}{56.02} - \frac{1}{T_{soil,i} - 227.13})} \tag{B.13}$$

$$f_{aera} = \frac{1 - \frac{\theta_i}{\theta_{sat}}}{1 - poro_{crit}} \tag{B.14}$$

with $poro_{crit}$ a critical porosity value calculated with a parameter and the clay content of the horizon and γ_{temp} the soil temperature parameter. The mineralized nitrogen is calculated as:

$$miner_{N,x,i} = \frac{miner_{C,x,i} * \beta_x}{CN_{x,i}^2} \tag{B.15}$$

with β_x a nitrogen mineralization parameter and $CN_{x,i}$ the C/N ratio. The humification is calculated as a ratio of the litter mineralization with:

$$hum_{N,i} = \gamma_{hum} * miner_{N,litter,i} \quad \text{and} \quad hum_{C,i} = hum_{N,i} * CN_{SOM,i} \tag{B.16}$$

with γ_{hum} the fraction of the mineralized nitrogen which is humified and $CN_{SOM,i}$ the C/N ratio of the SOM. No movements of the litter and the SOM are taken in account in the model.

B.4 Nitrogen cycle

Nitrogen deposition and symbiotic fixation

Nitrogen deposition covers the dry and wet depositions of NH_4 and NO_3, which are calculated as:

$$dep_{NO3} = dep_{NO_3,an} * \frac{prc}{prc_{an}} \quad \text{and} \quad dep_{NH4} = dep_{NH_4,an} * \frac{prc}{prc_{an}} \tag{B.17}$$

with $dep_{NO3,an}$ $dep_{NH4,an}$ the annual depositions of NO_3 and NH_4 in an open field measured by ICP (2010) (0.63 gN m^{-2} yr^{-1} for NH_4 and 0.54 for NO_3), prc and prc_{an} the precipitation during the time step and the year respectively. Equation B.17 illustrates that N depositions will gradually occur when precipitations are encountered. To simplify this phenomenon, the assumption is made that dry deposition are also incorporated in the soil profile with the incoming precipitations.

In TADA, unlike for forests, no symbiotic and non-symbiotic fixation is considered for grasslands and croplands, due to a lack of converging information in the literature.

Nitrification and denitrification

The nitrification is a chemical reaction converting NH_4 into NO_3 which occurs with a release of N_2O. The rate of this reaction in soil layer i is calculated with the following equation:

$$nitr_{NO_3,i} = NH_{4,i} * \min(\beta_{ph} * stress_{ph,i}, \beta_\theta * stress_{\theta,i}, \beta_T * stress_{T,i}) * rate_{nitr} \tag{B.18}$$

with $NH_{4,i}$ the ammonium content of soil layer i [gN m^{-2}], $rate_{nitr}$ the basal rate of nitrification [day^{-1}], β_{ph}, β_θ, β_T the coefficients traducing the importance of the stress factors $stress_{ph,i}$, $stress_{\theta,i}$ and $stress_{T,i}$ respectively. The calculation of these stress factors comes from ASPECTS and is fully described in Bureau (n.d.). The N_2O produced during this process is calculated as:

$$nitr_{N_2O,i} = nitr_{NO_3,i} * (rate_{N_2O} + rate_{stress} * (f_{nitr,\theta,i} + f_{nitr,T,i})) \tag{B.19}$$

where $nitr_{NO_3}$ is the NO_3 produced by nitrification, $rate_{N_2O}$ the minimal fraction of nitrification that create N_2O, $rate_{stress}$ the varying rate in function of the stress, $f_{nitr,\theta,i}$ is a factor introducing the influence of water availability. It is equal to 0 when the soil water content (SWC) is below the wilting point, grow linearly and is equal to 1 if SWC exceeds the saturation point. $f_{nitr,T,i}$ is a temperature factor equal to 0 when soil temperature is below 0°C, grow linearly and is equal to 1 if soil temperature is greater than 25°C.

The denitrification converts NO_3 into N_2 and N_2O. The total flux is calculated with the next equation:

$$denit_{tot,i} = \min(\frac{rate_{denit} * NO_{3,i}}{step}, \beta_{denit} * f_{denit,T,i} * f_{denit,\theta,i} * \min(\beta_{NO_3} * f_{NO_3}, \beta_{resp} * f_{resp})) \tag{B.20}$$

rate of denitrification [-], $NO_{3,i}$ the nitrate content in the soil [gN m^{-2}], $step$ the time step of the simulation [day], β_{denit} the denitrification factor, $f_{nitr,T}$, $f_{nitr,\theta}$, β_{NO_3}, f_{NO_3}, β_{resp} and f_{resp} are temperature, water, NO_3 content and respiration parameters and factors respectively. Refer to Bureau (n.d.) for the calculation of these factors. The fraction of N_2 and N_2O produced by denitrification is calculated according to the following equations:

$$denit_{N2O,i} = \frac{denit_{tot,i}}{1 + (\min(f_{NO3,i,bis}, f_{resp,i,bis}) * f_{WFPS,i})} \tag{B.21}$$

$$denit_{N2,i} = \frac{denit_{tot,i}}{1 + 1/(\min(f_{NO3,i,bis}, f_{resp,i,bis}) * f_{WFPS,i})} \tag{B.22}$$

where $f_{NO3,i,bis}$, $f_{resp,i,bis}$ and $f_{WFPS,i}$ are factors related to the NO_3 availability, the soil respiration and the water-filled pore space (WFPS). These three factors are calculated as follows:

$$f_{NO3,i,bis} = 12.5 - 25 * \tan(\pi * 0.01 * (NO_{3,i} - 190)/\pi) \tag{B.23}$$

$$f_{resp,i,bis} = 13 + 30.78 * \tan(\pi * 0.07 * (resp_i - 13.)/\pi) \tag{B.24}$$

$$f_{WFPS,i} = \frac{1.4}{13^{17/13^{2.2*WFPS_i}}} \tag{B.25}$$

with $NO_{3,i}$ the total soil nitrate content of the horizon in μgN g(soil)$^{-1}$, $resp_i$ the heterotrophic respiration of the previous time step and $WFPS_i$ the water filled pore space of the soil horizon of interest.

Nitrogen uptake

The nitrogen uptake subroutine does not change compared to ASPECTS and is completely detailed in Bureau (n.d.). Briefly, this process is based on the principle of supply from soil nitrogen and demand of the plant reserve. Fistly, TADA computes the maximum absorption rate of NO_3 and NH_4 either by diffusion or by mass flow transport (i.e. by water transport). Secondly, this maximum absorption rate is compared to the demand of the plant nitrogen reserve. If the supply exceeds the demand, the maximum amount of nitrogen is absorbed, until filling the reserve. Otherwise, the available nitrogen is entirely absorbed. The unique difference between forest and grassland or cropland ecosystems is the upper limit of the reserve. The maximum reserve of cropland is equal to a quarter of the total nitrogen content of plant organs while grassland species are assumed to store a tenth of their total nitrogen content.

Nitrogen allocation and translocation

As for nitrogen uptake, nitrogen allocation also follows the supply and demand principle. However, the supply now comes from the nitrogen reserve and the demand comes from the different plant organs. In order to compute the demand of these organs, their C/N ratios are compared to their optimal C/N ratios using the following equation:

$$dem_x = \frac{C_x * (\frac{1}{CNopt_x} - \frac{1}{CN_x})}{step} \tag{B.26}$$

with C_x the carbon content of a given organ x, $CNopt_x$ the optimal C/N ratio and CN_x the actual C/N ratio of this organ. The optimal C/N ratios come from the literature for ryegrass organs (data gathered from Li et al., 1994; Jongen et al., 1995; Thornley, 1998; Abdelgawad et al., 2014; Jiang et al., 2016; Wang et al., 2016; Roche et al., 2017) , and are modelled as a function of the growth stage for winter wheat (Kröbel et al., 2011). The total demand is then compared to the available nitrogen in the reserve (res_{disp}) which is estimated as follows:

$$res_{disp} = \frac{0.1 * res}{step} \tag{B.27}$$

with res the nitrogen content in the reserve computed into the nitrogen uptake module. The role of equation B.27 is to prevent the N reserve from being consumed in one time step, which would not stick to the reality. If res meets the demand of the organs, the amount of allocated nitrogen is dictated by the equation B.26 and is equal to the demand. If the total demand is greater than the value of res_{disp}, the allocation pattern is defined as:

$$alloc_x = \frac{dem_x}{\sum_{x=1}^{n_{org}} dem_x} * res_{disp} \tag{B.28}$$

with x corresponding to a given organ and n_{org} the total number of plant organs. According to this equation, each organ receives a fraction of the available nitrogen proportional to its demand.

As TADA has a more complex set of plant reservoirs for croplands, the allocation pattern shows some specificities. From the beginning of grain filling to the harvest of winter wheat, nitrogen is exclusively allocated to the grain and can be translocated from non-reproductive organs to the reproductive ones. The translocation occurs if the actual C/N ratio of an organ is lower than the optimal C/N ratio of this organ. If this is the case, the maximum translocation flux (i.e. supply from plant organs) is equal to the opposite value of dem_x calculated in equation B.26 ($offer_x = -dem_x$). If this supply exceeds the grain demand (dem_{grain}), the translocation flux from each organ is computed with:

$$trans_x = \frac{offer_x}{\sum_{x=1}^{n_{org}} offer_x} * dem_{grain} \tag{B.29}$$

Otherwise, if the demand exceeds the supply, all the nitrogen necessary and available in the reserve is allocated to the grain.

Nitrogen leaching

The nitrogen leaching module also follows the approach proposed by ASPECTS and is detailed in Bureau (n.d.). The NH_4 and NO_3 concentrations in soil solution are calculated from their total quantity and their solute buffer power, which is the ratio between ions adsorbed on the solid phase and ions in solution. These solute molecules follows the water movement which can be divided into a vertical and a horizontal component. The amount of leached NH_4 and NO_3 is therefore divided into a horizontal leaching flux and a vertical leaching flux. However, these dynamics do not occur if the NH_4 and NO_3 concentrations are below a given threshold defined by $azom_i$ and calculated as follows:

$$azom_i = azom_{min} * (\theta_{sat,i} - \theta_{fc,i}) * thick_i \tag{B.30}$$

with $thick_i$ the thickness of the soil horizon i, $azom_{min}$ the soil nitrogen content below which plants can no longer extract (4.889 gN m(micropore)$^{-3}$). If the NH_4 or NO_3 concentration in a given soil layer is below this threshold, the leaching transport of the concerned molecule is null.

Appendix C

Required data and parameters in TADA

C.1 Species and general parameters

Table C.1: Species parameters

Parameter	Description	Units	Value			References		
			Forest	Crop	Pasture	Forest	Crop	Pasture
Main characteristics								
SLA	Specific leaf area	$m^2\ gC^{-1}$	0.045	0.0365	0.0445	Aspects	measured in Lonzée	Lazzarotto et al., 2009
SSA	Specific stem area	$m^2\ gC^{-1}$	-	0.0067	-	-	Andrew & Storkey, 2016; Confalonieri et al., 2013	-
Phenological parameters								
A_p	Thermal semi-amplitude of the vernalizing effect	°C	-	10	-	-	Brisson et al., 2008	-
B_p	Subsoil plantlet elongation curve parameter	°C d	-	0.006	-	-	calibrated	-
C_p	Subsoil plantlet elongation curve parameter	-	-	3.8	-	-	calibrated	-
$dayl_{fal}$	Day length when leaf abscission starts	hr	10.5	-	-	Aspects	-	-
DS_{ear}	Developmental stage at ear emergence	-	-	-	0.55	-	-	Lazzarotto et al., 2009
DS_{veg}	Developmental stage at the start of vegetative growth	-	-	-	2	-	-	Lazzarotto et al., 2009
E_{max}	Maximum elongation of the coleoptile in darkness condition	cm	-	8	-	-	Brisson et al., 2008	-
f_{ear}	Shoot allocation coefficient after ear emergence	-	-	-	0.25	-	-	Lazzarotto et al., 2009
gdd_{bud}	Cumulative degree-days since FEB 10, over 5°C for budburst	°C	75	-	-	Aspects	-	-
iperm	Flag (0 = deciduous; 1 = evergreen)	-	0	-	-	Aspects	-	-
P_{base}	Base photoperiod for development	hr	-	6.3	-	-	Brisson et al., 2008	-
P_{sat}	Saturating photoperiod for development	hr	-	20	-	-	Brisson et al., 2008	-
S_p	Root sensitivity to drought (1=insensitive)	-	-	0.5	-	-	Brisson et al., 2008	-
S_v	Photoperiod sensitivity (1=insensitive)	-	-	0	-	-	Brisson et al., 2008	-

T_{base}	Minimum threshold temperature for development	°C	-	0	5	-	Brisson et al., 2008	Lazzarotto et al., 2009
T_{froid}	Optimum vernalization temperature	°C	-	6.5	-	-	Brisson et al., 2008	-
T_{stop}	High temperature stopping phasic development and leaf expansion	°C	-	35	-	-	Brisson et al., 2008	-
T_{rep}	Normalization factor for grass development	°C d	-	-	225	-	-	Lazzarotto et al., 2009
T_{max}	Maximum threshold temperature for development	°C	-	28	-	-	Brisson et al., 2008	-
$upvt_{germ}$	UPVT required to reach germination	°C d	-	50	-	-	Brisson et al., 2008	-
$upvt_{st3}$	UPVT required during stage 3 (germination to terminal spikelet)	°C d	-	275	-	-	Brisson et al., 2008	-
$upvt_{st4}$	UPVT required during stage 4 (terminal spikelet to flag leaf visible)	°C d	-	270	-	-	calibrated	-
$upvt_{st5}$	UPVT required during stage 5 (flag ligule visible to end of leaf growth)	°C d	-	105	-	-	calibrated	-
$upvt_{st7}$	UPVT required during stage 7 (grain filling to physiological maturity)	°C d	-	530	-	-	calibrated	-
$upvt_{veg}$	UPVT required during vegetative period	°C d	-	837	-	-	Brisson et al., 2008	-
VN	Number of vernalizing days required	d	-	55	-	-	Brisson et al., 2008	-
VN_{min}	Minimum vernalizing days required	d	-	7	-	-	Brisson et al., 2008	-
Photosythetic parameters								
a_1	Stomatal resistance factor	-	20	2.3	7.1	Aspects	calibrated	calibrated
χ_n	Ratio of photosynthetic capacity to leaf nitrogen at 25°C	mmol mol^{-1} s^{-1}	0.4567	0.21	1.02	Aspects	calibrated	calibrated
N_b	Leaf nitrogen not associated with photosynthesis	mmol m^{-2}(leaf)	1	25	25	Aspects	De Pury & Farquhar, 1997	De Pury & Farquhar, 1997
ibbl	Flag for Leuning (0) or Ball-Berry (1) stomatal resistance equation	-	0	0	0	-	-	-
θ_A	Curvature factor of response of canopy photosynthesis	-	1	0.8	0.8	Aspects	calibrated	calibrated
θ_J	Curvature factor of response of canopy photosynthesis to irradiance	-	0.7	0.7	0.7	Aspects	De Pury & Farquhar, 1997	De Pury & Farquhar, 1997
vpd_0	Stomatal resistance factor	Pa	1000	1000	1000	Aspects	Aspects	Aspects
k_n	Coefficient of leaf nitrogen in a canopy	-	0.713	0.713	0.713	De Pury & Farquhar, 1997	De Pury & Farquhar, 1997	De Pury & Farquhar, 1997
Radiation parameters								
β_0	Boland-Ridley-Lauret model parameter	-	-2.4	-2.4	-2.4	calibrated on Lonzée data	calibrated	calibrated on Lonzée data
β_1	Boland-Ridley-Lauret model parameter	-	2.77	2.77	2.77	calibrated on Lonzée data	calibrated	calibrated on Lonzée data
β_2	Boland-Ridley-Lauret model parameter	-	0.033	0.033	0.033	calibrated on Lonzée data	calibrated	calibrated on Lonzée data
β_3	Boland-Ridley-Lauret model parameter	-	0.054	0.054	0.054	calibrated on Lonzée data	calibrated	calibrated on Lonzée data
β_4	Boland-Ridley-Lauret model parameter	-	1.03	1.03	1.03	calibrated on Lonzée data	calibrated	calibrated on Lonzée data
β_5	Boland-Ridley-Lauret model parameter	-	0.63	0.63	0.63	calibrated on Lonzée data	calibrated	calibrated on Lonzée data
Carbon parameters								

a_{sigm}	Sigmoid function parameter	-	-	-0.3	-	-	Fitting from Ehdaie et al., 2008	-
c_{sigm}	Sigmoid function parameter	-	-	15	-	-	Fitting from Ehdaie et al., 2008	-
dm_c	Carbon content of dry matter	gC gDM^{-1}	-	0.449	0.4271	-	Measured in Lonzée	Measured in Dorinne
cvf_{cst}	Constant carbon assimilation efficiency	-	-	-	0.74	-	-	Choudbury, 2000
DG_0	CO2 gas diffusion coefficient in the air at 273.16K and 101.3kPa	m^2 s^{-1}	$1.39e^{-5}$	$1.39e^{-5}$	$1.39e^{-5}$	Fang & Moncrieff, 1999	Fang & Moncrieff, 1999	Fang & Moncrieff, 1999
$percent_{left}$	Percentage of C left in the reserve pool after grain remobilization	-	-	0.2	-	-	Ehdaie et al., 2008	-
$remobc_{eff}$	Carbon remobilization efficiency	-	-	0.75	-	-	Ehdaie et al., 2006	-
$time_{remob}$	Sigmoid function parameter	-	-	40	-	-	Ehdaie et al., 2008; Pheloung & Siddique, 1991	-
tns_c	Percentage of non structural carbohydrates in dry matter	gC gDM^{-1}	-	-	0.15	-	-	Downing & Gamroth, 2007
Respiration parameters								
a_κ	Teleonomic partitioning constant for grassland	gN gDM^{-1}	-	-	0.35	-	-	Lazzarotto et al., 2009
r_κ	Maintenance respiration constant	gC gDM^{-1}	-	-	0.03	-	-	Lazzarotto et al., 2009
c_κ	Teleonomic partitioning constant for grassland	gC gDM^{-1}	-	-	1	-	-	Lazzarotto et al., 2009
Q10	Maintenance respiration factor	-	2.7	2	2	Aspects	Spitters et al.,1989	Lazzarotto et al., 2009
rm	Maintenance respiration weightening coefficient	-	-	-	0.7	-	-	Lazzarotto et al., 2009
rm_0	Reference maintenance respiration rate at 20°C	gC gDM^{-1} day^{-1}	-	-	0.012	-	-	Lazzarotto et al., 2009
Temperature-dependent parameters								
T_{low}	Lower temperature for temperature function	C	-	0	0	-	Lazzarotto et al., 2009	Lazzarotto et al., 2009
T_{ref}	Reference temperature for temperature function	C	-	20	20	-	Lazzarotto et al., 2009	Lazzarotto et al., 2009
T_{up}	Upper temperature for temperature function	C	-	45	45	-	Lazzarotto et al., 2009	Lazzarotto et al., 2009
Nitrogen parameters								
azomin	Soil N content below which plant can not extract NO3	gN m^{-3} (μpore)	0.44	0.44	0.44	Gego, 1993	Gego, 1993	Gego, 1993
β_{lit}	Litter nitrogen mineralization	gC gN^{-1}	20	22	22	Aspects	calibrated on Dorinne data	calibrated
β_{som}	SOM nitrogen mineralization	gC gN^{-1}	15	16.5	16.5	Aspects	calibrated on Dorinne data	calibrated
dm_n	Nitrogen content of dry matter	gN gDM^{-1}	-	-	0.0275	-	-	Measured in Dorinne
$fresN_{max}$	Fraction of plant nitrogen defining the maximum nitrogen reserve	-	0.25	0.25	0.25	Aspects	Aspects	Aspects
$frNH4_c$	NH4 concentration on the root surface	molN cm^{-3}	$2e^{-8}$	$2e^{-8}$	$2e^{-8}$	Aspects	Robinson et al., 1991	Robinson et al., 1991
$frNO3_c$	NO3 concentration on the root surface	molN cm^{-3}	$2e^{-8}$	$2e^{-8}$	$2e^{-8}$	Aspects	Robinson et al., 1991	Robinson et al., 1991
$rate_{nitr}$	Optimum nitrification rate (ratio of NH4 content)	-	0.4	0.1432	0.1432	Aspects	calibrated on Dorinne data	calibrated
Animal parameters								
DM_{cap}	Intake capacity of dry matter per LSU per day	gDM LSU^{-1} day^{-1}	-	-	8900	-	-	Gourlez de la Motte et al., 2019

f_{meth}	Percentage of carbon intake lost as CH4 respiration	-	-	-	0.025	-	-	Gourlez de la Motte et al., 2019
f_{remove}	Percentage of shoot biomass removed by animal trampling	-	-	-	0.008	-	-	Vuichard et al., 2007
f_{resp}	Percentage of carbon intake lost as CO2 respiration	-	-	-	0.725	-	-	Gourlez de la Motte et al., 2019
$f_{ret,C}$	Percentage of carbon retained for milk or meat production	-	-	-	0	-	-	-
$f_{ret,N}$	Percentage of nitrogen retained for milk or meat production	-	-	-	0	-	-	-
f_{urine}	Percentage of urine present in excreta	-	-	-	0.6	-	-	Menzi et al., 1997 cited by Riedo et al., 2000; Oenema et al., 1997
f_{volat}	Percentage of nitrogen in excreta volatilized as ammonia	-	-	-	0.05	-	-	Menzi et al., 1997 cited by Riedo et al., 2000
h_{lim}	Grass minimum height under which animals can not graze	cm	-	-	3	-	-	Personal communication (J.Bindelle)
Root parameters								
α_{rt}	Parameter for root development	-	-	-	5.86	-	-	Arora & Boer, 2003
bd_{coef}	Bulk density coefficient for root sensitivity to soil strength	-	1550	1600	1600	Aspects	Jones et al., 1991	Jones et al., 1991
β_{rt}	Parameter for root development	-	-	-	7.67	-	-	Arora & Boer, 2003
$cr_{dpt,max}$	Maximum depth of the coarse root system	m	0.9	-	-	Aspects	-	-
fr_{dens}	Root carbon density	gC cm^{-3}(root)	0.075	0.075	0.075	Aspects	Aspects	Aspects
fr_{radius}	Root radius	cm	0.025	0.0077	0.0066	Aspects	Föhse et al., 1991	Föhse et al., 1991
$LW_{ratio,harv}$	Root length to weight ratio at maturity	m g^{-1}(root)	-	175	-	-	Barraclough & Leigh, 1984	-
ph_{max}	Maximum pH for root growth	-	9.25	9	8.4	Aspects	-	Hannaway et al., 1999
ph_{min}	Minimum pH for root growth	-	3.75	5	5.1	Aspects	Schroder et al., 2011	Hannaway et al., 1999
$ph_{op,low}$	Lower pH for optimum root growth	-	4.25	5.4	5.5	Aspects	Zhang et al., 2004; Johnson, 2011	Hannaway et al., 1999
$ph_{op,up}$	Upper pH for optimum root growth	-	8.25	8	7.5	Aspects	Johl, 1979	Hannaway et al., 1999
$GS_{dpt,max}$	Growth stage at maximum root depth	-	-	0.9	-	-	Jones et al., 1991	-
$poro_{h2o,crit}$	Critical water-filled porosity for root growth	-	0.4	0.4	0.4	Jones et al., 1991; Williams et al., 1989	Jones et al., 1991; Williams et al., 1989	Jones et al., 1991; Williams et al., 1989
rhizodep	Fraction of matter allocated to root going directly to the soil	-	-	0.134	0.134	-	Newman, 1978	Newman, 1978
$rt_{dpt,max}$	Maximum depth of the root system	m	-	2	-	-	Gregory et al., 1978; Kirkegaard & Lilley, 2007; Thorup-Kristensen, 2009	-
rt_{dens} (1:nhz)	Root length density in each soil layer	cm cm^{-3}(root)	-	8; 8; 4; 1; 0.5	-	-	Asseng, 1997; Hodgkinson et al., 2017	-
$LW_{ratio,seed}$	Root length to weight ratio at seeding	m g^{-1}(root)	-	200	-	-	Barraclough & Leigh, 1984	-
$Tp_{fr,base}$	Minimum soil temperature for root growth	C	5	2	0	Aspects	Porter & Gawith, 1999	Thornley, 1998

$Tp_{fr,op}$	Optimum soil temperature for root growth	C	20	16.3	20	Aspects	Porter & Gawith, 1999	Thornley, 1998
wcg	Coefficient for root distribution	-	-	2	-	-	Jones et al., 1991	-
Senescence parameters								
f_{depl}	Depletion factor of the total available water	-	-	0.55	0.6	-	Allen et al., 1998	Allen et al., 1998
γ_{temp}	Mineralization temperature parameter	-	308.15	277.33	277.33	Lloyd & Taylor, 1994	calibrated	calibrated
tau_l	Foliage lifespan at reference temperature (20°C)	d	219	70	83	Aspects	Van Heemst, 1988	Lazzarotto et al., 2009
tau_{fr}	Root lifespan at reference temperature (20°C)	d	-	58.97	100	-	Gibbs & Reid, 1992	Lazzarotto et al., 2009
tau_w	Woody biomass lifespan	d	54750	-	-	Aspects	-	-
$lifespan_{min}$	Litter lifespan	d	730	730	803	Aspects	Aspects	calibrated
$lifespan_{minc}$	Woody litter lifespan	d	7300	-	-	Aspects	-	-
$lifespan_{som}$	SOM lifespan	d	36500	36500	16100	Aspects	Aspects	calibrated

Table C.2: General parameters

Parameter	Description	Units
File names		
initialfile	Name of the initial values file	-
soilfile	Name of the soil characteristics file	-
managementfile	Name of the management file	-
pathres	Beginning of results file names	-
Type of simulation		
ecosyst	Type of ecosystem (1=forest;2=crop;3=grassland)	-
nhd	Number of data per day	d-1
nd	Numer of days in the one year	d
nnh	Number of time steps per half hour	-
nh	Number of time steps per day	d-1
nhwk	Number of days for average of N uptake	d
ifull	Flag to generate 1/2h results	-
nyrstart	Starting year of simulation	yr
nyrmax	Number of years to simulate	yr
ident_simul	Variable to choose the simulation type	-
ident_strs_n	Variable to choose to simulate nitrogen stress	-
ident_mana	Forest management type	-
ident_disease	Forest mortality due to disease	-
isteady	Flag to start a steady-state simulation	-
Numerical resolution		
niter	Maximum number of correction iteration	-
norder	Order of Runge-Kutta resolution	-
thick_layer1	Thickness of the first fictive soil layer	m

Environmental conditions		**Forest**	**Cropland**	**Grassland**	**Units**
ico2	Atmospheric CO2 concentration	360	360	360	ppm
idepot	Annual nitrogen deposition for forest	28	28	28	gN 10-1 yr-1
sNH4_depos_an	Annual deposition of NH4 in open fields	-	0,63	0,63	gN-NH4 m-2 yr-1
sNO3_depos_an	Annual deposition of N03 in open fields	-	0,54	0,54	gN-N03 m-2 yr-1
Reservoirs information					
nhz	Number of soil layers	6	5	3	-
ncp	Number of above-ground carbon pools	5	4	1	-
ncb	Number of below-ground carbon pools	6	4	4	-
nco	Number of carbon pools	41	24	13	-
nnp	Number of above-ground nitrogen pools	4	4	2	-
nnb	Number of below-ground nitrogen pools	7	5	5	-
nno	Number of nitrogen pools	46	29	17	-
nwp	Number of above-ground water pools	2	2	2	-
nwo	Number of water pools	8	7	5	-
ntp	Number of above-ground thermal pools	0	0	0	-
nto	Number of thermal pools	6	5	3	-
nres	Total number of pools	101	65	38	-
Site information					
xlat	Latitue	50,3050	50,3123	50,3123	deg
xlong	Longitude	5,9980	4,7464	4,9678	deg

C.2 Initial reservoirs values

Table C.3: Initial reservoirs values used for the cropland ecosystem (Lonzée).

				Horizon				
y	**Reservoir**	**Unit**	**Above-ground or horizon 1**	**2**	**3**	**4**	**5**	**Method**
1	storage organs (C)	g C m^{-2}	0					-
2	reserve (C)	g C m^{-2}	0					-
3	leaves (C)	g C m^{-2}	0					-
4	stems (C)	g C m^{-2}	0					-
5-9	root (C)	g C m^{-2}	0	0	0	0	0	-
10-14	litter (C)	g C m^{-2}	38.3481	76.8971	130.496	103.825	64.7867	†
15-19	SOM (C)	g C m^{-2}	619.424	1242.09	2107.86	1677.05	1046.48	†
20-24	CO_2 (C)	g C m^{-2}	0.61	1.23	1.62	2.05	2.46	Aspects
25	storage organs (N)	g N m^{-2}	0					-
26	reserve (N)	g N m^{-2}	0					-
27	leaves (N)	g N m^{-2}	0					-
28	stems (N)	g N m^{-2}	0					-
29-33	root (N)	g N m^{-2}	0	0	0	0	0	-
34-38	litter (N)	g N m^{-2}	1.25916	2.54575	4.32951	4.07448	2.97388	*
39-43	SOM (N)	g N m^{-2}	62.9584	127.287	216.476	203.724	148.694	*
44-48	soil NO_3	g N m^{-2}	0.42439	0.85801	1.45921	1.37325	1.00231	*
49-53	soil NH_4	g N m^{-2}	0.30222	0.61101	1.03913	0.97792	0.71376	*
54	snow	mm H_2O	0					Measure
55	soil water TOP	m^3 m^{-3}	0.37781					Measure
56-60	soil water	m^3 m^{-3}	0.37781	0.38622	0.39909	0.4186	0.43964	Measure
61-65	soil temperature	K	273.628	274.645	276.614	281.016	290.057	Measure

†Total carbon measured, partitioned with calibration

*Measure of the total soil nitrogen, partitioned with Sharpley & Smith (1995) between NO3, NH4 and organic, calibration between litter and SOM.

Table C.4: Initial reservoirs values used for the grassland ecosystem (Dorinne).

				Horizon		
y	**Reservoir**	**Unit**	**Above-ground or horizon 1**	**2**	**3**	**Method**
1	shoot	g C m-2	27.4497			*
2-4	root (C)	g C m-2	70.159	25.161	4.3375	Jackson et al. (1996)
5-7	litter (C)	g C m-2	1820.99	43.5049	0.01709	†
8-10	SOM (C)	g C m-2	2916.54	5749.14	4846.52	†
11-13	co2 (C)	g C m-2	0.61	3	2.87	Aspects
14	shoot (N)	g N m-2	2.83027			*
15	vegetation reserves (N)	g N m-2	4.132			Optimum reserve calculated
16-18	root (N)	g N m-2	2.71041	9.72013	1.67567	Jackson et al. (1996)
19-21	litter (N)	g N m-2	9.10774	12.1584	11.5528	‡
22-24	SOM (N)	g N m-2	455.387	607.921	577.642	‡
25-27	soil NO3	g N m-2	2.71726	3.62742	3.44675	‡
28-30	soil NH4	g N m-2	1.4177	1.89257	1.7983	‡
31	snow	mm H2O	0			Measure
32	soil water TOP	m3 m-3	0.4984			Measure
33-35	soil water	m3 m-3	0.4984	0.4759	0.438	Measure
36-38	soil temperature	K	279.844	280.231	280.366	Measure

*Measure of herbage height the 26/11/2013, changed in carbon by means of allometric equation and dm_c/dm_n

†Total carbon measured, partitioned with calibration

‡Measure of the total soil nitrogen, partitioned with Sharpley & Smith (1995) between NO3, NH4 and organic, calibration between litter and SOM.